MERCURY, SULFUR-METABOLIZING BACTERIA AND ORGANIC MATTER IN THE SEDIMENTS OF SUBARCTIC KUSAWA LAKE, YUKON

by

Jocelyn Anne Joe-Strack

B.Sc. University of Victoria, 2006

THESIS SUBMITTED IN PARTIAL FULFILLMENT OF
THE REQUIREMENTS FOR THE DEGREE OF
MASTER OF SCIENCE
IN
NATURAL RESOURCES AND ENVIRONMENTAL STUDIES
(GEOGRAPHY)

UNIVERSITY OF NORTHERN BRITISH COLUMBIA

April 2015

© Jocelyn Anne Joe-Strack, 2015

UMI Number: 1526529

All rights reserved

INFORMATION TO ALL USERS
The quality of this reproduction is dependent upon the quality of the copy submitted.

In the unlikely event that the author did not send a complete manuscript
and there are missing pages, these will be noted. Also, if material had to be removed,
a note will indicate the deletion.

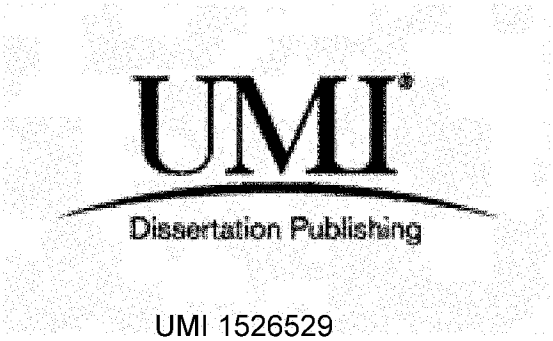

UMI 1526529
Published by ProQuest LLC 2015. Copyright in the Dissertation held by the Author.
Microform Edition © ProQuest LLC.
All rights reserved. This work is protected against
unauthorized copying under Title 17, United States Code.

ProQuest LLC
789 East Eisenhower Parkway
P.O. Box 1346
Ann Arbor, MI 48106-1346

Abstract

Recent studies of Arctic and Subarctic environments have detected rising levels of natural and anthropogenic mercury (Hg), putting northern residents at risk for Hg exposure. Within lake sediments, Hg can be methylated by certain species of Sulfate-Reducing Bacteria (SRB), a subset of Sulfur-Metabolizing Bacteria (SMB). This research assessed the controls of Subarctic SRB Hg-methylation in proglacial Kusawa Lake, Yukon, Canada. Kusawa was found to be oligotrophic, with very low primary productivity and an orthograde oxygen profile, conditions that inhibit Hg-methylation. In addition, the SMB proportion of total bacteria was small ($1.9x10^{-3}$ %), no known SRB Hg-methylators were detected, the total Hg sediment concentration was 0.022 ± 0.0009 $\mu g g^{-1}$ (±SE) and methylmercury was undetectable. The results support previous research that suggests the factors influencing SRB Hg-methylation in Kusawa Lake are: (i) the rate of algal-derived Hg-scavenging, (ii) the sediment concentration of total Hg and (iii) the diversity of sediment SRB.

Frontispiece: Kusawa Lake, Arc Mountain, near sample site, March 2010. (Photo credit: Pat Roach)

Contents

List of Tables

List of Figures

Acronyms

a.s.l above sea level

ADW accumulated dry weight

AMDE atmospheric mercury depletion events

Apr APS reductase

APS adenosine 5'-phosphate

BLAST Basic Local Alignment Search Tool

CRS constant rate of supply model

dH_2O distilled water

DO dissolved oxygen

Dsr dissimilatory sulfite reductase

EMR Energy Mines and Resources, Yukon

GEM gaseous elemental mercury

GSB green sulfur bacteria

HC hydrocarbon

HI hydrogen index

LOI loss on ignition

MeHg methylmercury

OICO carbon monoxide index

$OICO_2$ carbon dioxide index

OIRE6 oxygen index

OM organic matter

PC pyrolysable carbon

PCA Principle Components Analysis

PCR polymerase chain reaction

PSB purple sulfur bacteria

qPCR quantitative polymerase chain reaction

RC residual carbon

SAT sulfate adenylyltransferase

SE standard error

SB sulfur-reducing bacteria

SMB sulfur-metabolizing bacteria

SOB sulfur-oxidizing bacteria

SRB sulfate-reducing bacteria

SSC suspended sediment concentration

THg total mercury

TOC total organic carbon

Tbac total bacteria

UNBC University of Northern British Columbia

WRA White River Ash

Acknowledgements

This is the last section I am writing and I can only think of the fact that completing this project and writing this document has been extraordinarily challenging. I am amazed that it's almost complete and there are many to thank.

When I began my Master's, this project was intended to be different and I thank my supervisor, Dr. Ellen Petticrew for allowing me to follow my own direction and guiding me through this process. I thank my committee members, Dr. Phil Owens for sedimentology advice and Dr. Keith Egger for use of his lab and helping me plan and troubleshoot my lab work. I especially thank Pat Roach for inviting me to participate and contribute to the mercury research at Kusawa Lake and introducing me to Dr. Gary Stern.

I want to express my great appreciation to Dr. Stern and his collaborators, as I would not have been able to complete this work without their generous support. Particularly, I would like to thank them for collecting my samples and analyzing them for several of the variables used in my study. As well, I would like to thank Dr. Stern and Dr. Jessie Carrie for helping me interpret the Rock Eval results.

At UNBC, I want to thank Dr. Brent Murray for sharing his molecular biology expertise and Dr. Dezene Huber for use of his lab. As well, I'd like to thank the members of Dr. Egger's lab for their support and assistance in troubleshooting. I am very thankful for my fellow UNBC grad students for the opportunities to mutually commiserate in this experience. I'd especially like to thank Leah Vanden Busch for sharing the challenge of undertaking a similar path of writing from the north.

I am indebted and grateful to Champagne and Aishihik First Nation for supporting me throughout my post-secondary career and for donating resources for my lab work.

I'm also greatly appreciative to Darielle Talarico, for offering me the opportunity to advance my career while providing the time and wonderful support needed to complete this work.

So, in final reflection, I realize that when I think of this period of my life, I think of my mother. I strive to remember and invoke her lessons of how to live, how to work and how to be kind and patient and I thank her. When I moved to Prince George to begin this she missed me and as I finish, I miss her; but I can reflect in parallel the work this took, the path I've followed and people who held me along the way.

I would like to thank my family from both my mother and father's side who have been not only supportive of my educational goals but have also simply let me know they are proud of me. I have many wonderful friends and sisters that I thank for their love, for listening and sharing. I thank the Creator for my home the Yukon, Whitehorse and Riverdale, places that without I would have struggled to find the grounding needed to complete this task. Finally, I would like to thank sweet Scott Osborne, who has patiently listened, endured my exasperation and given me back the comfort and security of family.

I raise my hands to you all. Shäw nithän, kwänaschis, thank you.

Chapter 1 Introduction

1.1 Introduction

The United Nations Environmental Programme has identified Mercury (Hg) as a global threat to human and environmental health. It is responsible for toxicity that affects the gastrointestinal system and brain and is of particular concern to pregnant and nursing women (United Nations Environment Programme, 2013). Arctic and Subarctic residents are at risk for Hg exposure from naturally occurring sources of Hg and atmospherically transferred Hg emitted from distant industrial sources (Schroeder et al., 1998; Dunford et al., 2010). In lakes, algae and algal-derived organic matter (OM) can scavenge anthropogenic and naturally occurring Hg from the water column. They then form aggregates or flocs with suspended sediment that settle to the lake bottom where Hg species may be stored or re-suspended to the water column (Outridge et al., 2007; Stern et al., 2009; Sanei et al., 2014). At the sediment oxic/anoxic transition zone, Sulfate-Reducing Bacteria (SRB), a subset of Sulfur-Metabolizing Bacteria (SMB), can convert Hg to organic methymercury (MeHg) (Benoit et al., 1999; Gilmour et al., 2011). Methylmercury is of concern as it readily crosses cell walls to bioaccumulate and biomagnify up the food chain (Fitzgerald & Lamborg, 2003; Chételat et al., 2012).

In the Yukon Territory of northwestern Canada, many residents still harvest fish, animals and vegetation from the lakes and forests. Therefore, the need to determine the

risk of Hg exposure is important for those who regularly consume wild foods. This study intends to contribute to the understanding of the factors that influence the ability of SRB to methylate Hg in Subarctic lake sediments and inherently enable Hg uptake to the food web.

Much of this study augments previous work by Dr. Gary Stern and his team from the University of Manitoba where they have been examining the interaction between Hg and certain carbon fractions of organic matter (OM) as detected by Rock Eval Pyrolysis (Outridge et al., 2007; Stern et al., 2009; Carrie et al., 2012; Hare et al., 2014; Sanei et al., 2014). Their hypothesis proposes that climate change related increases in algal matter have resulted in a concurrent increase in algal scavenging of Hg from the water column to the lake sediments.

In 2005, Dr. Stern and his team collected duplicate sediment cores from the deepest region of Subarctic, Kusawa Lake (60°19'55"N, 136°4'48"W) in southwestern Yukon. From these two cores they analyzed the components of Total Organic Carbon (TOC) using Rock-Eval Pyrolysis and the Total Hg (THg) by cold vapour atomic absorption spectrometry. The outcome was that both cores exhibited a strong relation between THg and the Rock Eval fraction, S2 that consists of labile hydrocarbon-rich algal-derived OM. They also noted that the 20th Century S2 levels were 26-29% higher than the pre-1900 levels (Stern et al., 2009). This finding complemented previous works (Outridge et al., 2007) and was further investigated in a recent study that found that the ability of S2 algal-derived OM to scavenge Hg from lakes is dependent on the lake's overall productivity and the level of available Hg (Sanei et al., 2014). The algal-Hg scavenging hypothesis also suggests that post-1950 increases observed in sediment Hg records are not directly related to atmospheric Hg

deposits. Instead, the available organic carbon in a basin has the ability to strongly influence the rate of Hg sequestration in sediments (Outridge et al., 2007; Stern et al., 2009; Sanei et al., 2014).

In March 2010, members of Dr. Stern's research team took another set of duplicate sediment cores from ~700 m east of the previous 2005 sample site in Kusawa Lake, Yukon. These were the cores used in this study to assess the environmental controls of Hg-methylation and demethylation by SRB in Kusawa Lake's bottom sediments. To achieve this, the cores were analyzed to measure the concentration of total mercury, total bacteria and SMB, Rock Eval Pyrolysis, trace metals, particle size and ^{210}Pb and ^{137}Cs dating. Aspects of Kusawa's hydrology, climate conditions and other regional features were also considered. The overall intent of this study is to contribute to the understanding of Hg cycling in Subarctic aquatic systems so current and future generations of Yukoners can continue to safely harvest food from the lakes and forests and enjoy the Yukon's spectacular beauty.

An example of the importance of the wilderness to Yukoners is the joint creation of Kusawa Lake Park by an agreement between the Government of Yukon, the Champagne and Aishihik First Nation, Carcross/Tagish First Nation and Kwanlin Dun First Nation. These three First Nations have immemorially used Kusawa Lake when it was known as Nakhų Män, "rafting-across lake" by the Southern Tutchone and Kúsawau.â meaning, "long narrow lake" by the inland and coastal Tłingit. There is a large delta on the lake created by the Primrose River that was a gathering place to discuss traditional governance, concerns regarding animals and the forest and to celebrate in the abundance of fish and caribou that migrated

through the narrows. In planning the park, many of these traditional ideals are applied to ensure the longevity and vitality of the lake (Kusawa Park, 2014). Establishing a baseline biogeochemical understanding of mercury cycling in Kusawa Lake and the potential influence of climate change will aid current and future generations in monitoring and recognizing the extent of mercury accumulation and its impact on our culture, health and wellbeing.

1.2 Research Objectives

This project is a study of the interactions between OM, bacteria, and Hg in the bottom sediments of Kusawa Lake, Yukon Territory. It also takes into account the influence of the lake's limnology and sedimentation. In essence, the objective of this study is to evaluate and characterize the potential factors that control the interaction between SMB, particularly SRB and Hg in the bottom sediments of Kusawa Lake. It will also contribute to the body of research on Hg cycling and accumulation in Subarctic ecosystems. Overall, my thesis results are intended for researchers, the First Nations of Kusawa Lake and the current and future generations of Yukon people.

The primary objectives of this study are to:

1. examine the origin, concentration and composition of organic matter in the lacustrine sediments of Kusawa Lake (Chapters 3 and 4);

2. characterize the phylogeny and concentrations of sulfur-metabolizing bacteria and their interactions with the components of organic matter and sediment processes (Chapter 5);
3. discuss the mechanisms involved in mercury transport to the sediments and evaluate the potential for mercury methylation by sulfate-reducing bacteria (Chapter 6), and;
4. discuss the potential of climate change to influence the interactions between organic matter, sulfur-metabolizing bacteria and mercury (Chapter 6).

This thesis is structured into seven chapters where each chapter builds on the previous. Chapter 1 outlines the overarching questions and research objectives. Chapter 2 introduces the Kusawa Lake drainage basin, its historic climate conditions and other local features. Chapter 3 describes the limnology, bathymetry and the features of the sediment core's subsamples including the ^{210}Pb and ^{137}Cs dating, particle size and trace metal profiles. Chapter 4 is an overview of the Rock Eval Pyrolysis OM results and Chapter 5 depicts the downcore concentrations of total bacteria and SMB as well as phylogeny of SMB. Finally, Chapter 6 incorporates the findings from the previous four chapters to discuss the various influences on SRB-mediated methylation of Hg in the sediments. This chapter also postulates the potential influences of climate change on the processes studied and the implications for Yukon people. Finally, Chapter 7 summarizes the conclusions of the study, significance of this work and suggests supplementary research.

Chapter 2 Study Area, Kusawa Lake, Yukon

2.1 Creation and Physical Characteristics

"When Crow was making the world he was flying over thinking hard about what to do with the fish. He decided to go to Klukshu and held one wing towards the coast, the Alsek drainage, and declared that it should be filled with Sockeye, Coho and Chinook salmon. He held his other wing towards Kusawa, the Yukon drainage and said that will be filled with Chinook. That is why Klukshu has more salmon than the Yukon"

– Adapted from Mrs. Annie Ned (Kusawa Park, 2014)

2.1.1 Landscape and Sub-basins

Kusawa Lake (60°19'55"N, 136°4'48"W) is a proglacial fluvial system (Church & Gilbert, 1975) with a lake surface area of 142 km^2 that drains a watershed of 4292 km^2 to the Takhini River (Gilbert & Desloges, 2005), which enters the Yukon River just before Lake Laberge outside of Whitehorse, Yukon (Fig 2.1). The lake is located ~80 km southwest of Whitehorse and is accessible off the Alaska Highway between the Champagne and Aishihik First Nation communities of Takhini and Champagne. It has five major sub-basins shown in Figure 2.2 and described in Table 2.1.

2.1.2 Glacial History

Kusawa Lake lies at the southern extension of the Late Pleistocene glacially dammed Glacial Lake Champagne, which reached a maximum elevation of 853 m above sea level (a.s.l.) and spanned several valleys along the Shakwak Trench and Boundary Range Mountains. Its boundaries have not been definitively defined, but its strandlines have been

Study Area, Kusawa Lake, Yukon

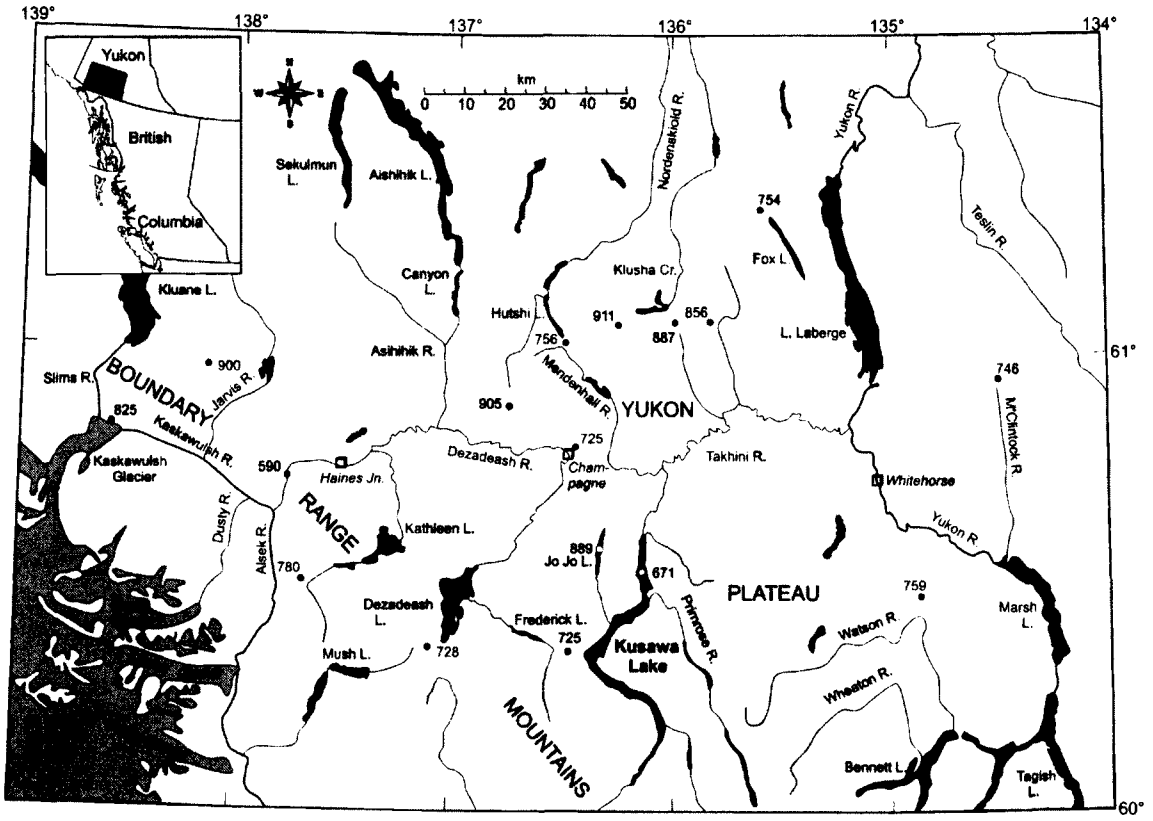

Figure 2.1: Overview of southwest Yukon drainage systems and topology surrounding Kusawa Lake. Regions over 1000 m a.s.l. are shaded in grey and spot elevations are identified for valley floors and lake surfaces (Gilbert & Desloges, 2005).

Table 2.1: Overview of Kusawa Lake sub-basins. Glacial cover is as of 2004 (Gilbert & Desloges, 2005)

Sub-Basin	Area (km^2)	Glacial Cover %	Description
[illegible]	[illegible]	[illegible]	[illegible]
Upper-most Takhini River	545	13.9	Smallest sub-basin; greatest glacial cover; Takhini lake likely a sediment trap
[illegible]	[illegible]	[illegible]	[illegible]
Jo-Jo Creek	330	0.0	Jo-Jo lake at 953 m a.s.l. in steep-walled valley; acts as a sediment trap
[illegible]	[illegible]	[illegible]	[illegible]

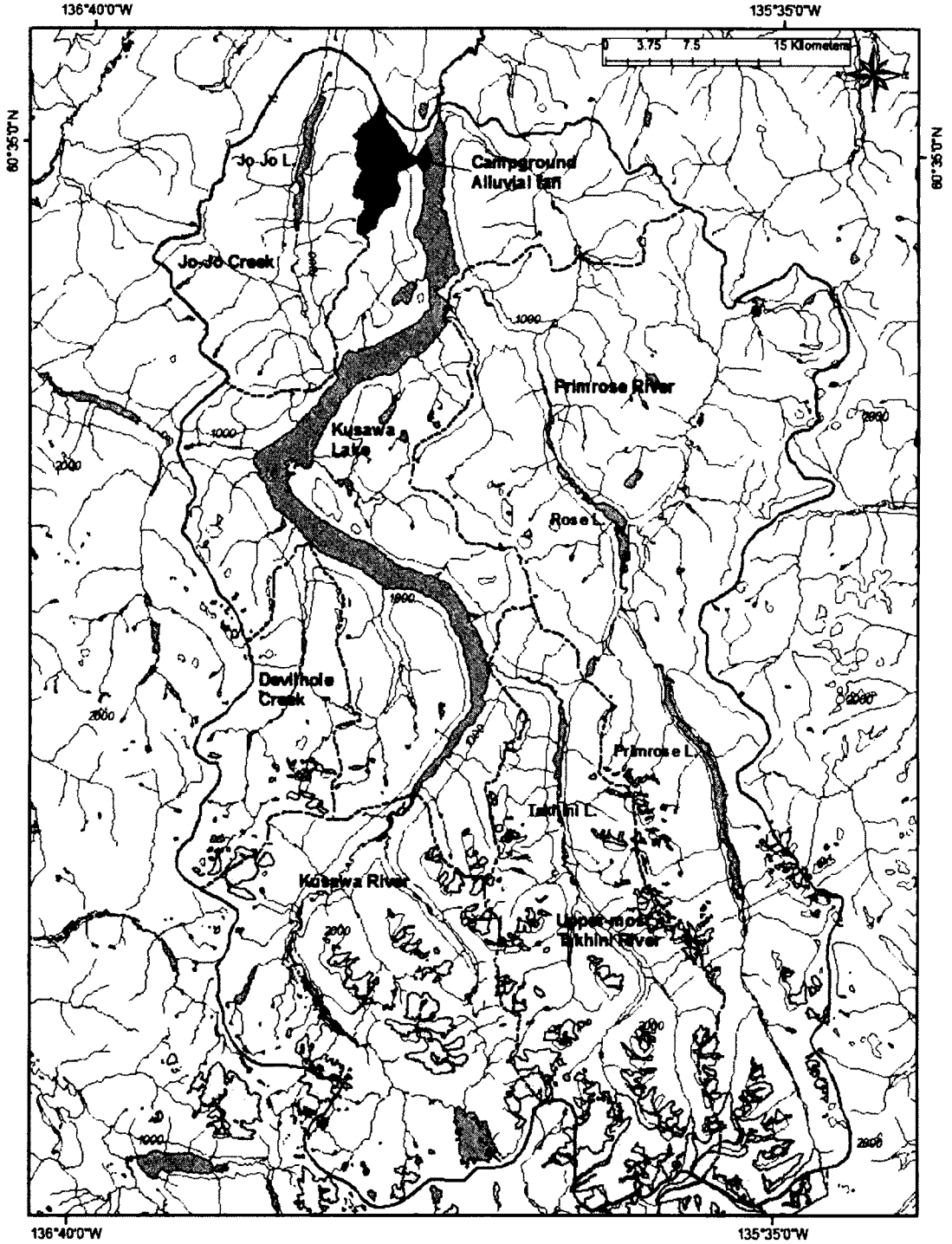

Figure 2.2: Overview of the Takhini River drainage basin and Kusawa Lake sub-drainage basins. The extent of glacial ice as of 2004 is shown in grey (Chow, 2009).

identified along the Dezadeash valley, including offshoots from the Kathleen valley and through the Frederick Lake valley to Kusawa Lake and the Takhini River valley (Fig 2.1) (Hughes et al., 1969; Jackson et al., 1991; Gilbert & Desloges, 2005). In the Kusawa region, Glacial Lake Champagne was dammed by a trunk glacier located at the southern end of the Takhini valley that resulted in moraines and a large delta at the outlet of Kusawa Lake. Failure of this ice dam lowered Lake Champagne and led to the separation and formation of Kusawa, which was further lowered to the modern day level of 671 m a.s.l. after a sediment plug at the lake outlet eroded enough to allow drainage (Gilbert & Desloges, 2005).

2.1.3 Bathymetry

In July 2004, Gilbert & Desloges (2005) conducted an acoustic survey of Kusawa Lake to determine the events involved in its formation during the Holocene deglaciation of Lake Champagne. From this, they identified five distinct bathymetric regions based on morphology, the acoustic character of the sediments and by inference of the sedimentary history and environment (Fig 2.3, Table 2.2).

2.1.4 Core Sample Location

The core sediment samples were taken from the area below the transect line shown in region IV (Fig 2.3). Region IV is the deepest part of the lake with the second deepest sediment fill. The acoustic profile of region IV taken by Gilbert & Desloges (2005) is shown

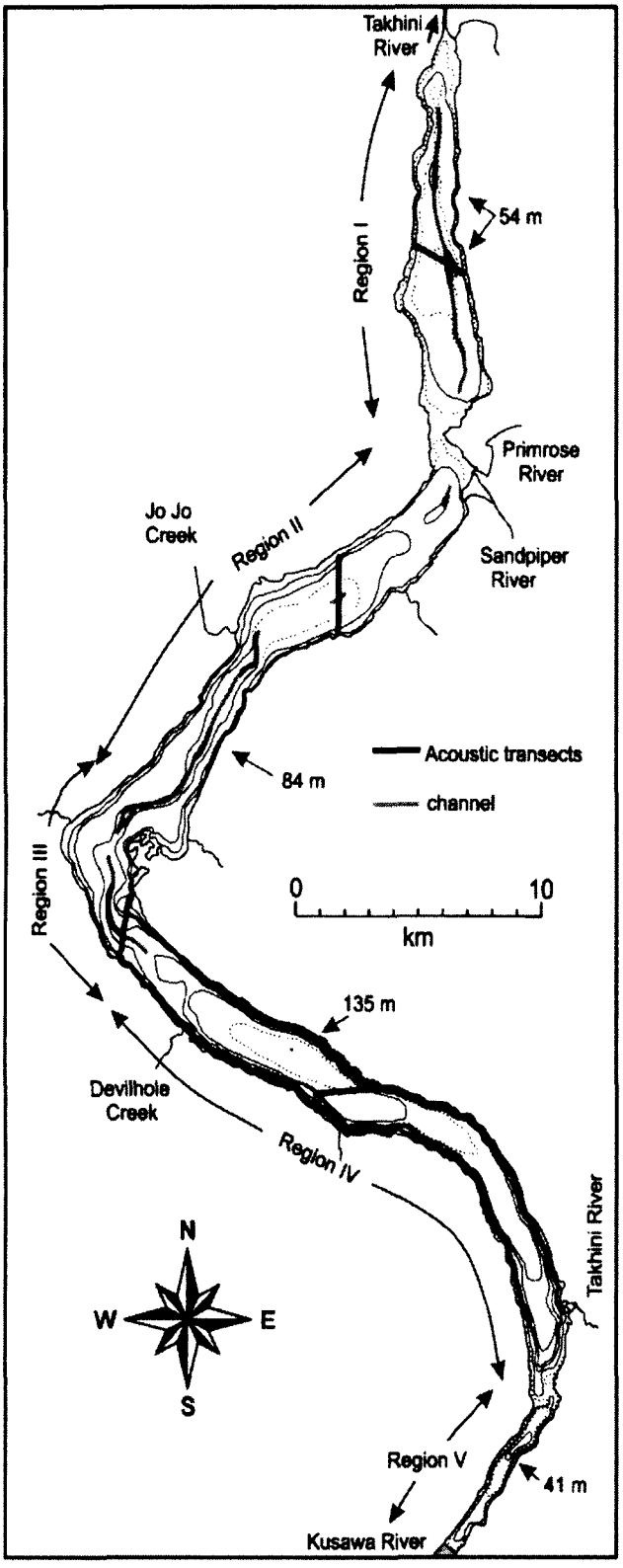

Figure 2.3: Bathymetry of Kusawa Lake determined from the July 2004 acoustic survey completed by Gilbert & Desloges (2005). Isobath interval is 20 m (solid lines) and 10 m (broken lines) below the normal summer water level. Maximum depths are indicated and acoustic transects are shown as horizontal lines. The velocity of sound in water was assumed to be 1430 m/s (corresponding to 5.5°C).

in Figure 2.4. From this profile, they inferred that region IV consists of one facies of well-layered sediment with reflectors parallel to the present lake bedrock. Further, they suggest that this sedimentation regime is due to a long period of deposition, largely from low-density turbidity currents that distribute sediment along the length of the lake floor (Gilbert & Desloges, 2005; Chow, 2009).

Table 2.2: Description of bathymetry of five regions in Kusawa Lake starting from head of the lake at Kusawa River (region V) to outlet at Takhini River (region I) based on acoustic profiles collected and characterized by Gilbert & Desloges (2005) and Chow (2009).

Region	Water Depth (m)	Sediment Depth (m)	Description
IV	135	82	Deepest part of lake, U-shaped valley. Well-layered sediment fill lies conformably on top of underlying basement (further discussion in Section 2.1.4 and Figure 2.4)
II	40-84	~40-100	After elbow, several depressions, thickest glacial-lacustrine sediment layer in lake. Before Primrose Delta in northern portion, the narrowest part of the lake there is nearly flat shallow sediment fill

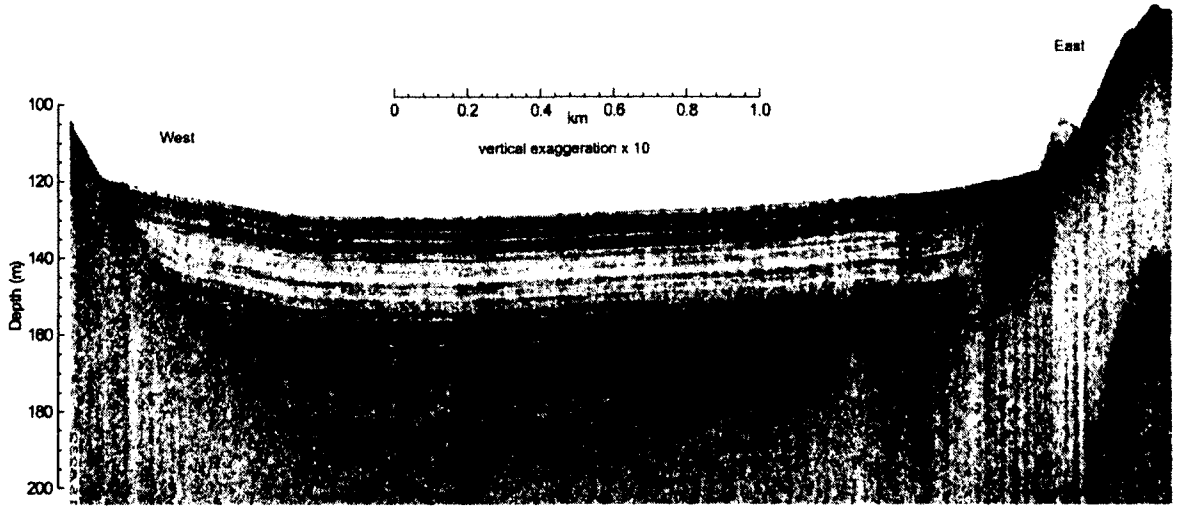

Figure 2.4: Acoustic section of region IV in Kusawa Lake. The perspective is looking down lake, to the North. Location of transect is shown in Figure 2.3 as a horizontal line across region IV (Gilbert & Desloges, 2005).

2.2 Climate History

With the exception of the Primrose River narrows, Kusawa Lake is ice covered from November/December until late May. One Yukoner who owns a cabin near the campground shared that the ice typically goes out around May long weekend and can be described as "thousands of smashing dishes, and it doesn't stop, its goes on and on for about 24 hours and then the lake's quiet again" (personal communication, Janssens, M, 2014).

Kusawa is located within the Dezadeash region and is moderated by warm air masses from the Pacific Ocean. It lies just to the east of the Boundary Range Mountains and can experience considerably lower temperatures and precipitation than locations further inland due to orographic effects cause by the Coastal and St. Elias mountain ranges (Lowey, 2002).

There are no long-term meteorological stations in the direct vicinity of Kusawa. The precipitation trends are assumed from the Environment Canada's Whitehorse Airport station located ~80 km northeast of the lake.

2.2.1 Temperature

Temperature was first recorded in Whitehorse in 1905, when the small town was the main rail and sternwheeler transportation hub for Stampeders on route to Dawson City during the Klondike Gold Rush. It was also a respite stop for rafters after Miles Canyon and the town's namesake, the treacherous Whitehorse Rapids. Activity then dropped off and temperature was not recorded from 1910 until 1941 when construction commenced for the Alaska Highway from Dawson Creek, B.C. to Fairbanks, Alaska during World War II. The

average annual temperature record at the Whitehorse Airport is shown in Figure 2.5. From 1970-2010 there is a 2.14°C increase in annual temperature with the warmest year recorded in 2004. This is evidence of climate warming, which is also observed in the longest climate proxy in the Yukon, the Yukon River break-up at Dawson City. The time and date of break-up has been recorded every year since 1896, with a raffle awarded to the ticket with the closest guess to when the ice goes out. In the first 20 years of the record, break up occurred around May 10th; in the past 20 years to date it has now advanced to May 4th (Janowicz, 2010). Another notable trend is that six of the seven April break-ups have occurred within the last 10 years (Joe-Strack, 2012).

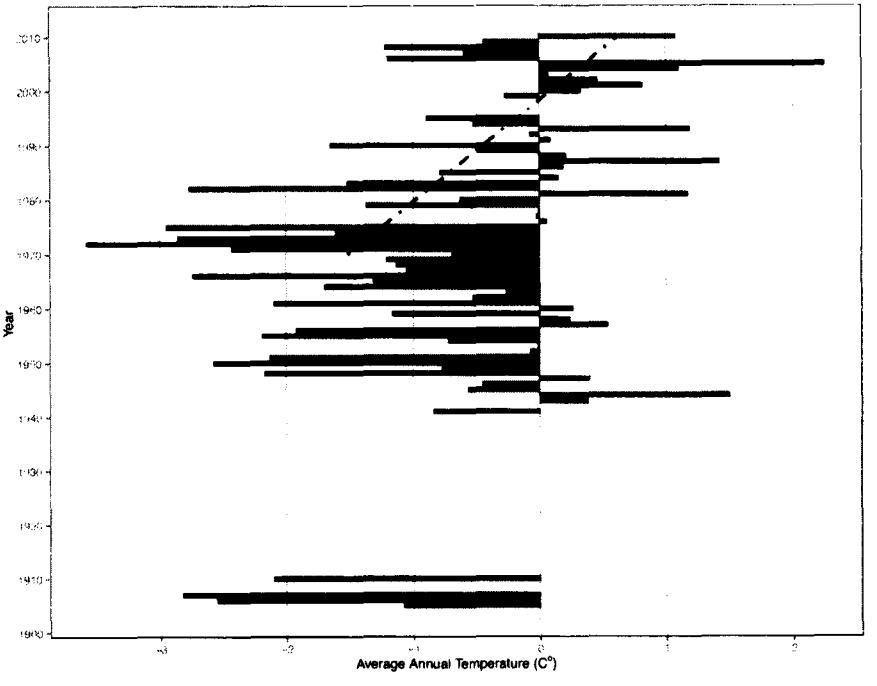

Figure 2.5: Average annual air temperature at Whitehorse Airport, located ~80km northeast of Kusawa Lake, from 1905-2010. The dash-dot regression line indicates a 2.14°C temperature increase from 1970-2010, r^2=0.229, p<0.01. (Environment Canada, 2014a)

2.2.2 Precipitation

The average rainfall and snowfall at Whitehorse Airport from the Environment Canada Canadian Climate Normals 1981-2010 was 160.9 mm and 141 cm, respectively (Environment Canada, 2014a). Ric Janowicz, the Yukon's hydrologist with Environment Yukon's Water Resources Branch noted inconsistent changes in annual precipitation throughout the Yukon. He states that winter precipitation has generally increased in northern and southeast regions and decreased in the southwest, while summer precipitation has increased slightly throughout the Territory, with greater increases in the southeast and central areas (Janowicz, 2010). The Kusawa region has experienced variable snow pack loads, for example, during the 2007 Southern Lakes flood event, Kusawa Lake had a 131-150% greater than normal snow pack, while in 2008 the snow-water equivalence was between 71-90 and 91-100% of normal and in 2013 the nearby measured snow packs were within the normal range (Environment Yukon, 2007, 2008 and 2010). These fluctuations may be due to the strong influence of atmospheric systems from the Pacific Ocean mixing with drier, cooler inland air masses (Lowey, 2002). Overall, the Kusawa watershed may have experienced a small increase in summer rain and possible decrease in winter snow, though this is uncertain due to the recent variability in snow pack.

2.2.3 Takhini River Discharge

The Water Survey of Canada and Yukon Water Resources Branch have operated three hydrometric stations that recorded discharge from the Takhini River watershed: the Primrose River above Kusawa 29AC006, operational from 1990-1998; the Takhini River at Kusawa outlet 09AC004, operational from 1952-1986 and 40 km downstream from there near the Champagne and Aishihik First Nation community of Takhini, the Takhini River near Whitehorse 09AC001, operational from 1948-current (Environment Canada, 2014b). The

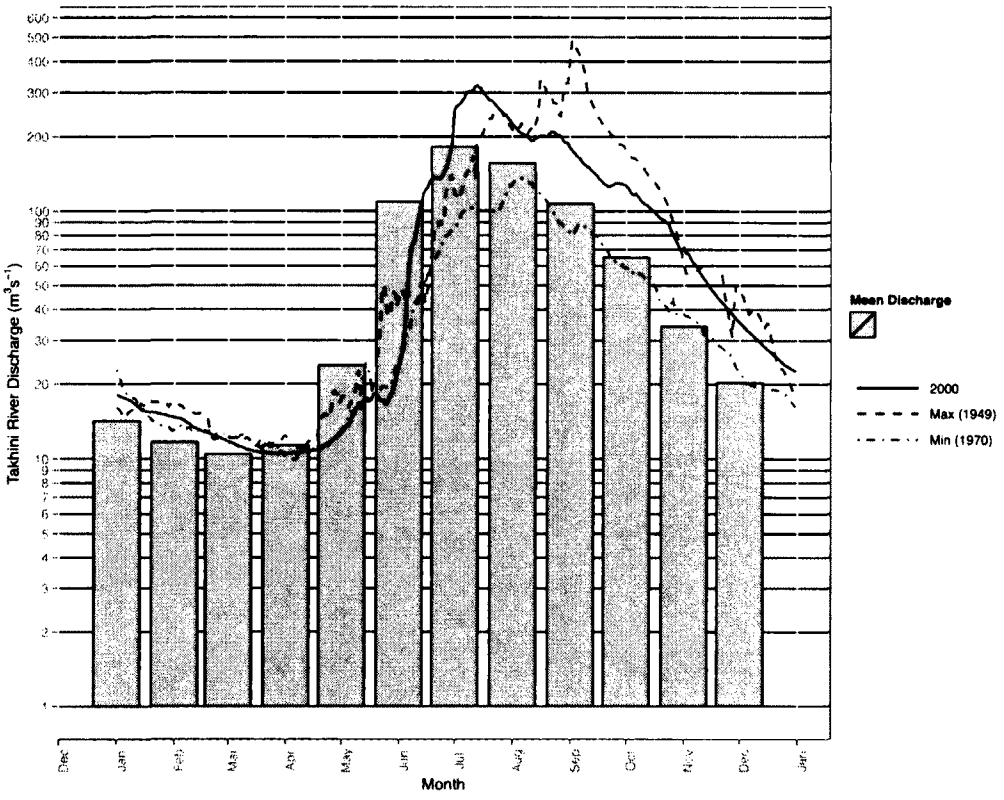

Figure 2.6: Average monthly discharge of the Takhini River near Whitehorse from the Water Survey of Canada (09AC001) from 1948-2012. Daily flows are shown for the two highest discharge years in 1948 and 2000 and minimal year in 1970 (Environment Canada, 2014b).

average discharge for the Takhini River near Whitehorse station (Fig 2.6) is shown as it has the longest record. The daily average hydrographs from 1949, 1970 and 2000 are shown and represent the maximum, minimum and second maximum discharge years on record. The peak flow occurs later in the summer as the watershed is glacially dominated as opposed to freshet, which typically occurs in early June in unglaciated systems.

2.2.4 Regional Disturbances

2.2.4.1 Torrent Systems

The Kusawa watershed is identified as a torrent system, which is common in mountainous terrain and implies that the system is prone to sporadic and sudden terrestrial discharges due to a cycle of subdued water discharge and short pulses of dynamic debris transport (Eisbacher & Clague, 1984). The most recent event was in 1982 where a flood event at the Kusawa Lake territorial campground was caused by a combination of rainfall flooding and slope failure and resulted in a catastrophic mudslide (Lowey, 2002); the affected area is shown in Figure 2.2 as the Campground Alluvial Fan.

2.2.4.2 Forest Fires

In 2005, Stern et al. (2009) analyzed a core from region IV for char deposited by nearby forest fire activity and detected major fire activity between 1917-1948, which has the potential to influence benthic activity and OM composition (Fig 2.7). More recent

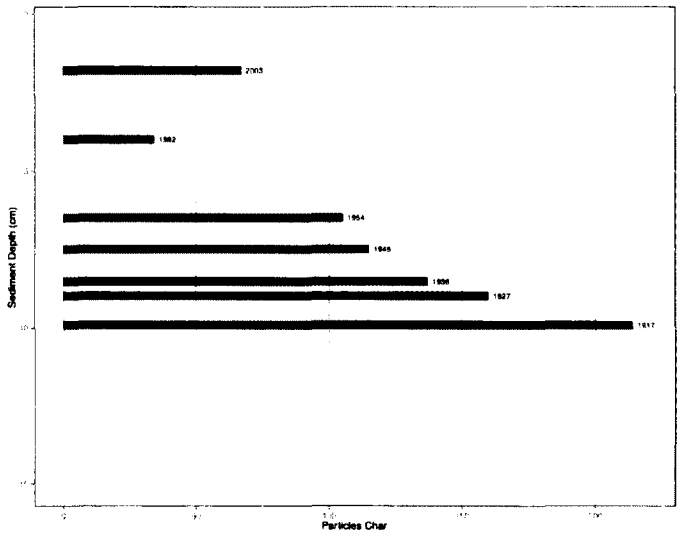

Figure 2.7: Particles of char associated with frequency of wildfire in the region determined by a core taken in 2005 where frequent wildfires were observed from 1917-1954 (adapted from Stern et al., 2009).

wildfire events were also reported in the Upper-Takhini and Kusawa watershed in 2000 and 1987, respectively (Kusawa Park, 2014).

2.3 Vegetation

The northern part of the Kusawa Lake watershed lies within the Yukon Southern Lakes ecoregion and the south within the Yukon-Stikine Highlands ecoregion. In the valleys, White Spruce and to a limited extend, Trembling Aspen dominate with a small population of Lodgepole Pine at the north end of the lake. The conifer and mixed forest trees are present to the tree line (~1200 m a.s.l.) where herbs, shrubs, willow, moss and lichen dominate the alpine tundra terrain (Smith et al., 2004).

Chapter 3 Limnology and Sedimentology of Proglacial Kusawa Lake

3.1 Introduction

Lake sedimentation in proglacial systems is dependent on several external factors such as summer and annual temperature, precipitation, rate of snow melt and rain storm events (Hodder et al., 2007). These climate driven factors control localized systems such as hydrology, lake stratification and terrestrial slope stability, all of which influence lake sedimentation and interpretation of lacustrine sediment core profiles.

3.1.1 Glacial Contributions

Glaciers act as water storage bodies that supply meltwater and sediment to a drainage basin on a diurnal, seasonal and temporal scale (Jansson et al., 2003). The quantity of glacial meltwater is highly seasonal, with peaks in larger southern Yukon drainage basins typically occurring in July or August (Environment Yukon, 2011). Glacial derived sediment transported with meltwater originates from ice shearing erosion of bedrock and can contribute up to 75-83% of the fine sediment load (Desloges & Gilbert, 1994). There is a strong relation between meltwater discharge and suspended sediment concentration (SSC) that fluctuates throughout the season and with extreme events such as landslides or rainstorms (Gurnell et al., 1994).

The sediment load originating from glaciers is influenced by events such as glacial surging, ongoing cycles of retreat (Gilbert et al., 2002) and jökulhlaups, which are catastrophic outburst flood events that release and transport large volumes of water and sediment (Desloges & Church, 1992; Ng & Björnsson, 2003). These extreme glacial events are predominately climate driven and can strongly influence the sediment record.

3.1.2 Terrestrial Contributions

Other sediment sources in proglacial systems include terrestrial inputs from land/mud slides and peri-glacial sediment slumped from lateral valley sides (Chow, 2009). Within the Yukon's various permafrost zones, land and mud slide potential is increasing due to climate warming and the concurrent increase of permafrost melt, leading to decreased land stability (Environment Yukon, 2011). Kusawa Lake lies within the sporadic continuous permafrost zone (10-50% permafrost coverage) of the Yukon, therefore the higher elevations of the southern basin are possibly permafrost bearing (Yukon Permafrost Network, 2011). Another terrestrial sediment pathway is via torrent systems where sediment is displaced and deposited to form alluvial fans or deltas along lakes. The system can be described as either dormant, where the region is stable and water is discharged without major landscape disruption or active, where short pulses of bulk debris transport result in catastrophic events such as mud or landslides and floods (Eisbacher & Clague, 1984). Torrent systems are also subject to climate change impacts such as changes in

vegetation, frequencies of storm events, permafrost melt and other factors that may alter slope stability (Stoffel & Huggel, 2012)

3.1.3 Fluvial Transport and Storage

River and stream dynamics play a key role in sediment transport and fate. The fluvial discharge (m^3/s) is directly related to seasonal temperature and precipitation. Winter river and stream discharges are mainly fed by groundwater and carry little sediment. Winter low flows in the southern Yukon typically occur just before the snow begins to melt in late March (Janowicz, 2008). The spring nival peak normally occurs in early June (Environment Yukon, 2011). During summer, rainfall may also cause peak discharge events, especially in the southwest Yukon where climate systems are strongly influenced by the Pacific Ocean and many ocean-derived storms can deliver large volumes of precipitation inland (Lowey, 2002). In the glacially dominated systems of the southwest Yukon, the annual peak water levels from glacial meltwater typically occur in early to mid August (Environment Yukon, 2011).

For coarse sediments, the available energy for a given discharge is related to a fluvial system's capacity to mobilize a given SSC and grain size. In other words, lower discharges are only capable of transporting a limited sediment load and maximum grain size, whereas higher discharges, such as flood events, have more energy and can transport a more substantial load and larger grain sizes (Knighton, 1998; Marren, 2005). The seasonal and annual variations in discharge energy and the corresponding sediment load are reflected in

lake sediment records, for example larger particles are transported and deposited during higher flow years and flood events. Fine sediments fluxes are controlled by supply, from sources such as land and channel bank erosion and typically are not limited by transport capacity as coarse sediments are.

Before sediment is delivered to lakes, it can be stored in sediment traps located higher in the basin, resulting in a lag in the lake sediment record if remobilization occurs (Hodder et al., 2007). Types of sediment traps include other upstream lakes that cause a decrease in flow and therefore deposit larger particle sizes, alluvial fans, deltas, sandbars and flood plains (Parker et al., 1998; Dirszowsky & Desloges, 2004; Lipowsky, 2006).

3.1.4 Lacustrine Processes

The dispersal of suspended sediment in lakes is influenced by a number of factors. One of interest is the Coriolis Effect, where the currents of all lakes in the northern hemisphere are deflected to the right due to the acceleration generated by rotation of the Earth (Hamblin & Carmack, 1978). Other significant factors include particle size, stratification, inflow, wind and turbidity currents.

3.1.4.1 Stratification

Characterization of lake types requires knowledge of stratification and mixing regimes. Lakes stratify into layers based on temperature and chemistry into the: epilimnion – the surface waters that are generally warmer and less dense, metalimnion – the transition

zone between the surface and bottom water, thermocline – located within the metalimnion and a region of rapid temperature shift, and hypolimnion – the bottom waters that are generally colder and more dense. Lakes are considered isothermal during mixing or when there is continuous mixing and as a result no stratification is observed.

Water column differences are also characterized by dissolved oxygen where regions may be: oxic – containing oxygen, anoxic – oxygen depleted or suboxic – region of low oxygen levels between the oxic and anoxic zones. Beyond this there are various classifications of vertical oxygen distribution, two of note are: orthograde profiles – when oxygen is present throughout the water column and is typical of low productivity lakes or oligotrophic systems, and clinograde – often occurs as a result of bacterial decomposition of organic matter and high algal productivity at some depth within the water column resulting in low oxygen availability in the hypolimnion, typical in more eutrophic systems (Dodson, 2005).

The frequency and mechanism of mixing these layers depends on various lake conditions, such as hydrostatic pressure, hydrology and climate. A previous study monitored the temperature profiles of several Yukon lakes in a summer and winter month and the majority of the lakes were found to be dimictic (Shortreed & Stockner, 1986), indicating they destratify twice a year (Dodson, 2005).

3.1.4.2 River and stream inflow

The differences in density between river and streams flowing into the main body of water in a lake results in three possible flow patterns (where density = ρ): overflow –

hypopycnal ($\rho_{lake}>\rho_{inflow}$), interflow – homopycnal ($\rho_{lake}=\rho_{inflow}$) and underflow – hyperpycnal ($\rho_{lake}<\rho_{inflow}$). The patterns are further dependent on the lake's hydrostatic pressure and temperature stratification (Middleton & Hampton, 1976; Edwards, 1992; Knighton, 1998).

Underflows are one of the principle mechanisms of sediment distribution in proglacial lakes (Chow, 2009). There are two types of underflows that are typical of glacial-fed lakes. First, quasi-continuous flows, where high-density river water flows under the hypolimnon as a bottom current resulting in long-term delivery of fines with intermittent pulses from upper basin activities (Smith & Ashley, 1985). The second is from catastrophic events and mass movements resulting in short-lived surge-type currents that are usually more localized and isolated (Serink, 2004). These two types of flows can be considered turbidity currents or underflows that carry sediment along lake or ocean beds (Chow, 2009).

The ability of turbidity currents to transport the sediment is dependent on temperature, salinity, hydrostatic pressure, current velocity and sediment composition. Any change in these variables can result in sedimentation of material to the lake bottom (Serink, 2004).

3.1.4.3 Wind and currents

Wind also plays a significant role in water-circulation and transporting sediment, though it is difficult to model and understand due to variations in wind strength and direction and the complexity of lake basins (Csanady, 1978). Wind stress primarily influences surface currents and is capable of re-suspending sediments at shallow locations

(Håkanson, 1977). Internal lake oscillations or lake basin-scale waves, called seiches, also contribute to ongoing sediment distribution and lake mixing (Wüest & Lorke, 2003).

3.1.5 Varves

The highly seasonal nature of sediment delivery in proglacial lakes often results in the formation of varves, seasonal layers of sediment deposited over the course of one year in deep-water lakes. Under desirable conditions, annual sediment couplets are formed with one thick light coloured sand/silt (minerogenic) layer derived from the nival peak and summer flows and the second, a thin darker layer of organics and silt/clay (organic-rich layer) accumulated during the autumn and winter (Desloges & Gilbert, 1994; Lamoureux & Bradley, 1996; Slaymaker et al., 2003). Due to their annual nature, varves are commonly used in paleolimnology to gain insight into a lake's environmental history and contemporary bed sediment processes, such as variations induced by climate change (de Geer, 1912; Desloges et al., 2002). However, the sedimentary record may not always reflect the true chronology, as the sediment lamination may not be truly laminar in nature due to post-settlement remobilization, discontinuous sedimentary processes or other interferences that disrupt the varve record (Hodder et al., 2007). To compensate for these potential errors in sediment chronology, other methods of dating, such as isotope dating can be used to verify accuracy.

3.1.6 Lead-210 and Caesium-137 Dating and Sedimentation Rates

Radiometric dating is a common technique used to date various materials such as carbon, oxygen and inorganics based on the comparison between the abundance of a naturally or artificial occurring radioactive isotope to its decay products and their known rates of decay (Olsson, 1986).

The annual laminar deposited sediment in lakes can be dated by measuring the downcore "unsupported" or excess ^{210}Pb isotope activity compared to the surface ^{210}Pb activity that corresponds to the sampling date (Fig 3.1). There are two natural origins of ^{210}Pb, the atmospheric decay of ^{222}Rn (unsupported) and ^{222}Rn production from natural ^{226}Ra within the sediments (supported). The unsupported or excess ^{210}Pb is calculated by subtracting the supported component from the total ^{210}Pb activity within each sediment layer. The dates are then determined by comparing the surface activity to the decayed activity at depth (de Souza et al., 2012).

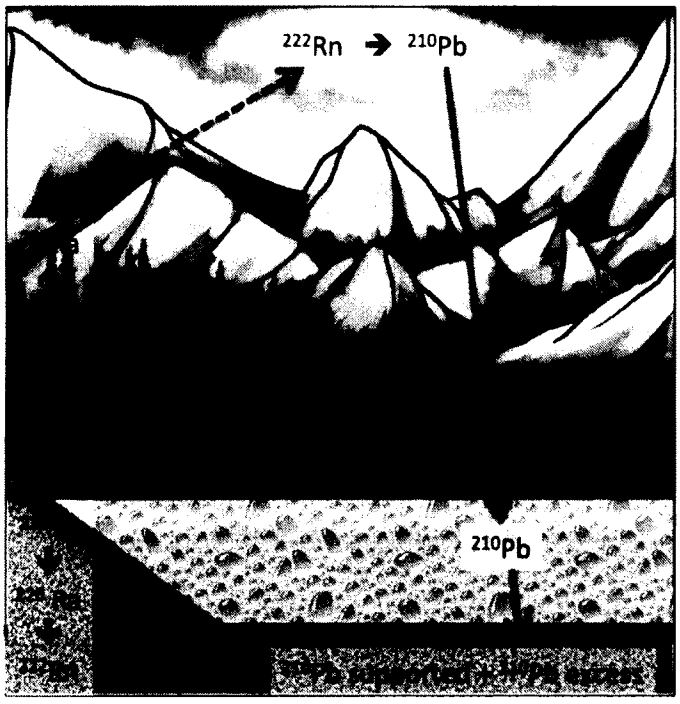

Figure 3.1: Overview of the ^{210}Pb cycle and decay of ^{238}U to supported (sediment) and unsupported (atmospheric) ^{222}Rn decay sources.

The resultant dates can be further confirmed by observing the independent ^{137}Cs peak, which is observed as a result of fall out during thermonuclear weapons testing between 1954 and 1963, the latter corresponding to the time of maximum fallout (Foster et al., 2006; Appleby, 2008). Once the sediment dates are known the sedimentation rate can be calculated as grams of sediment/m^2/year to indicate changes in the rate of sediment delivery to the sample site (de Souza et al., 2012).

3.1.7 Trace Metals

Trace metals profiles are commonly measured in lake sediments to discern an array of sediment and OM processes and mechanisms. They can be used to track sediment from their origin, assess contaminant transportation, heavy metal pollution and enrichment (AMAP, 1998). Once deposited in lakebed sediments, trace metals undergo various transformations depending on the metals reactivity, concentrations of other trace metals, redox conditions, and interactions with OM and sediment. In lakes, trace metals originate from: autochthounous sources from within the lake basin, allochthonous sources from within the local environment but outside the lake basin or anthropogenic sources from environmental pollution due to human activity (such as Hg, V, Cr, Ni, Zn, Cu, Cd and Ag) (Outridge et al., 2005; Heimbürger et al., 2012).

3.1.7.1 Redox Conditions

Trace metals can also be used to approximate redox conditions in downcore sediment profiles without oxygen or pH measurements. Under oxidizing conditions, redox sensitive metals are more soluble and under reducing conditions they are less soluble, which causes enrichment of redox sensitive trace metals during oxygen depletion (Tribovillard et al., 2006). Trace metals known to be redox sensitive include: As, Cu, Fe, Mn, Mo, Ni, Pb, Cd, Co, Cr, V, U and Zn (Boyle, 2001; Audry et al., 2006; Tribovillard et al., 2006; Ye et al., 2013).

One well-documented redox effect on trace metals is the reduction of soluble Fe and Mn oxyhydroxides (Mn or Fe-OH), which scavenge elements such as As, Cd, Cu, Mo, Pb and Zn to Mn/Fe–O^{+} adsorption sites (Boyle, 2001). Reduction of insoluble Fe^{2+} to soluble Fe^{3+} and resultant loss of the hydroxide group at approximately -100 mV – 100 mV, results in a sharp precipitation peak observable in the Fe trace metal profile along with subsequent peaks of previously bound metals (Audry et al., 2006). A similar sequence occurs with Mn at around approximately 100 – 300 mV redox potential. By noting the reduction peaks of Fe and Mn and associated precipitation of scavenged metals, the redox boundaries of the sediments can be hypothesized.

3.2 Methods

3.2.1 Core Sampling

Pat Roach, Contaminants Scientist with Aboriginal Affairs and Northern Development Canada and a team from Dr. Gary Stern's research group at the University of Manitoba collected duplicate 30 cm sediment cores from under ice in March 2010. The samples were collected from bathymetric region IV of Kusawa Lake at 60°15"46', 136°11"39', using a 10 cm diameter KB gravity corer (manufactured by Department of Fisheries and Oceans) (Fig 3.2). On site the first core, Core A, was sub-sectioned into 1 cm intervals from 0-30 cm; the second core, Core B, was sub-sectioned into 0.5 cm intervals from 0-10 cm and 1 cm intervals from 10-30 cm. All sub-sections were stored in Whirlpak bags at ambient temperature (0-10°C). Core B subsamples were shipped to the University of Manitoba in Winnipeg while Core A was stored at -20°C and transferred to UNBC.

In September 2010, Pat Roach collected three sediment grabs via boat using an Ekman grab within the vicinity of the main duplicate cores to increase statistical certainty. Each grab was assumed to reach approximately 7 cm in depth. The three surface grabs were shipped on ice to UNBC and subject to the same tests as Core A.

Figure 3.2: Kusawa Lake core sampling field trip in March 2010 showing the KB gravity corer at the sample site

3.2.2 Aerial Photos

The Government of Yukon's Energy Mines and Resources (EMR) SkyLine Air Photo Locator website (EMR, 2013) was used to determine the location and coverage of aerial photos available for Kusawa Lake, region IV. Photo originals taken in 2007, 1987, 1979, 1972 and 1948 were retrieved from the EMR Library and scanned into TIFF files. To stich the photos into panoramas, AutoPano Giga 3.0 software, developed by Kolor (Kolor SARL, 2013) was used. Final photos were optimized and cropped to highlight any temporal variations in topography, sediment plumes and overall conditions of the lake section. The sample site was identified in each photo by measuring relative distances from select topographic features, such as shoreline and creek outlets.

3.2.3 Limnology

Under ice water measurements for Kusawa bathymetric regions I and III and two locations within region IV near the sample site (IVa) and south of the sample site (IVb), were taken using the Sonde YSI 6000 (YSI Inc., Yellow Springs, OH, USA), which was lowered to depth using an electric winch through an ice auger hole on March 28, 2012 by Pat Roach. Measurements were taken to determine: dissolved oxygen (DO), temperature and pH.

3.2.4 Lead-210 and Caesium-137 Dating and Sedimentation Rate

Isotope analyses of ^{210}Pb and ^{137}Cs were conducted on Core B at the University of Manitoba's Department of Soil Science. Sediments were temporally characterized by depth and sedimentation rates were calculated using the linear and the constant rate of supply model (CRS) (Robbins, 1978). The CRS model assumes that the absolute ^{210}Pb flux rate of the bottom sediments remains constant regardless of background sedimentation, which is a more suitable assumption as compared to other sedimentation models. Caesium-137 activity is measured to verify ^{210}Pb dates in correspondence with nuclear weapons testing from 1954-1963 (Robbins, 1978; Stern et al., 2009). Final dates and trends were compared to the 2005 core taken by Stern et al. (2009) from approximately 700 m west of the current sample location.

3.2.5 Particle Size

Particle size distributions of each Core A sediment increment were measured using the Malvern Mastersizer 3000 (Malvern Instruments Ltd., Malvern, UK) at UNBC. The Mastersizer 3000 determines particle sizes from 0.01-3500 μm by measuring the intensity of light scattered as a laser beam passes through a dispersed particulate sample. Samples were not subject to H_2O_2 digestion or other methods to remove organics. Approximately 1 g of sediment from each subsection was resuspended in 5 mL of distilled water (dH_20) and left to soak overnight. A few drops of the sample solution were added to 120 mL of reverse osmosis dH_20 in the Mastersizer reservoir until ~11% light obscurity was measured. The samples were subject to pulse sonication for 60 s to break-up and prevent floc formations and false measurements of larger particle sizes. Particles sizes were represented using D_{50}, the median diameter grain size, D_{90} and D_{10}, to reflect the size of the 90th and 10th percentile of the grain size distribution respectively. The D_{10}, D_{50} and D_{90} and percent sediment size class were calculated from Udden (1914) and Wentworth (1922) using a semi-automated macro on MS Excel (Microsoft Inc.) called GRADISTAT v.4.0. (Blott, 2000). Changes in down core sediment size were used to identify historic sediment deposition events and to compare with other measured parameters

3.2.6 Trace Metals

Subsamples of Core B were sent to AcmeLabs in Vancouver, B.C. where 0.25 g of sediment sample was subject to four acid digestions in preparation for Inductively Coupled Plasma-Mass Spectrometry (ICP-MS) to determine the concentrations of 60 trace elements. ICP-MS detects sediment metals concentrations by counting the atoms for each element present in the solution (Acme Labs, 2013). The subsamples for Core B were divided into 0.5 cm increments from 0-10 cm and 1 cm increments for the remainder of the core to 30 cm. To allow direct comparison to Core A, which was sliced in 1 cm increments throughout the core, each x.5 and x.0 measurement was averaged to provide one measurement per centimeter. For example, 0-0.5 cm + 0.5-1 cm was averaged to yield the overall 0-1 cm or 0 cm measurement used in analysis. The downcore trace metal distribution trend was analyzed using Principle Components Analysis (PCA) in a variance-covariance cross-products matrix on three axes to discern temporal trends, major historic events and other notable downcore variations. The downcore trend of trace metals with known redox sensitivities were also used to estimate sediment redox boundaries and hypothesize the boundaries of the sediment oxic, suboxic and anoxic zones.

3.3 Results and Discussion

3.3.1 Aerial Photos

It is assumed that all the aerial photos were taken in the late summer (Fig 3.3). Though no specific date was recorded for the 1948 session, informal communication with EMR staff responsible for the Air Photo library confirmed that very few aerial flights have occurred outside of July or August in the Yukon. As well, visual observation of the 1948 photo (Fig 3.3d) indicates similar a sediment plume trend to other years. Photos from both 1972 and 1979 were stitched together to represent the 1970s.

In Chow's study (2009), she suggests that the Kusawa River carries a high sediment load from its upper tributaries of high valley walls and alluvial fans. The river then braids and decreases momentum as it enters Kusawa Lake, resulting in mass settling and sedimentation in bathymetric region V (Figure 2.3). Upper Takhini Lake has been reported to act as an efficient sediment trap (Chow, 2009), though the Upper-most Takhini River continuously delivers sediment to Kusawa Lake. The Upper-most Takhini sub-basin also has the greatest extent of glacial cover and is frequently subject to mass wasting events (Ng & Björnsson, 2003; Gilbert & Desloges, 2005; Chow, 2009). Both of these sediment sources are observed in Figure 3.3, where sediment plumes from both the Kusawa River and Upper Takhini River are observed in all years, varying in their dispersal and turbidity depending on the year and exposure of the photographs.

Observations of the sediment plume and flow patterns in Figure 3.3 show that this narrow, deep valley lake exhibits river-like characteristics. One illustration of this is that the

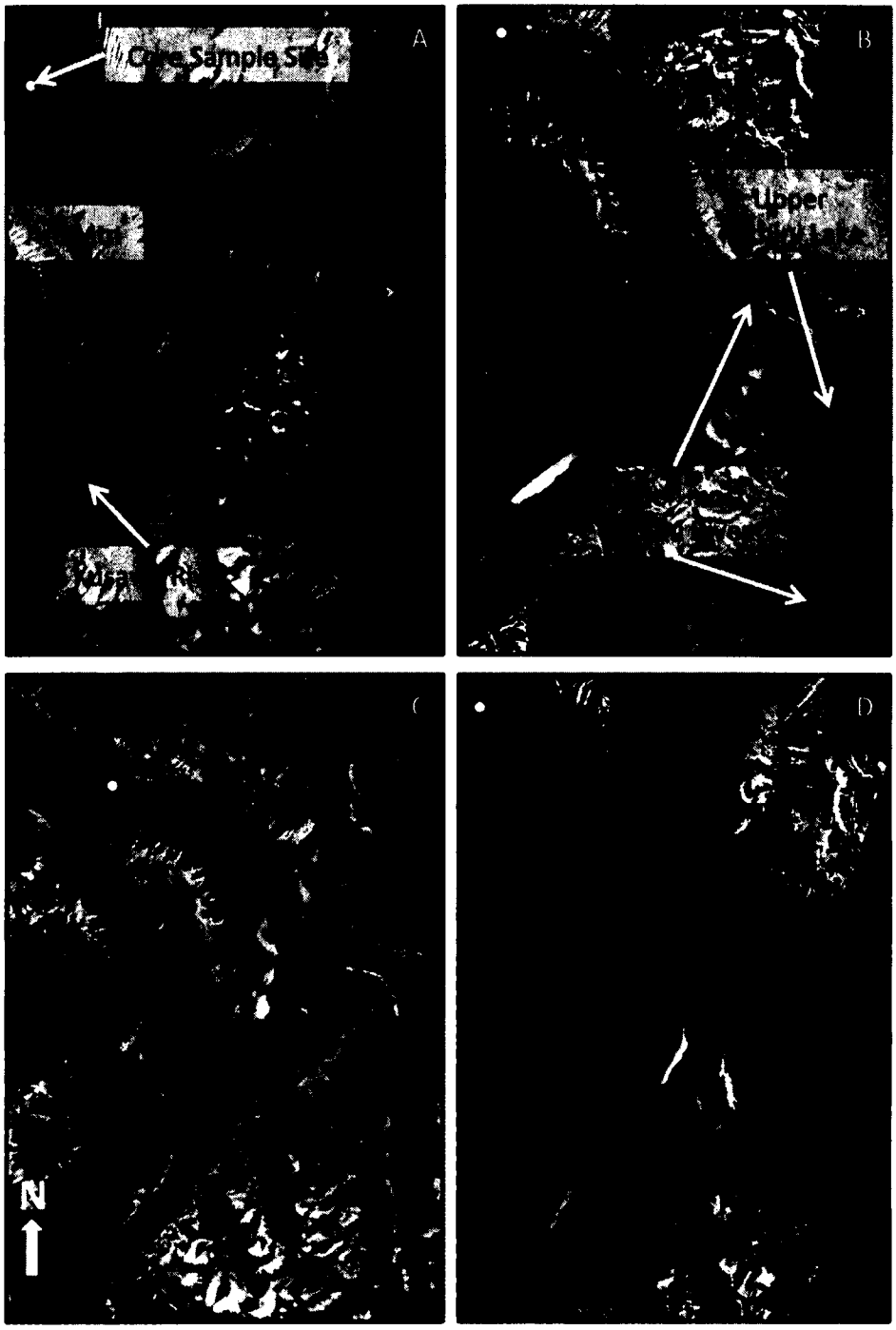

Figure 3.3: Aerial photos taken in, a: August 2007, b: July 1987, c: August 1972/1979, and d: 1948 unknown time of year. The white circle identifies the sample site, located within the sediment plume from the Upper-Takhini and Kusawa Rivers.

highest sediment concentration occurs around the outside edge of the lake bends, which could be considered river-like meanders. This is most evident in the westward turn around Arc Mountain where the sediment is concentrated to the outside eastern shore. The Coriolis Effect may also influence sediment distribution by moving water currents to the right or east in the Northern Hemisphere (Hamblin & Carmack, 1978).

The white dot on each panorama indicates the sample site, which is located within the dispersal path of the sediment plume in each photo. Therefore, the cores collected were subject to ongoing sedimentation from mass wasting, flooding and other events that impact the volume of sediment delivered from the Kusawa and Upper Takhini Rivers. As a result, when interpreting the core sedimentation rates and downcore relations, it cannot be assumed that sediment delivery is constant, although the sample was taken from the deepest region of the lake. A more ideal sample site would have been on the western side of the meander around Arc Mountain, where Stern's et al. (2009) first core in 2005 was collected.

3.3.2 Limnology

The water column temperature, pH and DO were measured under ice for bathymetric regions I, III, IVa (near sample site) and IVb (south of sample site) on March 28, 2012 (Fig 3.4). For regions I, III and IVa there was a thermocline observed at approximately 2.5 m below the water surface (Fig 3.4a). Below 2.5 m the temperature increased gradually

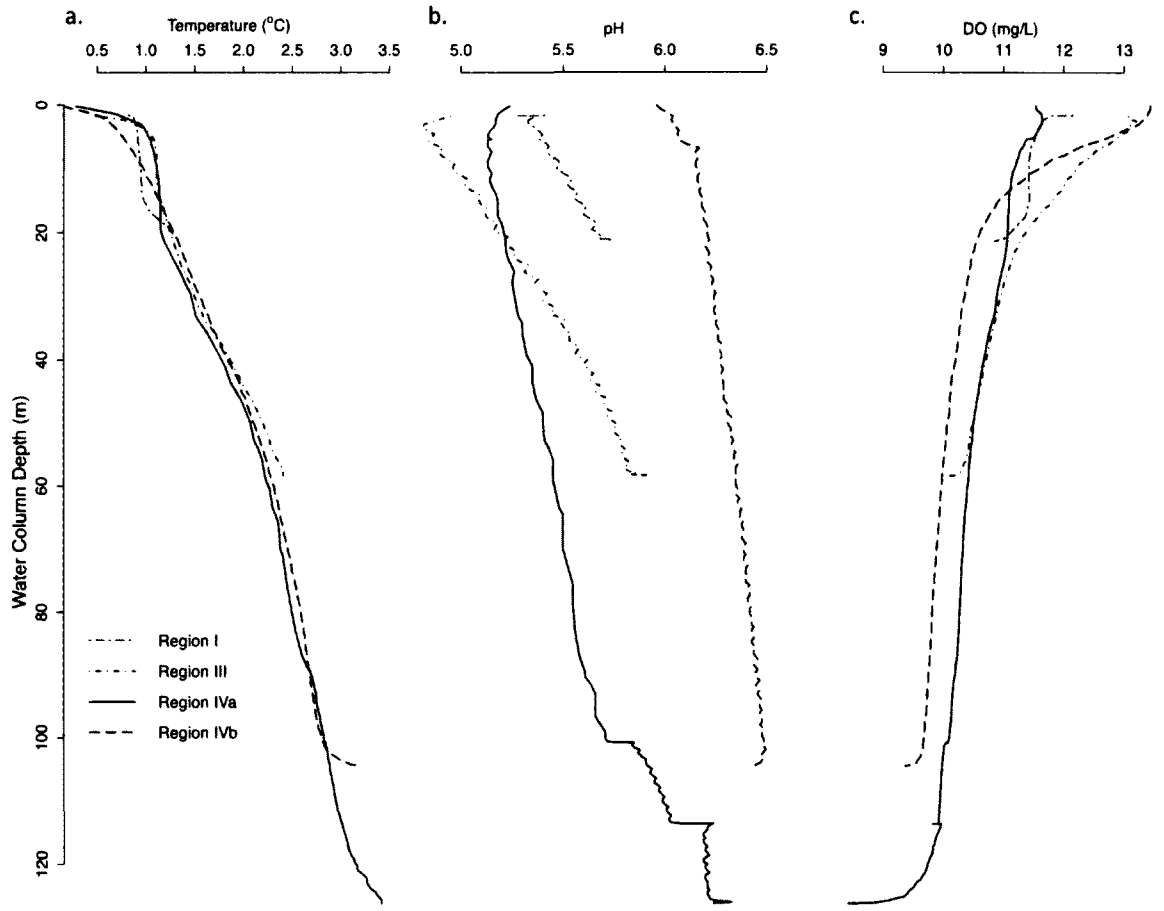

Figure 3.4: Graph of under ice limnology measurements taken on March 29/2012 by P. Roach (unpublished) at four of the five bathymetric regions of Kusawa Lake. The max depth at regions I, III, IV and V are 21 m, 58 m, 126 m and 104 m, respectively (a: temperature; b: pH and c: dissolved oxygen)

to the bottom at each location. The most distinct thermal stratification was observed at region I, the shallowest section of the lake.

The pH profiles were more varied between regions with region III being the most acidic and region V the least (Fig 3.4b). At each site the pH increased gradually with increasing depth but did not exceed 6.5. The most notable trend was a sharp increase in pH at region IVa around depths of 100 m and 112 m. These two distinct shifts may be

indicative of high-density underflow currents that originated from the glacially dominated Upper-Takhini basin. Another possibility is that the bathymetric hole located in region IVa may have a distinct current from the southern overflow, resulting in a shift in pH.

One interesting observation from the limnology measurements is the presence of oxygen throughout the water column in all regions. These orthograde oxygen profiles indicate abundant oxygen availability even in late winter, which suggests oligotrophic conditions. A small decrease in DO is also observed in region IVa around the pH shift at 100 m, further suggesting a separate underflow current and independent cycling in the deep bathymetric hole.

While minimal stratification is observed at near the lake outlet, little to no layering is displayed near the lake head. Chow's (2009) took a similar set of limnology measurements in July 2004, the warmest summer recorded in Yukon history (Environment Canada, 2010). When compared to the 2012 winter measurements used in this study, an inverse trend between summer and winter is observed for temperature. This supports classification of Kusawa Lake as dimictic, indicating that it destratifies twice a year, which is typical of Yukon lakes (Shortreed & Stockner, 1986).

Together, analysis of the sediment plume from the aerial photos along with the summer and winter limnological record suggests that the flow pattern at the head of the lake, and the core sample site, is more fluvial. When the lake current slows before the Takhini River outlet in region I more lake-like characteristics such as distinct thermal stratification are observed.

3.3.3 Lead-210 and Caesium-137 Dating and Sedimentation Rate

3.3.3.1 Lead-210 and Caesium-137 Dating

When initially reviewing the original ^{210}Pb and ^{137}Cs down core profiles (Fig 3.5a) two anomalies were noted: first, if the dating is based on the ^{210}Pb measurements, then the ^{137}Cs peak aligned to 1972, instead of the expected peak in ^{137}Cs fallout in 1963 and second, there was a large dilution event observed at 1925. Aside from the 1925 event, the downcore pattern of excess ^{210}Pb exhibited a consistent linear decrease with accumulated dry weight.

To provide some insight into these two anomalies, the measurements were compared to the core taken in 2005 by Stern et al. (2009) (Fig 3.5a) that was sampled from ~700 m west of the 2010 core site within region IV. The two cores were not directly comparable, as the 2005 core was taken from outside of the major lake current described in section 3.3.2. The 2005 core has a lower linear sedimentation rate of 323 $g/m^2/yr$ (Stern et al., 2009) compared to 518 $g/m^2/yr$ for the 2010 core. As it could not be confirmed whether the ^{210}Pb measurements or ^{137}Cs measurements for the 2010 core were incorrect, a method of relative interpolation was used to provide a reasonable estimate of the sediment dates. Two similar peaks were identified in each profile at the ^{210}Pb dates of 1999/1996 and 1925/1911 for the 2010/2005 cores, respectively. These values were interpolated to calculate new dates, which were anchored at 1963 to reflect the ^{137}Cs peak (Fig 3.5b). In other words, the excess ^{210}Pb profile for the 2010 core was "forced" by the 1963 ^{137}Cs peak. This approach was employed, as the ^{137}Cs peak is considered a more reliable chronological

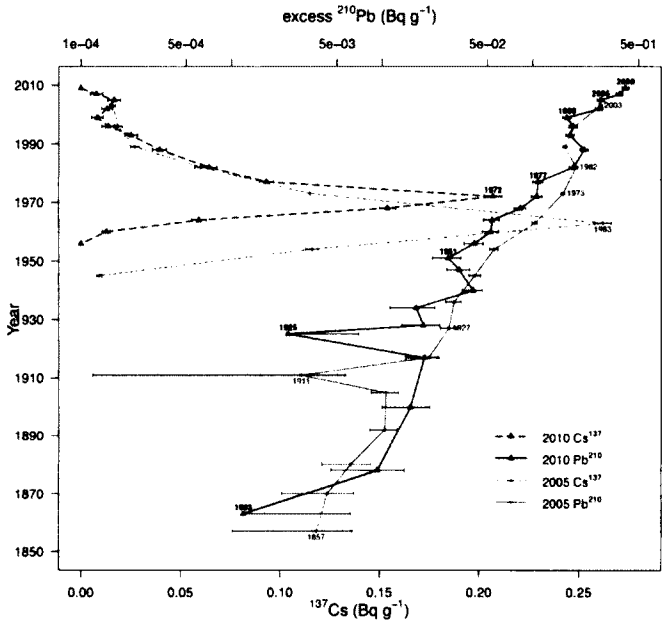

Figure 3.5a: Alignment of 2005 and 2010 ^{137}Cs and ^{210}Pb profiles to compare and interpolate differences. The estimated dates were determined by linear alignment between peaks at 1999/1996, 1972/1964 and 1925/1911 for the 2010/2005 cores, respectively.

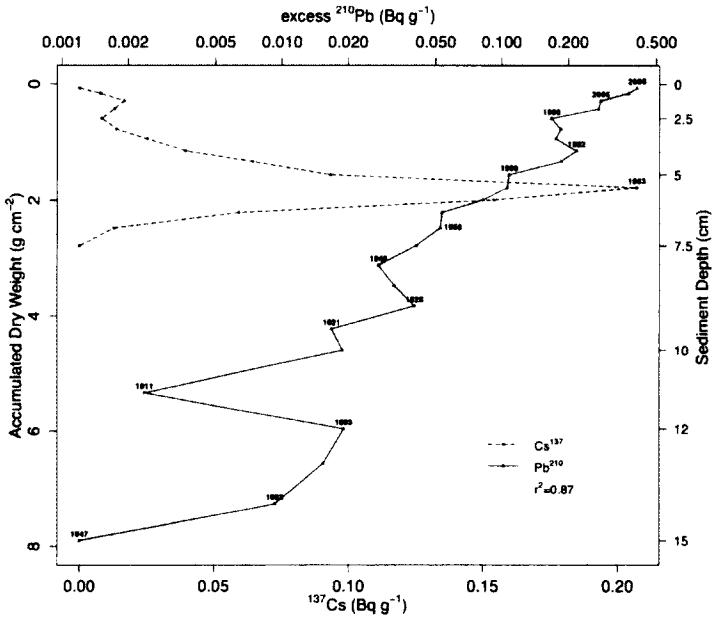

Figure 3.5b: Estimated ^{210}Pb downcore activities anchored to the ^{137}Cs peak at 1963 with accumulated dry weight and depth of sediment. The annual linear sedimentation rate is 0.092 cm/yr.

measure than the excess ^{210}Pb profile (Benoit & Rozan, 2001), especially when dealing with two cores from different sedimentation environments. This new data set does not provide reliable dates, however, given the similarity of the shapes of the two data sets, the downcore trends are considered valid. Correction for focusing and the ^{210}Pb flux for the 2010 ^{210}Pb profile was not calculated. Table 3.1 describes the differences and results for the original and adjusted ^{210}Pb profile along with sedimentation rates, which are discussed in the next section.

Table 3.1: Comparison of calculated year vs. depth and sedimentation rates for the original 2010 ^{210}Pb profile that was adjusted to the 2005 core taken from ~700 m west of the 2010 core.

2010 ^{210}Pb V	^{137}Cs	10 cm dilution	# Years	Avg Linear	Annual Linear
[illegible]	1972	1925	147	[illegible]	[illegible]
Adjusted	1963	1911	162	548 g/m^2/yr	0.092 cm/yr

3.3.3.2 Sedimentation Rate

The sedimentation rate was calculated by:

$$\frac{\text{ADW(g)} / \text{Volume Sediment (m}^3\text{)}}{\text{\# years} / \text{slice (m)}} = \text{Sedimentation Rate (g/m}^2\text{/yr)} \qquad \text{(Equation 3.1)}$$

Where: ADW is Accumulated Dry Weight and volume of sediment is determined using πr^2, (r=radius of corer or diameter/2 = 0.05 m) by thickness of slice and #years are based on the number of years calculated by the ^{210}Pb and ^{137}Cs dating profile per slice thickness. These results are shown in Figure 3.6 plotted against both depth and year. The average linear sedimentation rate was calculated to be 548 ± 47 g/m^2/yr (± SE). The annual linear

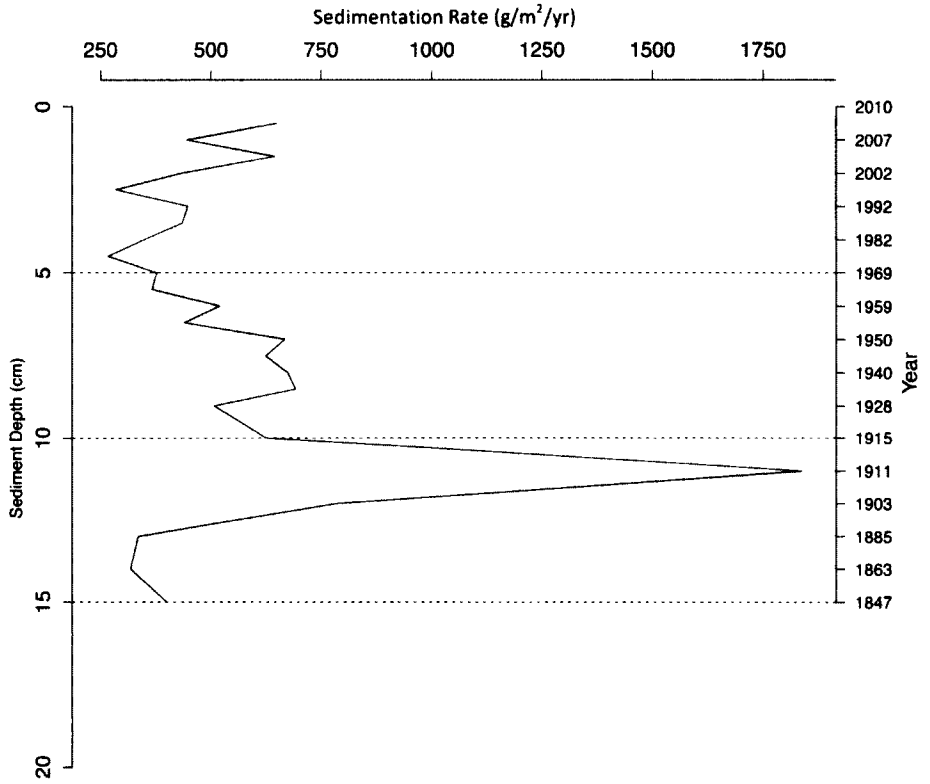

Figure 3.6: Sedimentation rate determined by adjusted ^{210}Pb dating profile and Equation 3.1. Note the anomalous sedimentation event at 1911.

sedimentation rate was determined by the slope of the ADW versus excess ^{210}Pb curve to be 0.092 cm/yr, r^2=0.87 (Fig 3.5b).

3.3.3.3 1911 Sedimentation Anomaly

There is an anomalous sediment delivery event of 1837 g/m^2/yr that occurred in 1911 at 11 cm (Fig 3.6) in the core that is also reflected as a dilution in ^{210}Pb activity (Fig 3.5b). Unfortunately, no historical climate data was recorded at that time period. It can be speculated that some large event such as a flood, jökulhlaup or release of previously damned sediment from moraines, ice or some other mechanical barrier occurred. Prior to

the event the average sedimentation rate was 350 g/m^2/yr and after it was 500 g/m^2/yr. This suggests that a previously unconnected sediment source was activated and increased the annual volume of sediment delivered to region IV. The source is either from the Upper-Takhini River or Kusawa River, as both are glacially moderated, it is difficult to determine which sub-basin the large sediment load originated from.

3.3.4 Particle Size

Overall there is little downcore particle size variability in the core subsamples from 0-30 cm (Table 3.2, Fig 3.7). The particle size is very small with a D_{50} of 3.9 ± 0.087 μm (± SE). These and other grain size measurements are shown in Table 3.2 and depicted in Figure 3.7. The 1911/11 cm sediment event is reflected as a sharp increase in the proportion of clays and medium silts and then a decrease in these fractions at 10 cm. The average D_{10} is 0.70 μm prior to the event and 0.77 μm after. This supports the hypothesis presented in section 3.3.2 that a previously inactive sediment source released a higher concentration of fine sediment to region IV.

Table 3.2: Down core particle size and % average sediment size class distributions.

Particle Size	D_{10} (μm)	D_{50}	D_{90}	Clay (%)	Fine Silt	Med Silt	Fine Sand
[illegible]	[illegible]	[illegible]	[illegible]	[illegible]	[illegible]	[illegible]	[illegible]
Average	0.73	3.90	16.05	28.5	45.5	25.3	0.5
[illegible]	[illegible]	[illegible]	[illegible]	[illegible]	[illegible]	[illegible]	[illegible]
Standard Error	0.012	0.087	0.58	0.004	0.004	0.002	0.0008

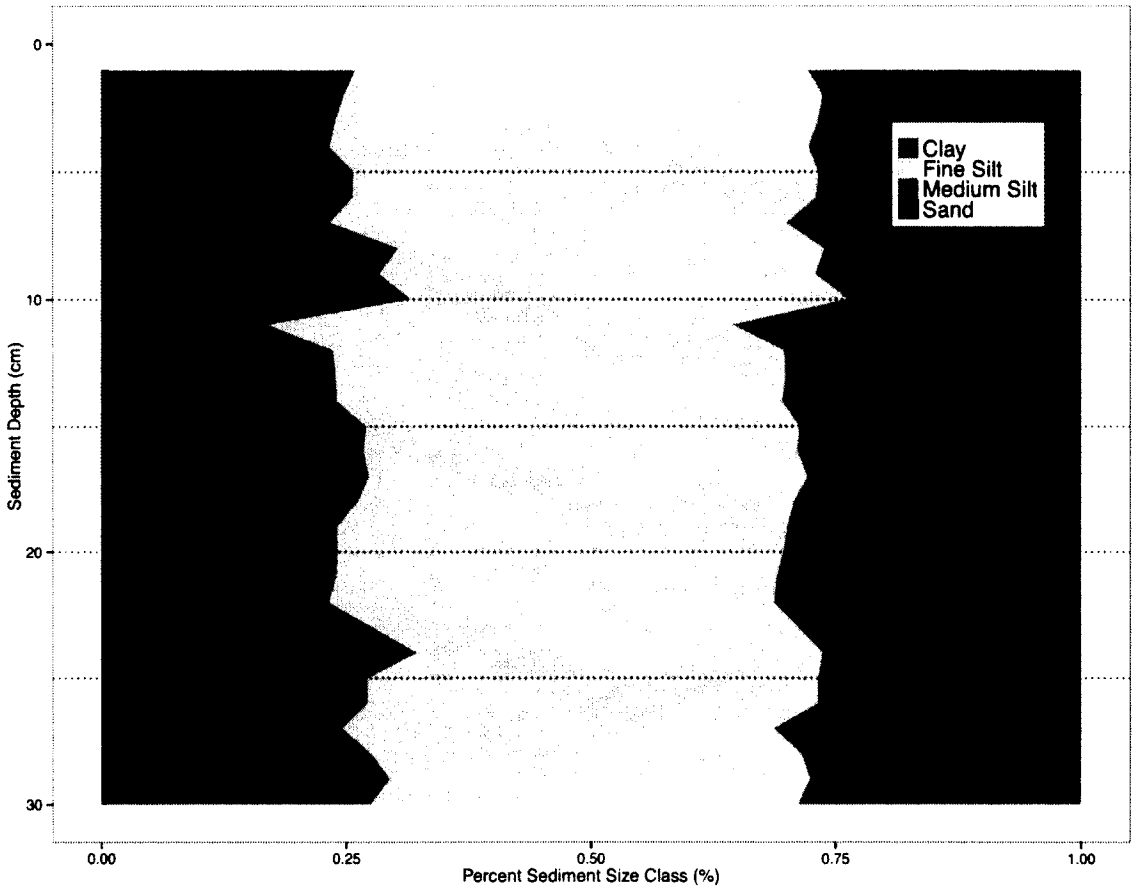

Figure 3.7: Downcore Percent Sediment Size Class (%) variations. Note that the sample consists predominately of clays and silt.

3.3.5 Trace Metals

Of the 60 trace metals analyzed, Au and Re were below the minimum detection limit and the following trace metals displayed little to no down core variation and were not included in any analysis: Be, Lu, Tm, Ho, Tb, S, Se, Eu, Er, Yb and Te. Sulfur (S) was only detected in the top centimeter at 0.045% and was below the limit of detection for the remainder of the core. Full sediment profiles of each detected trace metal are presented in the Appendix.

3.3.5.1 Core Alignment

The trace metal and sediment size profiles were used to align the two 30 cm duplicate cores for cross-core correlation. Core A was subsampled in 1 cm increments and Core B in 0.5 cm increments to 10 cm and 1 cm slices to 30 cm. As the two cores were taken from the same ice hole in March 2010 in succession, they are assumed to have comparable depths and sedimentation rates, though they are not identical. The strong association between sediment size and trace metal concentrations is well documented (Horowitz, 1991; Sutherland, 2000; Outridge et al., 2005; Ye et al., 2013). When sediment size and trace element trends were compared directly, no significant correlations were observed. However, when the surface of Core A was aligned to 1 cm on Core B (therefore, losing the surface measurement for Core B), 41.5% of the trace metal profiles had a significant regression relation with D_{10} ($p<0.05$). This alignment was further confirmed by visual inspection and alignment of similar peaks found on both the trace metal and sediment size profiles. Therefore, all cross-core correlations and regressions used in this study were constructed by aligning Core A at 0 cm to Core B at 1 cm.

3.3.5.2 Trace Metal Distribution

A 3D-PCA was prepared to analyze the overall trace metal distribution and variation by sediment depth (Fig 3.8). While the majority of the depths group together, there are a few notable exceptions. The surface sample at 0 cm divergence is likely due to sediment-water interactions occurring at the bed sediment surface. The samples from 9 cm and 10 cm also separate and are potentially affiliated with the 1911 sedimentation event.

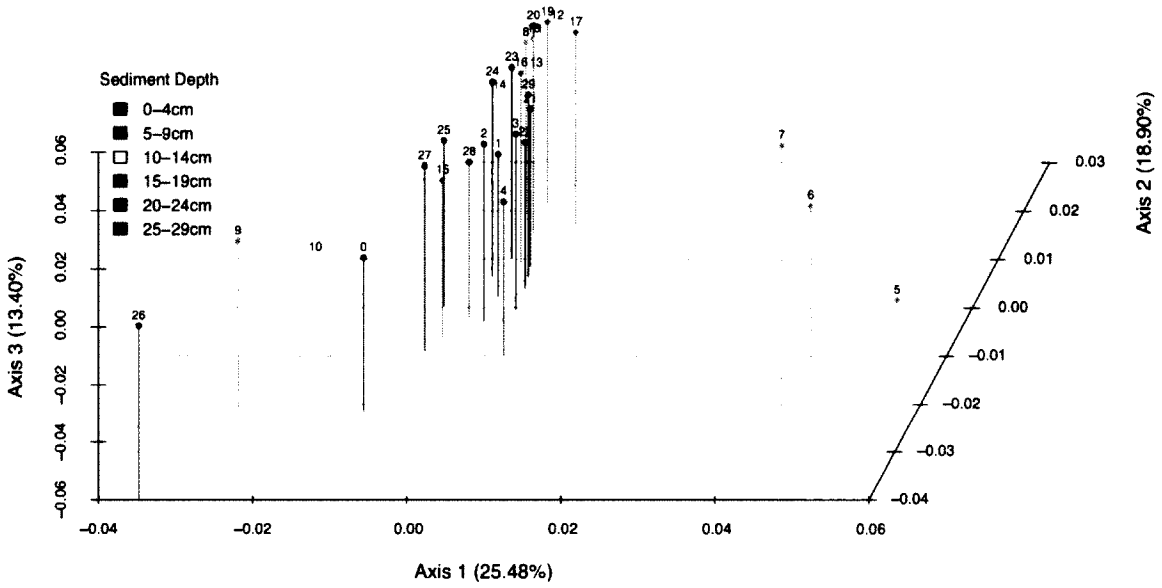

Figure 3.8: PCA analysis of downcore trace metal distribution. Note shift between 5-7 cm, likely associated with enrichment of redox sensitive metals, 9-10 cm, likely associated with the 1911 sedimentation event and 26 cm, likely associated with the White River Ash layer.

One of the more interesting deviations occurs at 26 cm. A small increase in % clay is noted here along with a concurrent decrease in D_{10} at 27 cm. This drastic change in trace metal composition is hypothesized to be the White River Ash (WRA) layer. The WRA is a product of two volcanic eruptions that are estimated to have occurred at 1150 calendar yr BP from Mount Churchill located in the southeast portion of the Wrangell Mountains in Alaska. The resultant ash covered over 340,000 km^2 of eastern Alaska and the southwestern Yukon (Clague et al., 1995). The ash layer is visible along clay cliffs and remembered in local First Nations legends as it resulted in a major displacement of many inhabitants (Workman, 1979, personal communication with local elders). Chakraborty (2010) identified the ash layer at 20 cm in a core taken from Kusawa Lake in region IV. The annual linear sedimentation rate of that core was 0.022 cm/yr, compared with the current

core of 0.092 cm/yr (Chakraborty et al., 2010). The higher rate of sediment delivery to the 2010 core would account for observing the ash layer at a deeper level.

Depths 5-7 cm diverge to the far right of the PCA distribution due to large peaks in Mn, Mo and As at 5, 6 and 7 cm, respectively. When these elements are excluded from the trace metal composition, the samples group with the majority of samples. The peak succession is likely due to changes in redox potential and is discussed in the next section.

3.3.5.3 Redox conditions revealed by trace metal reductions

As no oxygen or sulfur species measurements were taken, trace metal reductions were used to estimate redox potentials and oxygen availability within the sediments. One well-understood oxidation-reduction processes is the reduction of Mn followed by Fe oxides that scavenge metals to the pore water across the oxic-suboxic boundary (Schaller et al., 1997; Audry et al., 2006; Ye et al., 2013). The redox zones were estimated using the Mn and Fe reduction peaks, which occurred at 5.5 cm and 7 cm, respectively. The resultant proposed oxic, suboxic and anoxic boundaries are depicted in Figure 3.9, where the oxic/anoxic boundary is estimated to occur around 9 cm depth. The assumed sigmoidal depletion of oxygen across the suboxic zone and the onset of sulfate reduction in the anoxic zone are also presented for reference. The subsequent Mn and Fe oxyhydroxide scavenging metals released were observed as major enrichment of As, Mo, Cr, Zn and V (Appendix) across the suboxic zone (Boyle, 2001).

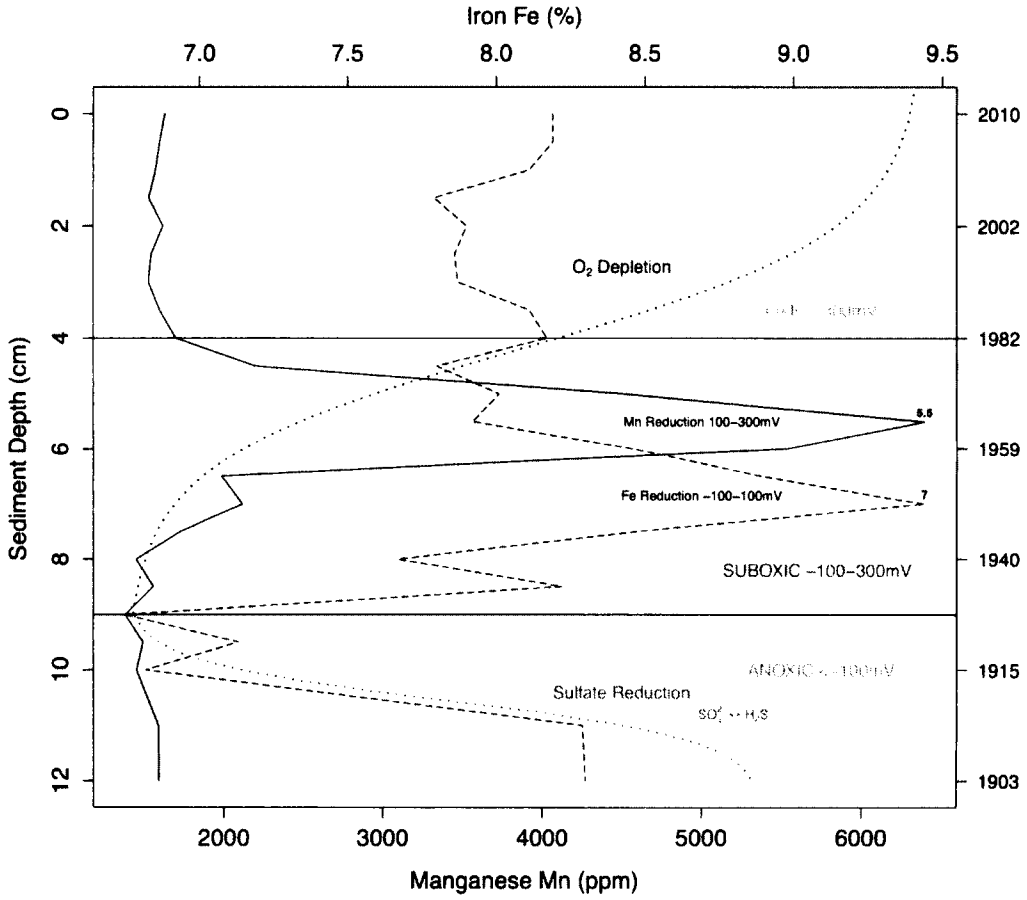

Figure 3.9: Determination of down core redox values based on Mn and Fe reduction at 5.5 cm and 7 cm, respectively. The hypothesized trend in oxygen and hydrogen sulfide levels are shown as dotted sigmoidal lines as suggested by Schaller (1997) and Manceau (1992).

Chapter 4 Rock-Eval Pyrolysis of Organic Matter in Kusawa Lake Sediments

4.1 Introduction

The carbon cycle is one of the most important on the planet as it drives every process necessary for life along with oxygen and hydrogen. Carbon is responsible for joining with other elements to form organic compounds such as lipids, carbohydrates and proteins and accounts for half the dry weight of each cell (Nelson & Cox, 2000). To achieve this organic carbon undergoes several transformations depending on its state and association with other elements (UNH, 2011). Carbon may also be present in inorganic forms, such as charcoal, graphite or coal or as inorganic matter compounds like calcite ($CaCO_3$) and dolomite [$CaMg(CO_3)_2$] (Schumacher, 2001). Organic Matter (OM) is a measure of the compounds that make up dead cells and includes elements carbon, oxygen, hydrogen, nitrogen, phosphorus and other organic and inorganic elements and molecules (Hedges & Keil, 1995).

4.1.1 Sediment-Associated Organic Matter

Within aquatic systems, OM can associate with fine sediments to form flocs and/or aggregates that may become suspended or dissolved and transported downstream with

lake and fluvial currents. This sediment-associated OM then settles out through the lake water column and is deposited at the sediment-water interface of the lake bottom (von Wachenfeldt & Tranvik, 2008). The deposited OM typically originates from either allochthonous, or autochthonous sources (Dodson, 2005). Allochthonous OM includes terrestrial sediments and soils that are introduced to aquatic systems via shoreline erosion, river discharge or more extreme events such as land mass movements. This type of OM consists of forest material, degraded animal matter, humic substances and soil-associated prokaryotes and other primary consumers such as fungi. In aquatic systems, allochthonous OM and sediment also originates from outer basin sources such as incoming rivers and upper basin stream that feed into the lake. Autochthonous OM is derived from primary producers and autotrophs such as algal and bacterial matter that reside in the lake basin and benthic sediment (Brady & Weil, 1996).

All OM found within the sediments can be altered or degraded via microbes, photochemical reactions, biotic alterations to the water column or benthic zone, chemical redox reactions, diagenesis and other reactions (Hedges & Keil, 1995; Carrie et al., 2012). The rate of bacterial degradation is influenced by several factors such as temperature, redox potential, nutrient availability and carbon sources (Staehr et al., 2012). The influence of climate change on primary productivity and bacterial metabolism has been the focus of several studies. Many have observed an increase in algal matter in recent sediment records that is attributed to an increase in primary productivity caused by warmer annual

temperatures (Macdonald et al., 2005; McBean, 2005; Walsh, 2005; Arctic Council, 2007; Outridge et al., 2007; Stern et al., 2009; Van Oostdam et al., 2009; Jiang et al., 2011).

Another product of OM degradation is petroleum hydrocarbons. When OM contained in sedimentary rock is subject to subsurface extreme thermal degradation at constant temperatures between 50°C and 175°C they can produce petroleum molecules. These molecules may then migrate to a reservoir and undergo further alteration to yield economical and retrievable hydrocarbons (Nuñez-Betelu & Baceta, 1994). Several methods and applications have been developed to determine the viability, state, presence and quality of hydrocarbons associated with sedimentary rock formations; these procedures are also relevant in environmental studies that evaluate more recent and less degraded hydrocarbons and carbon compounds.

4.1.2 Organic Matter Applications

There has been great interest in developing methods to determine the amount, source and make up of total organic carbon (TOC) in the environment. Total organic carbon is a measure of the carbon components of OM in water, soils and sediments and other environmental samples (Dodson, 2005). Examples of some of these methods include: loss on ignition (LOI), hydrogen peroxide digestion, isotope markers ($\delta^{13}C$) and chemical or thermal production of CO_2 (Schumacher, 2001; Carrie et al., 2012).

4.1.2.1 Rock-Eval Pyrolysis

Rock-Eval Pyrolysis is an analysis of TOC that was traditionally used to assess economic hydrocarbon potential in sedimentary rock. The technique is based on thermal release of carbon compounds in a two-step process: first, pyrolysis in an inert atmosphere (nitrogen), followed by combustion in an oxic atmosphere (air) (Nuñez-Betelu & Baceta, 1994; Lafargue et al., 1998). This characterizes TOC (wt % of sediment) as either Residual Carbon (RC) or Pyrolysable Carbon (PC). Residual carbon consists of degraded material and humic and detritus (dead organic material) substances that are not readily available for further metabolic processing. Pyrolysable carbon consists of labile material and smaller molecules such as amino acids, fatty acids, vitamins, nucleotides and steroids (Carrie, 2012) and is partitioned into hydrocarbon (HC) containing fractions, S1 and S2, and oxygen containing fractions, $S3CO_2$ and S3CO. In some studies, the S2 fraction is further defined by separation into $S2_{400}$ (detected from 300-400°C during pyrolysis) and $S2_b$ (400-650°C). Carrie et al. (2012) observed that the $S2_{400}$ fraction is likely better suited for assessing the interaction between elements bound to algal-derived organic sulfur compounds and labile OM in sediments and soils (Lafargue et al., 1998; Disnar et al., 2003; Sanei et al., 2005; Carrie et al., 2012). A summary of each of these fractions is outlined in Table 4.1.

Rock-Eval Pyrolysis was originally used to determine the HC ratio of kerogen, the OM portion of sedimentary rock that is used as a measure of petroleum potential in hydrocarbon exploration. Kerogen can be broadly classified using a Van Krevelen Diagram,

Table 4.1: Overview of OM fractions released and measured from Rock-Eval Pyrolosis 6 (version 6) that are measured as TOC per g of dry weight sediment. TOC (Total organic carbon) = PC (pyrolysable carbon) + RC (residual carbon) and PC=S1+S2+S3CO_2+S3CO (Carrie et al., 2012).

TOC	Fraction	Measure	Temperature	Description
PC				
	S1	mg HC g^{-1}	0-300°C	Small (<500 Daltons) volatile and easily degraded molecules such as small sugars and lipids
	$S2_b$	mg HC g^{-1}	400-650°C	More refractory larger kerogen-like biomoecules
	$S3CO_2$	mg CO_2 g^{-1}	100-650°C	CO_2 containing molecules such as carbohydrates, lignins
RC		wt %	650-850°C	Strongly refractory and refractory compounds

a calculated plot that segments the ratio of hydrogen to carbon (H/C) using Rock-Eval measurements (Nuñez-Betelu & Baceta, 1994). This method has been reformed to study more recent sediments and assess the temporal variations in OM as well as its content and origin. More recent OM sources typically have lower H/C ratios, as they are associated with less degraded material (Stern et al., 2009; Sanei et al., 2005 & 2014; Carrie et al., 2012). A study by Carrie (2012) worked towards standardizing the Rock-Eval technique by comparing known amino acid, sugar and lipid compounds, with source matter such as terrestrial and aquatic material and measuring their contribution to each OM fraction.

4.1.2.2 Rock-Eval Pyrolysis and Algal-Derived Organic Matter

Another recent application of the Rock Eval technique is to study the role of algal-scavenging of Hg from the water column to lake sediments in Arctic and Subarctic lakes (Outridge et al., 2007 & 2011; Stern et al., 2009; Sanei, 2005 & 2014). A key finding from these studies is that in many of the lakes the S2 fraction of PC, related to the amount of algal-derived OM found in the sediments, is strongly correlated with the concentration of total Hg (THg). These studies and others (Dirszowsky & Desloges, 2004; Carrie et al., 2009; Hare et al., 2014) have generally observed a recent temporal increase in S2 with correlating Hg taken from northern lake sediments. The hypothesis is that the increase in S2 and THg is due to climate change related increases primary productivity and a corresponding increase in algal Hg-scavenging from the water column, which will be discussed further in Chapter 6.

4.2 Methods

4.2.1 Rock-Eval Pyrolysis

Rock-Eval 6 (Vinci Technologies, France) was used to assess the OM content of a 30 mg sediment subsample of each slice of Core B by Dr. Hamed Sanei and Dr. Jessie Carrie at the University of Manitoba.

To determine the quantity and type of OM present, two heating stages progressing at a rate 25˚C/min are required. The first stage takes place in a pyrolysis oven under inert,

O_2-free conditions (nitrogen) to measure S1 and S2 hydrocarbon pyrolysates (300-650°C) by flame ionization detection. At the same time, online infrared detectors continuously measure the two S3 components (100-650°C), S3CO and $S3CO_2$, which are released due to thermal cracking of oxygen bearing compounds. For the second step, the sample is transferred to an oxidation oven and heated to 850°C to burn off the remaining OM and release the RC fraction. TOC can then be determined by the sum of the total quantity of carbon detected during pyrolysis, PC and oxidation, RC (Nuñez-Betelu & Baceta, 1994; Lafargue et al., 1998). In this study, only the S1, S2 and S3CO fractions of PC and their derivatives, HI and OICO, are considered.

From these components, the Hydrogen Index (HI) and carbon monoxide index (OICO) can be calculated using the following equations (Carrie et al., 2012):

$HI = 100 \times S2/TOC$ (mg HC g^{-1} TOC^{-1}) (Equation 4.1)

$OICO = 100 \times S3CO/TOC$ (mg CO g^{-1} TOC^{-1}) (Equation 4.2)

For comparison with each other the S1, S2 and S3CO measurements were converted to % TOC and % PC. To achieve this, S1 and S2 were multiplied by 0.083, as 83% of the signal is related to C by mass and the conversion of mg/g to wt%, i.e. 0.01. Using the same logic, S3CO was multiplied by 12/280 to determine the amount of carbon in the CO signal (Carrie et al., 2012).

To allow direct comparison to Core A, (sliced in 1 cm intervals throughout) the first 10 cm of Core B (sliced in 0. 5cm intervals) were averaged and aligned as described in Section 3.3.5.1.

4.3 Results and Discussion

4.3.1 TOC, RC and PC Fractions

Due to laboratory error, no measurement was recorded for RC at 4.5 cm; therefore the 4.0-4.5 cm measurement was used to represent the 4-5 cm or 4 cm value for TOC, RC, HI and $OICO_2$, OICO and OIRE6. This is not expected to drastically influence the overall results. A downcore view of the major OM components determined by Rock-Eval Pyrolysis is shown in Figure 4.1.

The amount of TOC (Fig 4.1a) in the sediments was very low at an average of 0.70 ± 0.005 wt% (± SE), indicating the sediments were highly inorganic, as expected in a glacio-lacustrine oligotrophic system. The greatest amount of TOC was observed in the top 5 cm of sediment along with one notable peak at 15 cm. The %RC (Fig 4.1c) was quite high with an average of 77.9% of TOC and made up 0.54 ± 0.003 wt% of the sediments, indicating that majority of the carbon compounds are strongly resistant and refractory (Carrie et al., 2012). Accordingly, the average labile OM or PC (Fig 4.1d) fraction had an average of 22.1% TOC and contributed 0.16 ± 0.001 wt%.

4.3.1.1 S1 and S2

The breakdown of PC components is shown in Figure 4.1 along with their percentages of both TOC and PC in Table 4.2. S1 (Fig 4.1e), being the most labile portion of organic matter, contributes the lowest amount of carbon of all the PC components with a mean of 5.37 ± 0.29 % PC. This is expected as S1 consists of small compounds such as lipids,

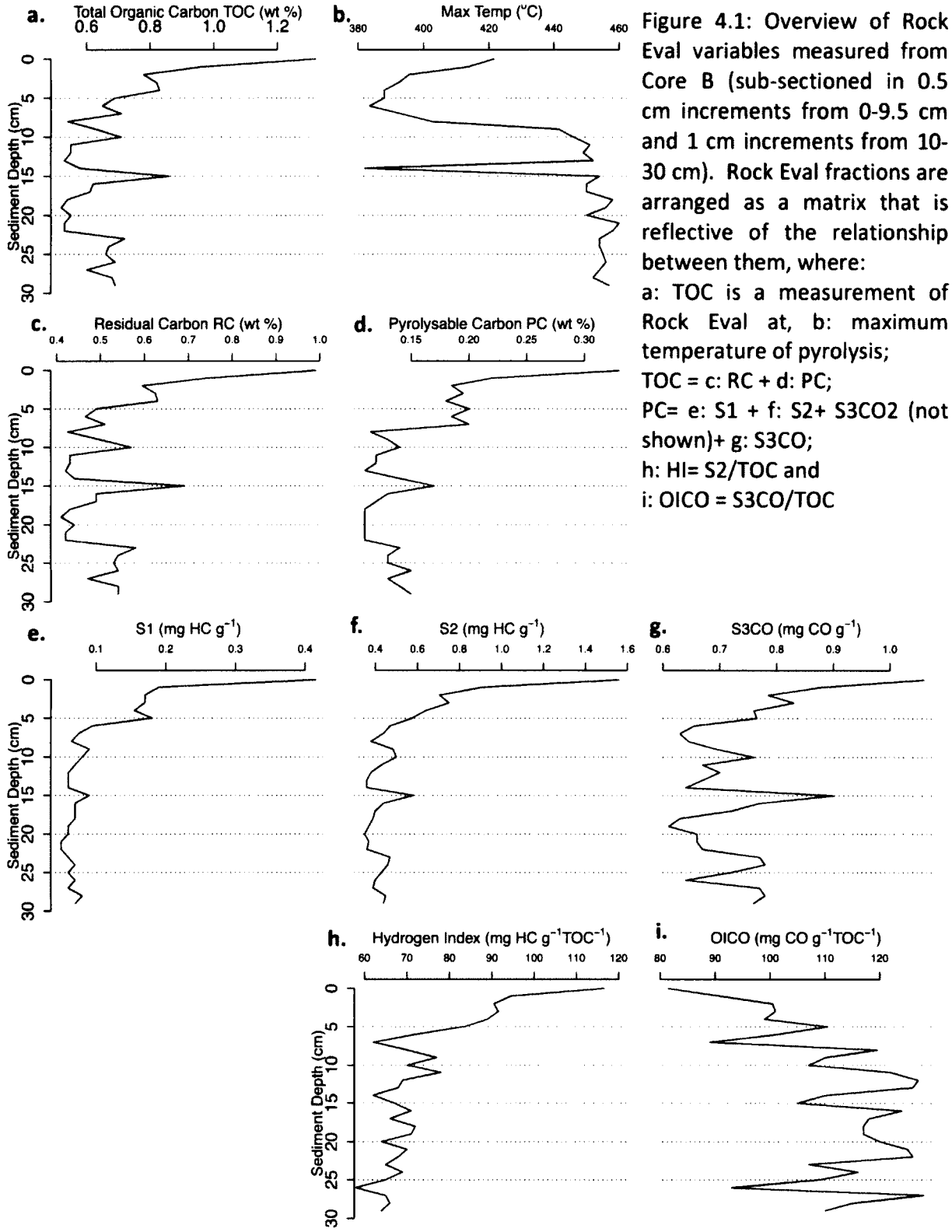

Figure 4.1: Overview of Rock Eval variables measured from Core B (sub-sectioned in 0.5 cm increments from 0-9.5 cm and 1 cm increments from 10-30 cm). Rock Eval fractions are arranged as a matrix that is reflective of the relationship between them, where:
a: TOC is a measurement of Rock Eval at, b: maximum temperature of pyrolysis;
TOC = c: RC + d: PC;
PC= e: S1 + f: S2+ S3CO2 (not shown)+ g: S3CO;
h: HI= S2/TOC and
i: OICO = S3CO/TOC

Table 4.2: Comparison of PC components as percentages of TOC and PC.

Fraction	S1		S2		S3CO	
	TOC	PC	TOC	PC	TOC	PC
Min	0.69	2.64	4.81	16.22	3.16	11.49
	1.83	5.37	6.27	27.84	4.05	20.30
Max	3.12	11.92	10.86	41.50	5.50	26.10
	0.06	0.29	0.18	0.72	0.07	0.65

smaller proteins and sugars that are quickly degraded through various mechanisms (i.e. bacterial degradation) (Stern et al., 2009; Carrie et al., 2012).

The S2 (Fig 4.1f) made up a higher percentage of the HC portion of PC than S1 with a mean of 27.84 ± 0.72% PC. S2 is more stable than S1 and is known to consist of algal-derived lipid cell wall material and some minor inputs from plant material (Carrie et al., 2012). As it is more stable and less prone to bacterial degradation, S2 is considered a better representative of algal-derived OM in the sediments than S1. Similar to S1 and TOC, the largest concentration of S2 is near the sediment-water interface with a 5.5-fold and 3.5-fold post-1950 increase in S1 and S2, respectively. Stern et al.'s (2009) 2005 core observed a 4-fold, post-1950 increase in S1 and S2 HCs that was attributed to an increase in primary productivity related to climate change, specifically the annual temperature increase of 2.14°C since 1970.

Separation of the $S2_{400}$ and $S2_b$ fractions can be visually inferred by comparing S2 to the maximum temperature of pyrolysis (i.e. the temperature at which the S2 signal was detected) (Fig 4.2). There is a distinct separation between the surface layers to 8 cm along with 14 cm that are detected below 400°C and the remainder of the core samples, detected

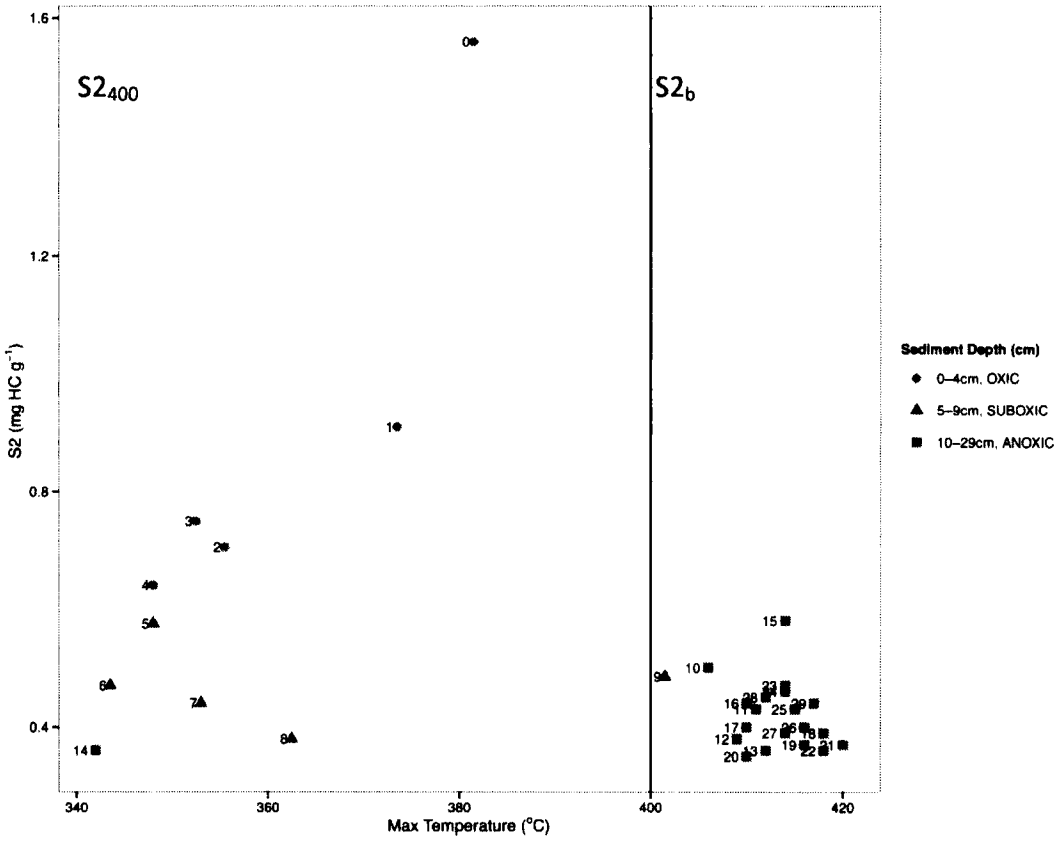

Figure 4.2: Biplot of S2 vs. max temperature, where sediment subsamples that released OM below 400°C are designated $S2_{400}$ and those above 400°C are $S2_b$.

above 400°C. This indicates that 0-8 cm and 14 cm samples are composed of more labile OM and from 9 cm and below (excluding 14 cm) consist of more degraded and processed OM (Disnar et al., 2003; Carrie et al., 2012).

4.3.2 HI versus OICO

A Pseudo Van Krevelen diagram of HI vs. OICO (Fig 4.3) was used to infer between allochthonous and autochthonous sources of OM. Carrie et al. (2012) concluded that

terrigenous and aquatic OM have significantly different HI:OICO ratios for recent sediments. However, they did caution that interpretations of the S3CO measurements are influenced by mineral carbon and therefore decarbonation, which was not completed for this study, is recommended. They also noted that this interpretation is intended for recent, less degraded OM, as the ratio is influenced by the state of degradation. Therefore, it will be assumed that decreasing HI:OICO ratios are related to a higher degree of degradation. In Figure 4.3, there is a downcore degradation trend (indicated by the oval) where all samples have an HI:OICO <1.5, implying that all samples are from a similar source, likely autochthonous aquatic OM. Two exceptions to this are from the 7 cm and 26 cm depths, which are visually considered outliers from the general trend. Note that in this arrangement the 14 cm sample groups as expected, indicating that its divergence is not due to a shift in OICO or HI and it is likely of the same or similar OM origin. At this stage, it is assumed that the 7 cm sample diverges due to the increase in proposed redox activity and the 26 cm outlier can be attributed to the WRA layer. Both occurrences were identified in in Section 3.3.5.2 in the trace metal PCA diagram (Fig. 3.6). Overall, with the exception of 26 cm, it appears that the OM source is consistent and is inherently assumed to be autochthonous aquatic OM with little to no major terrestrial or upper basin input. This is also supported by the relatively stable particle size profile, excluding the 1911 large sedimentation event, which will be addressed in the next section.

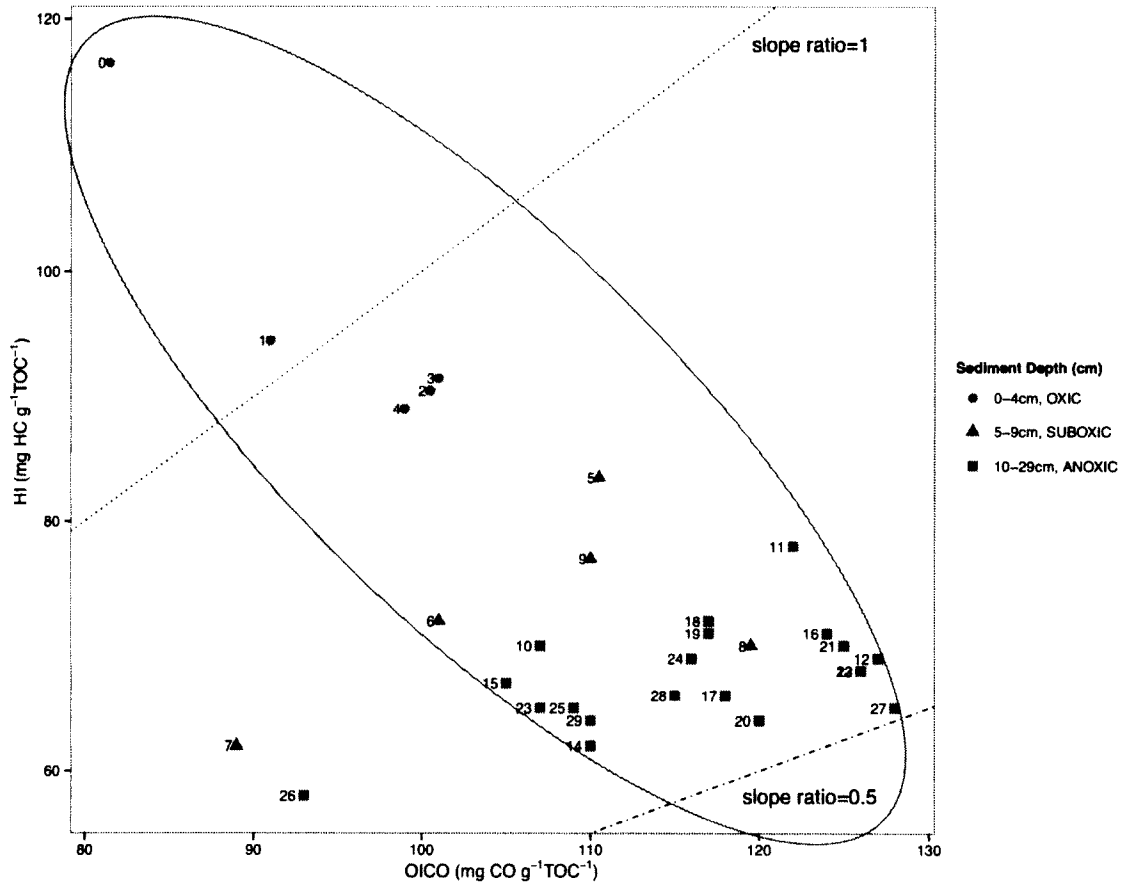

Figure 4.3. Pseudo Van Krevelen diagram of HI vs. OICO. The dotted line is the 1 HI:OICO ratio line and the dot-dash line is the 0.5 HI:OICO ratio line. The oval indicates a negative downcore degradation trend that excludes samples from 7 cm and 26 cm.

4.3.3 Organic Matter and Particle Size

Autochthonous OM in the sediments is presumed to originate in the lake water column and by association with suspended mineral particles from aggregates that ultimately settle to the lake bottom (Dodson, 2005). To further assess OM transport and source, TOC was compared to fine particle content (% particles <3.9 μm) in a bi-plot (Fig 4.4).

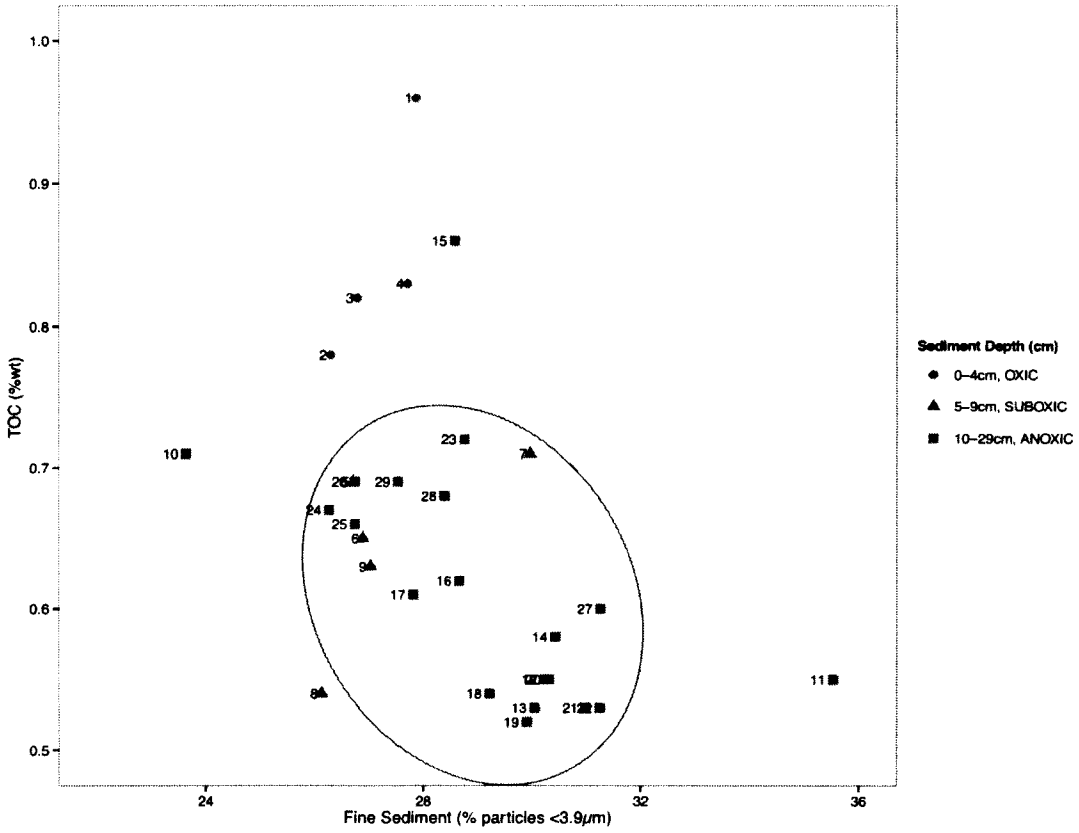

Figure 4.4: Relation between TOC and fine sediment particles (r^2=0.194, p<0.01). The oval displays two visually observed clusters that include sediments from below 12 cm, excluding 15 cm.

The surface sediments to 4 cm and the sample from 15 cm have the highest TOC while the majority remains clustered together as indicated by the oval. The outliers at 10 cm and 11 cm are linked to the 1911 major sedimentation event where the higher proportion of small sized particles at 11 cm are associated with a lower TOC. Overall, the figure suggests that the OM association with small particles is relatively low and constant being between 0.7 and 0.5%, indicating that variable inputs of OM from the watershed are not apparent here but rather the majority of the OM is autochthonous from in-lake sources. This also implies that

settling of this material did not involve OM-mediated aggregation or flocculation and that sedimentation from the watershed does not deliver large amounts of OM to the lake bottom. These findings correspond with the assumption from Figure 4.3 that majority of the OM originates from autochthonous sources and is likely associated with primary productivity and bacterial matter.

One notable discrepancy is the high TOC %wt at 15 cm core depth. Within the assessed OM profiles a 15 cm sample peak is observed in all measurements except S1, the most labile and easily degraded OM fraction. Figure 4.4 also indicates that there are no obvious allochthonous inputs to the core with the exception of the WRA layer at 26 cm depth, making it likely that the sediments at 14-15 cm contain some unknown labile authochthonous OM accumulation.

4.4 Summary of Rock-Eval Pyrolysis

Evaluation of the sediment core using Rock-Eval Pyrolysis 6 suggests that the OM is predominately from autochthonous limnetic sources. The surface sediments from 0-4 cm are associated with recently deposited labile OM and sediment associated OM found below 9 cm in the anoxic zone is largely refractory with the exception of some unknown possibly labile OM accumulation at 14-15 cm depth. Finally, the WRA layer was identified as an allochthonous OM source observed at 26 cm depth.

Chapter 5 Total Bacteria and Sulfur Metabolizing Bacteria in Kusawa Lake Sediments

5.1 Introduction

5.1.1 Review of Bacterial Metabolism

Bacteria are capable of using several different compounds and molecules for their metabolism. How each microorganism generates energy is dependent on oxygen availability and what molecule it uses as its source of electrons. In aerobic respiration, oxygen is used as the terminal electron acceptor, while in anaerobic respiration a compound other than oxygen such as nitrate (NO_3^-) or sulfate (SO_4^{2-}) is used. Heterotrophic bacteria are capable of using a variety of inorganic and organic electron acceptors under either oxic or anoxic conditions for their metabolism. While, obligate or facultative aerobes require high or limited levels of oxygen and conversely obligate or facultative anaerobes require strictly anoxic or tolerate suboxic conditions, respectively.

Within lake sediments the mode of bacterial respiration is primarily driven by sediment depth, oxygen availability and redox potential (Fig 5.1). This relates to downcore microbial mediated OM degradation and the corresponding available electron acceptors and donors. First, large labile OM macromolecules are deposited at the sediment-water interface and subject to microbial aerobic respiration and hydrolysis within the oxic and

suboxic zones. These marcromolecules are broken down into OM monomers such as nucleic acids, sugars and amino acids. As oxygen is depleted through the suboxic zone, the molecules are fermented to produce carboxyl groups, such as lactate and propionate and used as substrates by microbes in the suboxic and anoxic sediments. The final OM breakdown of carbon takes place in the strictly anoxic lower sediments where CO_2 is reduced to either methane (methanogenesis) or acetate (acetogenesis) and carbon mineralization may occur (Jørgensen, 2000; Madigan et al., 2003).

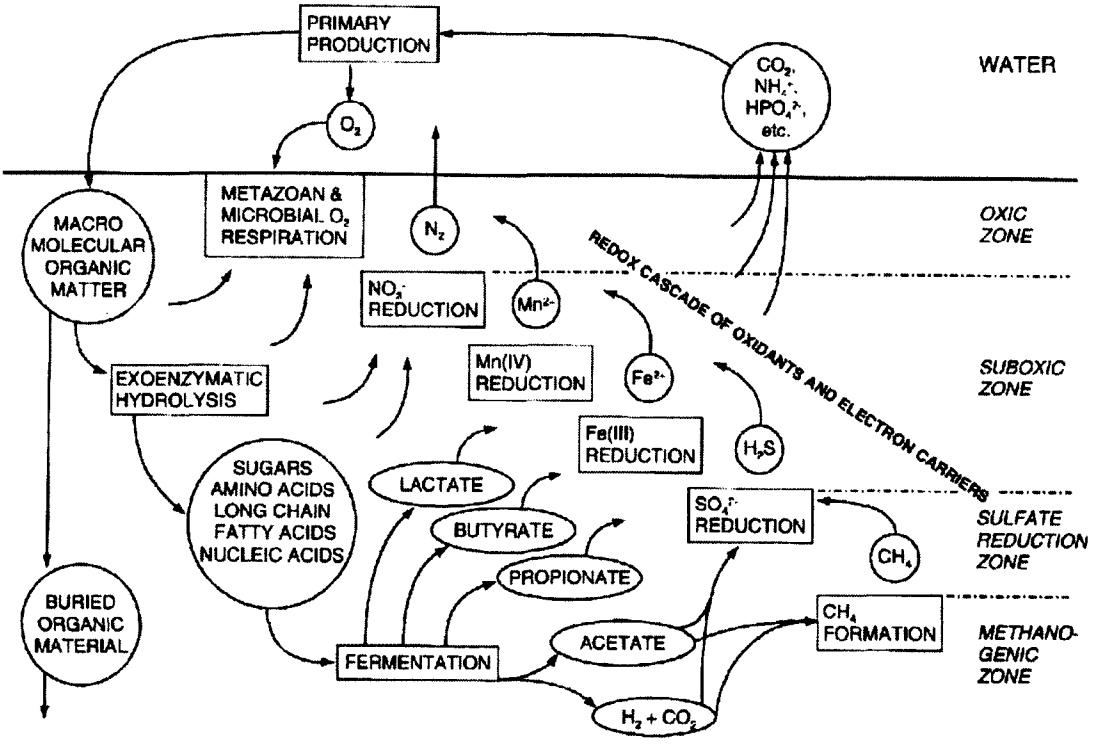

Figure 5.1: Schematic microbial processing of organic matter in lakes sediments and the associated reduction pathways and resultant products of various modes of metabolism. From Jørgensen (2000).

5.1.2 Sulfur-Metabolizing Bacteria

There has been extensive study on sulfur-metabolizing prokaryotes from both Bacteria and Archaea. Sulfur-Metabolizing Bacteria (SMB) are studied for their metabolic diversity, environmental ubiquity and usefulness in biotechnology applications such as soil remediation, metal precipitation and wastewater treatment (Muyzer & Stams, 2008). They are one of the key groups of organisms that drive the global sulfur cycle and also play a significant role in the cycling of carbon, nitrogen and various metals (Barton & Hamilton, 2007).

5.1.2.1 Sulfur Origin

In freshwater environments, elemental sulfur (S_0) originates from autochthonous bacterial storage of sulfur globules, allochthonous weathered rocks, terrestrial OM, wildfire and volcanic ash and anthropogenic sources such as fossil fuels, wastewater discharge, long range atmospheric transfer and acid mine drainage (Holmer & Storkholm, 2001). In oligotrophic lake sediments, the overall level of sulfate, the most oxidized form of sulfur, is typically <300mM, while it can occur at 700-800 mM in some eutrophic lakes (Pester et al., 2012). Within low productivity lake sediments, autochthonous sulfur-species and compounds generally originate from organic sulfur compounds, such as the proteins of aquatic organisms (Holmer & Storkholm, 2001).

5.1.2.2 Sulfur Cycling

Sulfur-metabolizing bacteria (SMB) are capable of either the reduction or oxidation of various inorganic chemicals such as iron, nitrogen, hydrogen and phosphorus, however they are most recognized for their role in sulfur cycling. Sulfur is typically involved in redox processes (Norici et al., 2005) with an overview of the redox couples involved in the sulfur-reduction pathway are show in Table 5.1.

Redox Couple	$E^{0'}$ (mV)
[illegible]	[illegible]
$S_2O_3^{2-} + 2e^- \rightarrow SO_3^- + H_2S$	-402
[illegible]	[illegible]
$SO_4^{2-} + 8e^- \rightarrow H_2S$	-217
[illegible]	[illegible]

Table 5.1: Overview of redox potentials $E^{0'}$ of reduction intermediates of the sulfate reduction cycle, where $E^{0'}$ are at pH 7 (Thauer et al., 2007).

To utilize sulfur, SMB employ a suite of enzymes that catalyze either the oxidation from hydrogen sulfide to sulfate or the reduction in reverse. The different species of SMB and their mode of respiration are discussed in the next section. SMB use four primary protein clusters to drive sulfur metabolism (Fig 5.2). The first three are located in the cytoplasm and utilize sulfite as an intermediate as follows: (i) the first reaction in the reduction pathway is catalyzed by sulfate adenylyltransferase (SAT) for $SO_4^{2-} \leftrightarrow$adenosine 5'-phosphosulfate (APS); (ii) APS reductase (Apr complex) catalyzes APS$\leftrightarrow SO_3^-$; (iii) and the final reaction is facilitated by dissimilatory sulfite reducatase (Dsr complex) for $SO_3^- \leftrightarrow H_2S$. The fourth protein is located in the periplasm, where sulfur and thiosulfate are oxidized to sulfite using the SOX protein complex that converts $S_0 \leftrightarrow S_2O_3^{2-} \leftrightarrow SO_4^{2-}$ (Madigan et al., 2003; Muyzer & Stams, 2008; Hokenbrink et al., 2011; Stewart et al., 2011).

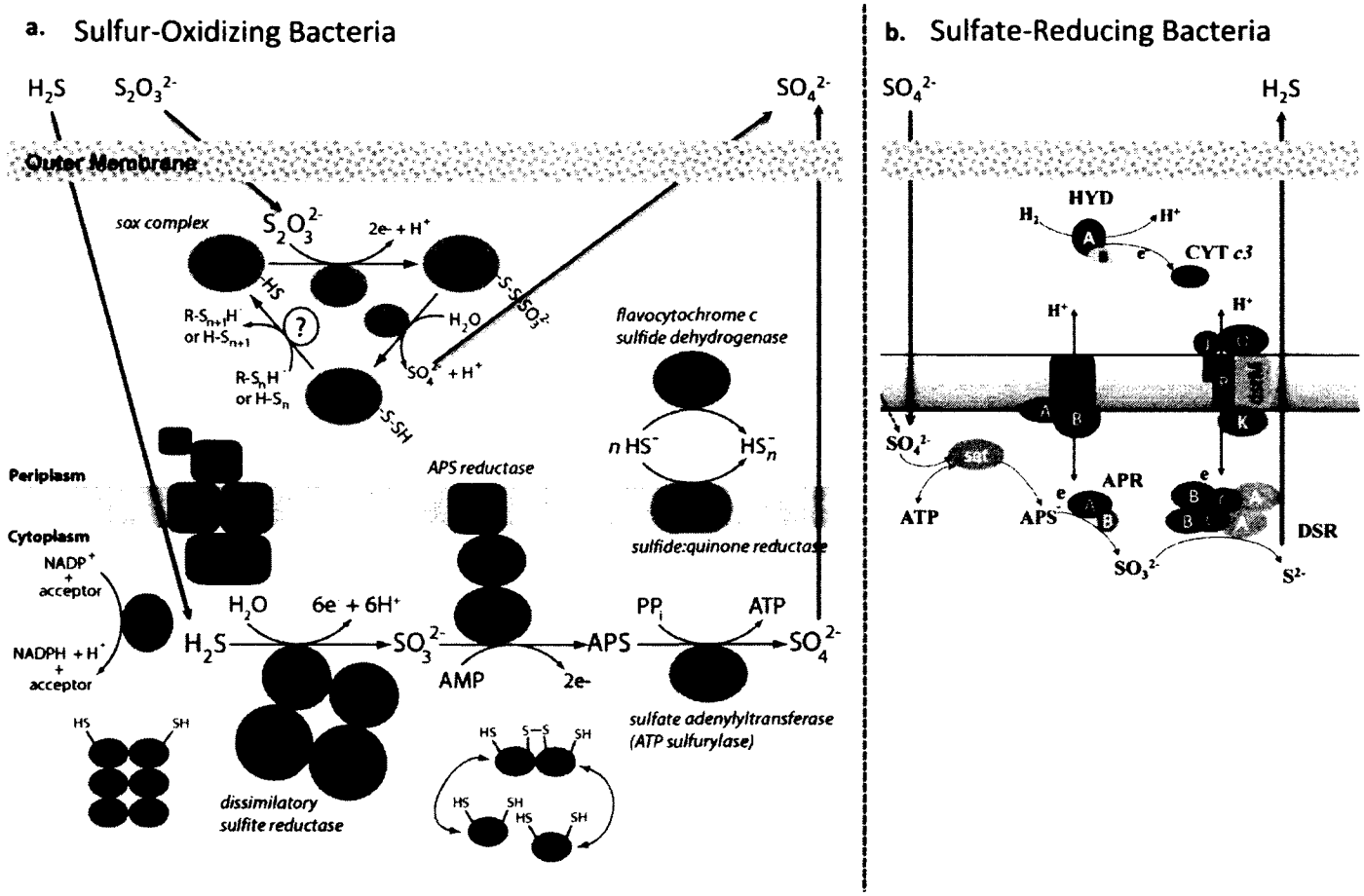

Figure 5.2: Generalized overview of the SMB enzyme pathway for sulfate reduction and sulfide oxidation. a: Sulfur-Oxidizing Bacteria (SOB) that take up H_2S or $S_2O_3^{2-}$ as an electron donor to produce SO_4^{2-} through the *Dsr/Apr/SAT* or *Sox* pathways, respectively (adapted from Stewart et al., 2011; Gregerson et al., 2011); b: Sulfate-Reducing Bacteria (SRB) take up extracellular SO_4^{2-} and reduce it to H_2S through the *SAT/Apr/Dsr* pathway to produce SO_4^{2-} that is excreted (adapted from Cao et al., 2014).

5.1.2.3 Organic Matter Metabolism

In highly active environments, such as shallow marine systems, SMB can contribute to more than 50% of organic carbon mineralization (Jørgensen, 2000). They can be broadly categorized into five groups based on their carbon metabolism and preferred electron acceptor or donor: (i) phototrophic sulfur-oxidizing bacteria; (ii) sulfur-oxidizing bacteria (SOB); (iii) sulfur(S_0)-reducing bacteria (SB); (iv) sulfate-reducing bacteria (SRB) and (v) organic sulfur utilizing bacteria (Giovannoni & Stingl, 2005; Sievert et al., 2007). A general overview of sulfur-based reactions coupled with OM breakdown is depicted in Figure 5.3 (Zhou et al., 2011; Pester et al., 2012).

Anoxygenic photosynthetic Purple Sulfur Bacteria (PSB) and Green Sulfur Bacteria (GSB) contain highly efficient bacteriochlorophylls that drive photosynthetic growth and require very little light. Manske et al. (2005) successfully cultured GSB from a depth of 100 m in the Black Sea where only 0.00075 μmol quanta m^{-2} s^{-1} of light was measured, the lowest reported values for photosynthetic growth at that time. Cold and low light adapted photosynthetic proteins have also been described for a strain of GSB isolated from an Antarctic Lake (Ng et al., 2010). Phototrophic SMB use H_2S as an electron donor for CO_2 fixation and store globules of elemental sulfur that are eventually oxidized to produce SO_4^{2-}. They can also use $S_2O_3^{2-}$ or Fe^{2+} as an electron donor instead of H_2S. One notable difference between PSB and GSB is that the elemental S_0 globules produced by GSB are stored outside of the cell, whereas PSB store them intracellularly (Madigan et al., 2003; Dahl et al., 2005; Hokenbrink et al., 2011).

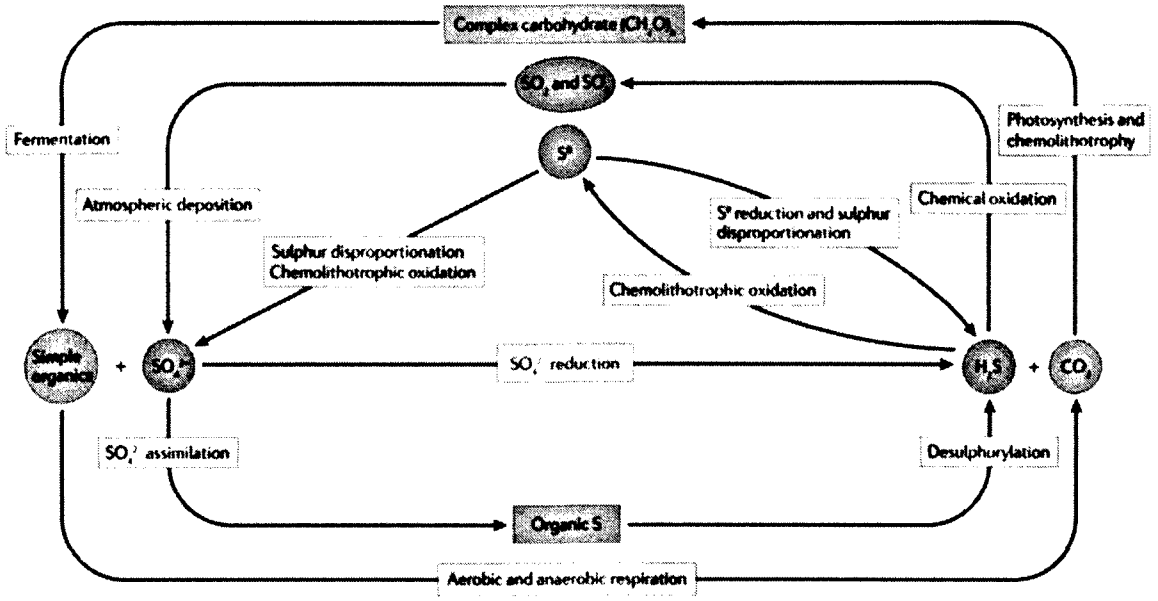

Figure 5.3: Schematic of the role of SMB in the carbon and sulfur cycle to provide an overview of coupling mechanism of using sulfate as an electron acceptor to degrade fermented organic matter (i.e. simple sugars such as lactate) to produce hydrogen sulfide and either CO_2 or acetate. Figure from Zhou (2011).

Chemolithotrophic SOB oxidize a broad array of reduced inorganic sulfur-compounds such as S_0 and H_2S via the *Dsr* and *Sox* enzymes or the reverse sulfate-reduction pathways to produce SO_4^{2-} and H^+. While the majority of these species are aerobic there are also facultative and obligate anaerobes that oxidize sulfur and are commonly found in hydrothermal vents or hot springs (Ruby, 1981; Madigan et al., 2003). SOB can use an array of carbon substrates, though it appears most are autotrophic and therefore, only consume CO_2 (Cypionka, 2000).

Sulfate-reducing bacteria (SRB) are facultative and obligate anaerobes that reduce SO_4^{2-} to H_2S and can be divided into two groups based on their completeness of carbon breakdown. The first group degrades carbon compounds to acetate and the second

completely oxidizes to carbon dioxide. Common SRB substrates include H_2, acetate, fermentation products (i.e. succinate, malate, lactate, pyruvate and formate), aromatics (i.e. toluene and benzene) and alcohols, particularly ethanol and propanol. Several species that completely oxidize carbon compounds to CO_2 use fatty acids as electron donors, and are also capable of autotrophic growth using H_2 as their electron source. Under both regimes, produced H_2S is either assimilated and converted to amino acids or dissimilated and excreted from the cell (Madigan et al., 2003).

Many SRB are found in oxic environments and are presumed to still be utilizing the sulfate-reduction pathway, though this mechanism is poorly understood (Sass & Cypionka, 2007). Some SRB are capable of using oxygen as an electron acceptor though it does not sustain growth and can lead to the production of oxygen radicals along with increased pH, which in turn is toxic. This suggests that it is not the oxygen itself the SRB are sensitive to but the products of its metabolism (Cypionka, 2000). Several mechanisms have been proposed to describe how SRB cope with oxygen stress in sediments: (i) they utilize various enzymes that detoxify oxygen radicals (Cypionka, 2000); (ii) they form cell aggregates with anoxic interiors (Sass et al., 1998); (iii) they migrate diurnally to avoid high oxygen concentrations produced by photosynthetic organisms during the day (Krekeler et al., 1998) or (iv) they employ a mechanism called aerotaxis, where several cells migrate to some oxygen threshold with an adequate substrate supply and remove oxygen to restore anoxic conditions (Cypionka, 2000).

Sulfur (S_0)-reducing bacteria (SB) are unable to reduce sulfate to sulfide ($SO_4^{2-} \rightarrow H_2S$) but they can reduce elemental sulfur to sulfide and therefore live in syntrophy (shared use of metabolic products between various bacterial species) with bacteria that oxidize $H_2S \rightarrow S_0$ (Madigan et al., 2003; Stahl et al., 2007).

Under extreme anoxic conditions found much deeper in the sediments, methanogenesis and acetogenesis occurs. Here, autotrophic SRB compete with methanogens and acetogens for CO_2, as majority of the bacteria present are autotrophs that use H_2 as an electron donor and CO_2 as their electron acceptor (Madigan et al., 2003; Thauer et al., 2007).

5.1.2.4 Sulfur cycling in Oligotrophic Lakes

Under low sulfate conditions, such as in oligotrophic lakes, sulfate levels are typically below 1 mM and SMB sustains growth by continuously cycling H_2S to SO_4^{2-} across oxic/anoxic interfaces within the sediment or water column. As a result, SMB communities support each other where SOB and phototrophic bacteria provide SO_4^{2-} for SRB and SB, which in turn provide S_0 and H_2S for oxidation. For this reason, many SRB are found near the oxic/anoxic interface. As a consequence, in low sulfate environments, growth of SMB populations is restricted by the concentration of metabolically available sulfur compounds. (Holmer & Storkholm, 2001; Thauer et al., 2007).

5.1.2.5 Metal Ion Metabolism

In aquatic systems, SRB interact with various metals to influence their speciation, solubility and mobility. This is driven by a unique metal interaction with sulfides to produce bioprecipitated metal-sulfides, a phenomenon that is applied in biotechnical methods to remove metals from wastewater, such as acid mine-drainage runoff. Common metals that bind with sulfide include Cd, Co, Cu, Fe, Mn, Hg, Ni and Zn (Hockin & Gadd, 2007).

SRB are also capable of using Fe(III) and Mn(IV) as terminal electron acceptors instead of sulfate under anaerobic conditions and play an important role in the redox cycling of Fe^{2+}/Fe^{3+} and Mn^{2+}/Mn^{4+} across the oxic/anoxic interface. One hypothesis is that reduced sulfide can be re-oxidized to sulfate by coupling and stabilizing with Mn and Fe-oxides in the suboxic transition zone (Thamdrup et al., 1994; Thauer et al., 2007).

5.1.2.6 Phylogeny

An overview of the diversity and metabolic preferences of SMB and their distribution within 11 of the 21 phyla of the Domain Bacteria is shown in Figure 5.4. Traditionally the 16S rDNA gene was used to detect unculturable SMB until degenerate primers were designed to target *AprA*, the alpha subunit of APS reductase and *DsrAB*, the alpha and beta subunits of the dissimilatory sulfite reductase enzyme complex (Wager et al., 1998; Klein et al., 2001; Leloup et al., 2009). Both *Apr* and *Dsr* gene targets recover representatives from almost all SMB lineages (Wagner et al., 1998; Klein et al., 2001; Loy et al., 2004; Stahl et al., 2007), although some SMB may not contain *AprA* and/or *DsrAB* if sulfur cycling occurs via

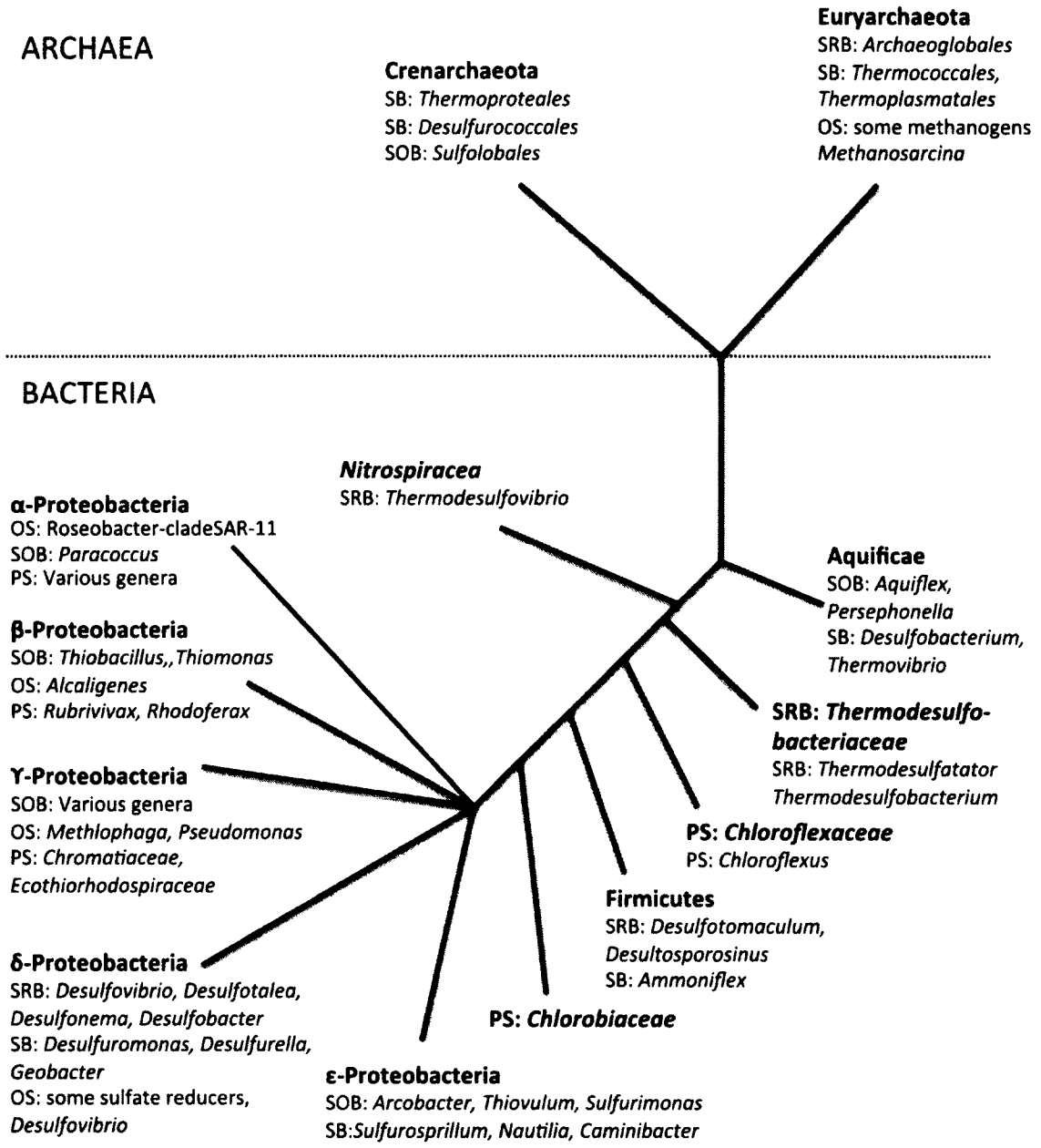

Figure 5.4: General representation of phylogenetic tree that depicts the broad diversity sulfur-metabolizing bacteria and archaea and their major phylogenetic lineages and method of sulfur metabolism. PS: Phototrophic Sulfur Bacteria; SOB: Sulfur-Oxidizing Bacteria and Archaea; SB: Sulfur (S_0)-Reducing Bacteria and Archaea; SRB: Sulfate-Reducing Bacteria and Archaea; OS: Organic Sulfur Utilizing Bacteria and Archaea. Adapted from Sievert et al. (2007).

another enzyme pathway (Stahl et al., 2007). In Figure 5.4, the *DsrAB* gene is not confirmed in all of the species shown; it has been detected in phyla that contain phototrophic SOB, SOB or SRB and is unconfirmed in phylum ε-proteobacteria, Aquificae and Crenarchaeota (Wagner et al., 1998; Stahl et al., 2007; Zhou et al., 2011).

The evolution of the *dsrAB* gene is dominated by vertical transmission along each lineage with a few lateral transfer events from δ-Proteobacteria species to *Archaeoglobus, Thermodesulfobacterium*, phototropic SMB and members of the Gram-positive Firmicutes (Klein et al., 2001). The exact mechanism of this transfer is unknown with theories that it occurred through xenologous (horizontal gene flow) displacement of a single gene *in situ* (Omelchenko et al., 2003) or a large 'metabolic island' containing sulfate-reduction genes was transferred by some mobile element in one single event (Mussmann et al., 2005). As a result, when constructing *dsrAB* dendrograms, two distinct lineages of *Firmicutes* species are commonly observed (Castro et al., 2002; Dhillon et al., 2003; Kaneko et al., 2007; Schmalenberger et al., 2007; Wu et al., 2009).

5.2 Methods

5.2.1 Nucleic Acid Extraction

Nucleic acids were isolated from each 1 cm slice of Core A from 1-30 cm in duplicate using the MO BIO Laboratories Inc. Ultra Clean Soil DNA Isolation Kit (MO BIO Laboratories Inc., 2010). Approximately 0.25-1 g of dry sediment was weighed on a precision scale before extraction. DNA concentration was determined using the Quanti-iT dsDNA HS kit with the Qubit fluorometer (Invitrogen, 2010b) and the Nanodrop ND-1000 spectrometer; 2 μL of template was used for both apparatuses. DNA concentration decreased with sample depth until no DNA could be detected past 22 cm. The low extraction efficiency was presumed to be from a combination of increased DNA degradation at lower levels and possible changes in sediment composition that impeded DNA extraction (Frostegard, 1999). To increase extraction efficiency the MO BIO Laboratories Inc. Power Soil DNA Isolation Kit (MO BIO Laboratories Inc., 2009) was used for samples from 11-30 cm. While extraction concentrations were still low, they were detectable on the Qubit fluorometer.

All extractions were cleaned and concentrated using the Favorgen Genomic DNA Clean-up kit (Favorgen Biotech, 2009). The 50 μL of cleaned template was eluted from the full 50 μL and 100 μL original template obtained from both the Ultra Clean and Power Soil kits, respectively.

5.2.2 Sequence Analysis of *DsrAB*

The *dsrAB* gene was PCR-amplified using primers Dsr-1F-GC (5'-ACS CAY TGG AAR CAC G-3') and Dsr-4Rdeg (5'-GTG TAR CAG TTD CCR CA-3') to yield a 1.7 kb fragment as described by Klein (2001) and Wagner (1998). The optimal $MgCl_2$ concentration was determined to be 2.5 mM, where higher concentrations increase annealing efficiency but decreased specificity. A touch down gradient for the annealing temperature from 65°C-59°C was also used to increase annealing efficiency as well as decrease specificity. The final PCR reaction conditions using the Platinum Taq PCR Kit (Invitrogen, 2010c) were as follows: 1 μL of 10 pmol/μL of each primer, 5 μL of DNA template, 2.5 μL of 10X PCR buffer, 1.25 μL of $MgCl_2$ (2.5 mM), 0.675 μL of BSA (3 mg/mL), 0.2 μL of deoxynucleoside triphosphate mix (dNTPs) (2 mM [each] dATP, dCTP, dGTP and dTTP), 1 Unit of *Taq* Platinum polymerase and nuclease free water to the final reaction volume of 25 μL. Reactions were distributed to 0.2 mL PCR tubes and amplified under the following conditions: initial denaturation of 90 s at 94°C followed by 30 cycles of 15 s at 94°C, touch down gradient from 65°C-59°C for 20 s, 54 s at 72°C and a final extension of 1 min at 72°C.

Clone libraries were constructed using TOPO® XL PCR cloning kit (Invitrogen, 2010a). The initial attempt of gel purification using the Crystal Violet provided with the TOPO XL cloning kit was not successful due to low PCR concentrations and inability to visualize the band. Alternatively, the Qiagen QIAQuick Gel Extraction kit (Qiagen ®, 2008) was used as per the manufacturer instructions to isolate the 1.7 kb fragment. Successful PCR reactions

were combined for ligation as follows: the three Ponar Grabs and core slices from 1-3 cm, 4-5 cm, 6-7 cm, 8-9 cm, 10-13 cm, 14-17 cm, 18-21 cm, 22-25 cm and 26-30 cm. Cloning attempts using the purified combined PCR products with the TOP10 *E. coli* strain provided with the TOPO XL kit were unsuccessful due to the long-term storage and improper handling of the cells that rendered them no longer viable. Instead, *E. coli* JM109 cells (provided by B. Murray, UNBC) were used to transfect the ligated TOPO XL plasmid and PCR products. Cells were grown overnight at 37°C on LB-Kanamycin (50 μg/mL) - X-Gal (80 μg/mL) - IPTG (0.05 mM) plates and blue-white screening was used to determine successful reactions. Approximately 1-12 successful bacterial colonies were picked from each plate and inoculated into 5 mL of LB Broth with 50 μg/mL Kanamycin and incubated overnight at 37°C with shaking at 225 rpm. Plasmids were isolated using the QIAgen MiniPrep Kit as per the manufacturer's instructions (Qiagen ®, 2006). The plasmid concentration was determined on the Nanodrop. Insert size was verified using universal M13 forward and reverse primers under the following conditions: 0.5 μL of 10 pmol/μL of each primer, 1 μL of 1:10 plasmid dilution, 2.5 μL of 10X PCR buffer, 0.75 μL of $MgCl_2$ (2.5 mM), 0.25 μL of deoxynucleoside triphosphate mix (dNTPs) (2 mM [each] dATP, dCTP, dGTP and dTTP), 1 Unit of *Taq* Platinum polymerase and nuclease free water to the final reaction volume of 25 μL. Reactions were distributed to 0.2 mL PCR tubes and amplified under the following conditions: initial denaturation of 93°C for 5 min followed by 35 cycles of 94°C for 30 s, 56°C for 30 s, 72°C for 90 s and a final extension of 72°C for 5 min (Invitrogen, 2010a).

Plasmids with the correct fragment length were sequenced using the universal primers M13F-Forward and M13R-Reverse to sequence the *dsrA* and *dsrB* subunits found at either end of the 1.7 kb fragment. Plasmids were prepared for sequencing in 96-well plates with ~450 ng of plasmid, 10 pmol of primer to a final volume of 15 μL and sent to Fragment Analysis and DNA Sequencing Services at the University of British Columbia, Okanagan in Kelowna, BC for sequencing using the ABI 3130xl Genetic Analyzer (UBC Okanagan, 2012).

Obtained sequences were manually reviewed using CodonCode Aligner 4.04 (CodonCode Corporation, 2013) to optimize and verify the nucleotide signal. Sequences were then compared to the online Basic Local Alignment Search Tool (BLAST) to verify the presence of the *dsrA* or *dsrB* gene and select the nearest related sequences from the GenBank database for alignment and comparison. All nucleotide sequences obtained in this study and from GenBank were aligned using MUSCLE (a multiple sequence comparison by log-expectation computer program) in MEGA 5.2.2 (Tamura et al., 2011). Sequences were then translated to amino acids and the best-fit MEGA 5.2.2 model analyzer was run to determine the optimal model to construct a maximum-likelihood tree using 500 replicate bootstrap analysis. The same tree building process was done for the un-translated nucleotide sequences to visually assess any ambiguities. The tree was grouped into clusters based on 87% amino acid sequence homology and into operational taxonomic units based on 97% amino acid sequence homology. Environmental conditions such as climate, sulfate and oxygen levels of the sequences obtained from the BLAST database were also recorded (Wagner et al., 1998; Klein et al., 2001; Dhillon et al., 2003; Leloup et al., 2009).

5.2.3 Quantification of *DsrA*

Sulfur-metabolizing bacteria were quantified using the SyBr® Green qPCR method by targeting the *dsrA* gene (Applied Biosystems, 2006). Previously prepared Plasmid 13167 from the cloning experiment was used as the standard and the plasmid concentration was confirmed using the Qubit. The plasmid was linearized using restriction enzyme *HindIII* to prevent supercoiling and enable qPCR amplification as follows: 5 μL enzyme buffer, 1 μL *HindIII*, 5 μL plasmid and fill to 50 μL with nuclease free H_20. The reaction was incubated at 37°C using a heat block for 1 hr (Promega, 2011).

A 6-times 10-fold serial dilution of the standard was run on every plate in duplicate to determine the standard curve used for absolute quantification. A duplicate 'no-template' negative control was also run for each plate to account for contamination and primer dimers. A melting curve for each plate was run from 65°C-95°C to assess non-specific amplification and the presence of primer dimers.

The *dsrA* genes present is each DNA sample was amplified and detected in duplicate using the Bio-Rad MiniOpticon™ Real-Time PCR Detection System (Bio-Rad, 2014). The primers used are described by Kondo et al. (2004) and Leloup et al. (2007) and are as follows: forward DSR-F+ (5'-ACS CAC TGG AAG CAC GGC GG-3') and reverse DSR-R (5'-GTG GMR CCG TGC AKR TTG G-3') to yield a 221 bp fragment. Primers were optimized by running variations of concentration for each forward and reverse primer at 50 nM, 300 nM and 900 nM. The lowest positive detection concentration was determined to be 50 nM for both the forward and reverse primers.

Annealing temperature was optimized to 63°C and the following conditions were used for all unknown samples: in 48-well plates, 2 μL DNA template or plasmid standard, 12.5 μL SyBr® Green PCR Master Mix, 50 nM DSR-F+ and DSR-R primers and filled to 25 μL with nuclease free H_2O and run on the RT-PCR machine at 50°C for 2 min, 94°C for 15 min and 35 cycles of 94°C for 15 s, 63°C for 60 s and 72°C for 45 s (Wagner et al., 1998; Kondo et al., 2004; Applied Biosystems, 2006; Leloup et al., 2007).

5.2.4 Quantification of 16S rDNA

Total Bacteria (Tbac) were quantified using the SyBr® Green qPCR method by targeting the 16S rDNA gene. The standard was isolated from a stock of *E. coli* that was grown overnight at 37°C on LB plates and one colony was picked to inoculate 5 mL LB Broth, which was grown overnight at 225 rpm at 37°C. Total genomic DNA of the inoculation was isolated using the MO BIO UltraClean® Microbial DNA Isolation Kit (MO BIO Laboratories Inc., 2010). DNA was quantified using the Qubit and used as the standard for Tbac quantification.

A 6-times 10-fold serial dilution of the standard was run on every plate in duplicate to determine the standard curve used for absolute quantification. A duplicate no-template negative control was also run for each plate to account for contamination and primer dimers. A melting curve for each plate was run from 65°C-95°C to determine non-specific amplification and the presence of primer dimers. qPCR products were amplified and

detected in duplicate using the Bio-Rad MiniOpticon™ Real-Time PCR Detection System. Two universal primers were used as described by Lopez-Gutierrez et al. (2004) to detect members of Eubacteria to amplify a 174 bp region and are as follows: 341f (5V-CCT ACG GGA GGC AGC AG-3V) and 515r (5V-ATT CCG CGG CTG GCA-3V). Primers were optimized by running variations of concentration for each forward and reverse primer at 50 nM, 300 nM and 900 nM. The lowest positive detection concentration was found to be 300 nM for the forward and reverse primer.

Annealing temperature was also optimized to 56°C. The following conditions were used for all unknown samples: in 48-well plates, 5 µL DNA template or plasmid standard, 12.5 µL SyBr® Green PCR Master Mix, 300nM 341f and 515r primers and filled to 25 µL with nuclease free H_2O and run on the RT-PCR machine at 50°C for 2 min, 95°C for 15 min and 40 cycles of 95°C for 15 s, 56°C for 30 s and 72°C for 30 s (Lopez-Gutierrez et al., 2004).

5.2.2 qPCR Calculations and Analysis

5.2.2.1 qPCR Calculations

The following equations and variables were used to calculate the final DNA concentration per gram of sediment at each sediment depth:

- C_t, the number of cycles required to reach the certain threshold florescence measured and reported by the RT-PCR detection system;

- *E,* amplification efficiency was determined using the following equation:

$$E = 10^{(-1/\alpha)} \qquad \text{(Equation 5.1)}$$

where, α is the slope of the curve calculated by the known concentration of the serial dilution of the sample vs. the threshold florescence.

- Environmental inhibitors of amplification efficiency (versus the cleaned and concentrated plasmid templates) were corrected for using the One-Point-Calibration method described by Brankatschk (2012) where,

$$N_{0\ sample} = N_{0\ standard} \times \frac{E_{standard}^{C_t\ standard}}{E_{sample}^{C_t\ sample}} \qquad \text{(Equation 5.2)}$$

where, N_0 is the concentration of the standard and template in ng/µL of DNA based on the known template concentration. Therefore the ng/µL DNA of each sample can be calculated to incorporate the differences in efficiency due to environmental impurities.

- The number of copies of genes detected is then calculated by:

$$Copy\# = c_{target} \times \frac{N_{0\ sample} \times N_A}{l_{Fragment} \times M_{bp}} \qquad \text{(Equation 5.3)}$$

where, *Copy #* is the number of gene copies detected per µL, c_{target} is the estimated copy number DNA strand (for 16S rDNA estimate 3.6 copies/cell and *dsrAB* one copy per cell), N_A is Avogadro constant (6.022×10^{23} bp/mol); $l_{fragment}$ is the length of the amplified DNA fragments, in this study 174 bp for 16S rDNA and 221 bp for *dsrA* and M_{bp} is the average weight of a double-stranded base pair (6.6×10^{11} ng/mol).

- From this the number of detected gene copy number per gram of sediment was calculated by determining the dilution factors imposed by the DNA extraction, cleanup and PCR steps and dividing by the grams of sediment analyzed (Leloup et al., 2009; Applied Biosystems, 2010; Brankatschk et al., 2012).

5.2.2.2 qPCR Analysis and Statistics

The SMB and Tbac ratio was calculated by dividing each of the four SMB qPCR replicates with each of the four Tbac qPCR replicates to yield 16 ratios that were multiplied by 100 to reflect percent and were arranged into a boxplot. The median of each 16 replicate set was used as the final percentage to assess its downcore relation with other variables.

All variables used in correlation or regression analysis were tested for normality using the Sharpiro-Wilk normality test ($p>0.05$ indicates normal distribution). All particle size datasets and trace metals of interest with the exception of Mn, As and Mo were normally distributed. The three bacteria variables and several of the Rock-Eval variables, with the exception of TOC, RC, S3CO and OICO, were all found to be non-normal. Tbac, SRB and Ratio were normalized by log-transformation and Hg and S2 were normalized by reciprocal (1/x) transformation. For visual ease, all the figures displaying bacterial distributions use a log-scale axis.

The statistical test selected to measure the significance of a relation between variables was dependent on the variables tested and their alignment with the requirements

to satisfy the assumptions for correlation or regression. The Spearman's Rank-Ordered Correlation assumes that the variables are continuously random intervals or ratios and they do not need to be normally distributed. It gives a measure of the strength of a non-linear monotonic relationship (as the value of one variable increases or decreases the other variable also increases or decreases) between the variable, which was verified graphically if required (Laerd Statistics, 2013). The Pearson's Correlation includes the assumption of a normal distribution, though it has been recognized as a powerful and useful test for continuous non-normal data (Chok, 2010). This correlation test was used in certain cases where a non-linear monotonic relation was not observed graphically or statistically but a non-normal linear one was. If both variables were normally distributed then simple linear regression was used.

5.3 Results and Discussion

5.3.1 Total Bacteria Quantification

The downcore distribution of Tbac is shown in Figure 5.5 along with the corresponding SMB distributions, which will be discussed in the next section. The minimum Tbac concentration was 1.81×10^{10} 16S rDNA/g sediment at the surface sample, 1 cm of; the

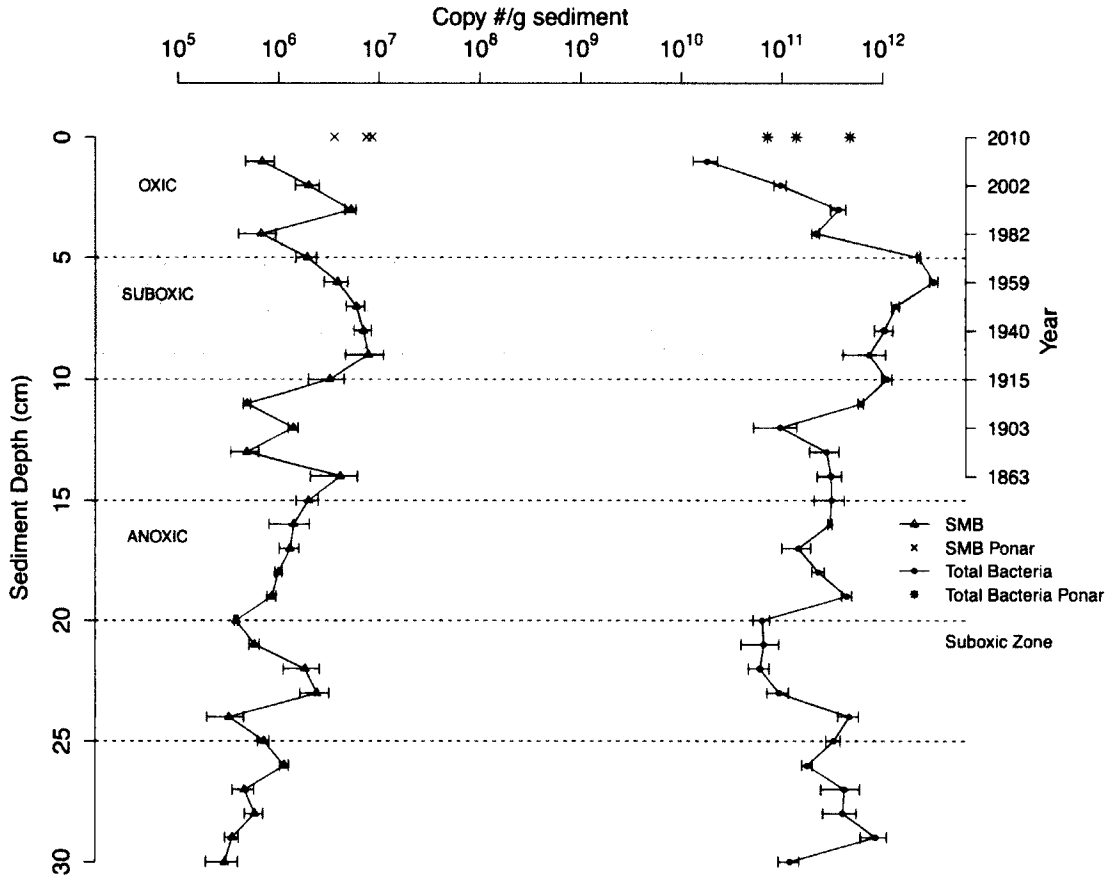

Figure 5.5: Overview of the downcore distribution SMB (*DsrAB*) and Tbac (16S rDNA) by gene copy#/g sediment with standard deviation error bars and the redox boundaries proposed by Mn and Fe reduction peaks (Chapter 3). Ponar grabs are representative of top ~7 cm.

maximum of $3.21x10^{12}$ 16S rDNA/g sediment occurred at 6 cm and the overall average was $5.40x10^{11} \pm 3.22x10^{9}$ 16S rDNA/g (± SE) of sediment. The average of the three Ponar Grabs (representative of a mixture of the top 7 cm from the surrounding region) is shown as asterisks * in Figure 5.5 and was $2.28x10^{11}$ 16S rDNA/g of sediment, which is comparable to the average number of bacteria in the sediment core. The number of bacteria increases at the onset of the suboxic zone and maintains a high concentration until 6 cm where it rapidly decreases and remains somewhat constant to the core bottom.

5.3.1.1 Total Bacteria and Particle Size

No significant correlation was found between Tbac and any of the particle size measurements indicating that there is no obvious relationship between particle size and the number of bacteria present in the bottom sediments. However, within the water column, bacteria are dependent on the large surface area of suspended clay that adsorbs dissolved organic matter to provide a concentrated nutrient and energy source (Donohue & Molinos, 2009). The lack of correlation observed in the sediment core may be due to several factors. For example, once the clay-OM-bacteria aggregates are deposited to the sediment, bacteria may migrate to the optimal redox zone for their metabolism (von Wachenfeldt & Tranvik, 2008; Gudasz et al., 2012). As well, the capacity of clay particles to form an aggregate is not necessarily dependent on particle size as it also involves the strength of ion adsorption, physical structure of the clay, extent of surface area and its affinity for OM (Donohue & Molinos, 2009).

5.3.2 Sulfur-Metabolizing Bacteria Quantification

The downcore distribution of SMB in the sediments is shown with Tbac in Figure 5.5. The minimum, 2.94×10^5 *dsrAB*/g sediment occurs at 30 cm, the maximum, 7.86×10^6 *dsrAB*/g sediment occurs at 9 cm and the overall average was $2.01 \times 10^6 \pm 5.22 \times 10^5$ *dsrAB*/g (±SE) sediment. The three Ponar Grabs, shown as the three boxes located about the 0 cm line represent the mixture of the top 7 cm of the region surrounding the core site and have an

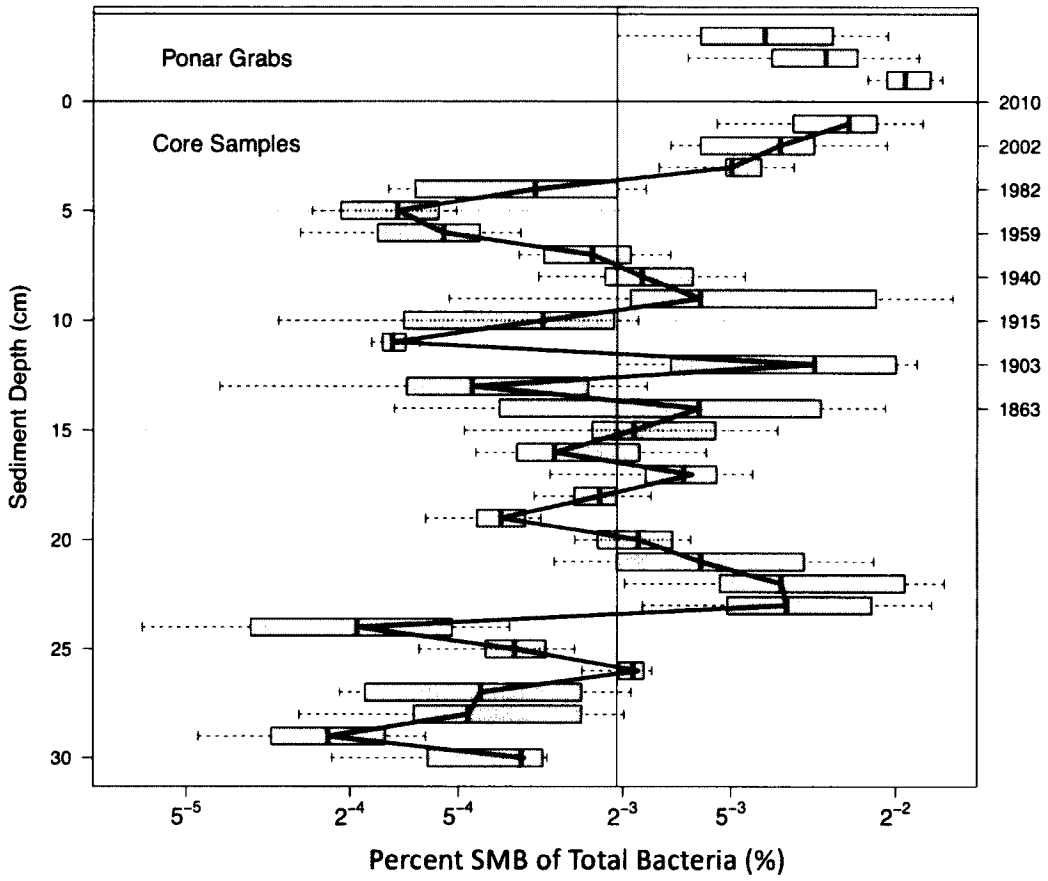

Figure 5.6: Boxplot of %SMB of Total Bacterial qPCR replicates (16 ratios for each sample). The black line in each box represents the sample median and the overall median is shows by the vertical line as 1.9×10^{-3}. The Ponar Grabs are separated to the top but are presumed to be a homologous sampling of the top ~7cm.

average of $6.54x10^6$ *dsrAB*/g sediment.

Visually, the SMB and Tbac downcore profiles (Fig 5.5) appear to follow a similar trend, especially within the top 10 cm, however the Spearman Correlation of Log(Tbac) to Log(SMB) is very weak (ρ=0.30, $p<0.1$). A better representation of the abundance of SMB is shown as the percent SMB of total bacteria (%SMB) as a box plot in Figure 5.6. This is a depiction of the percent SMB of Tbac calculated from the four qPCR replicates, to give a total of 16 ratios used to calculate the median SMB% of each sediment sample. The vertical line indicates the overall %SMB median, $1.9x10^{-3}$ %SMB, while the maximum was 0.013 %SMB and the minimum $1.6x10^{-5}$ %SMB. The three Ponar grabs are shown at the top with a median of 0.01%.

The downcore trend of %SMB indicates the overall abundance is very low. Other studies have reported %SMB anywhere from 10^{-5} to 3% with the higher concentrations typically found in marine environments (Holmer, 2001; Barton et al, 2007; Leloup, 2009; Pester 2012). The low proportion is likely related to the Subarctic oligotrophic lake conditions of Kusawa, such as cooler temperatures, higher oxygen and lower sulfate levels.

The greatest proportion of SMB occurs at the surface and then decreases to 5 cm. A second peak follows from 5 cm to 11 cm with the apex at 9 cm. A sharp peak with the second highest abundance occurs at 12 cm, which is followed by several irregular fluctuations to 19 cm. A third peak is then observed from 19-24 cm and the remaining samples are all below the overall median. Several publications (e.g. Mussmann et al., 2005; Stahl et al., 2007; Muyzer & Stams, 2008) have reported that SMB typically exhibit two

population peaks within the oxic and anoxic zone, here it is proposed that these are located at 5-9cm and 19-24cm respectively.

5.3.2.1 Sulfur Bacteria and Particle Size

No significant relation was found between SMB or %SMB and any of the particle size measurements indicating that there is no direct relation between particle size and the number of SMB present in the sediments. These relationships were evaluated here as SMB are presumed to be a part of the community developed in the suspended clay-organic-bacterial aggregate formations discussed in Section 5.3.1.1.

5.3.3 Sulfur-Metabolizing Bacteria Diversity

The *dsrAB* gene was sequenced to assess the diversity of the SMB present in Kusawa Lake sediments. PCR amplifications that contained the expected 1.7 kb fragment were isolated and combined as follows: Ponar Grabs, 1-3 cm, 4-5 cm, 6-7 cm, 8-9 cm, 10-13 cm, 14-17 cm, 18-21 cm, 22-25 cm and 26-30 cm. Up to twelve clones were sequenced from each group, except for the following groups where only a few clones were grown: 6-7 cm (7 colonies); 8-9 cm (6 colonies); 10-13 cm (1 colony); 14-17 cm (0 colonies) and 26-30 cm (2 colonies). The unsuccessful cloning was possibly due to laboratory error or inadequate competent cells for transformation. Sequences obtained from the 76 successful clones were compared to the GenBank database and 39 *dsrAB* sequences were confirmed. The

unsuccessful sequences were either not the *dsrAB* gene, the sequencing reaction was contaminated or it was unsuccessful.

5.3.3.1 Maximum Likelihood Tree

The nearest BLAST sequence for each clone was added to a *dsrAB* library along with the Kusawa clones. Using MEGA 5.2.2 the sequences were aligned and a 177 amino acid maximum likelihood tree was constructed using the Whelan and Goldman model based on 500 bootstraps (Fig 5.7). Eight clusters based on 87% amino acid identity and 16 Operational Taxonomic Units (OTUs) based on 97% amino acid identity were identified. The probable bacterial order for each cluster was determined by comparison with the associated clones obtained from the BLAST database. The environmental condition of each BLAST clone isolate was also considered to make inferences about the sediment conditions at Kusawa.

As with many environmental studies of *dsrAB* (Holmer & Storkholm, 2001; Loy et al., 2004; Leloup et al., 2009; Pester et al., 2012), uncultured SMB were detected in clusters I and II and comprised of five OTUs. The associated BLAST sequences were all uncultured SMB from freshwater wetlands and paddy soils from a range of sulfate and oxygen concentrations. Cluster I includes all the Ponar Grabs except one and isolates from 6-7 cm, 14-17 cm, 22-25 cm or 26-30 cm. As no BLAST search results were linked to OTU1 and OTU2, it is proposed that these comprise a novel lineage of subarctic, psychrophilic (cold tolerant) SMB that function under limited sulfate availability (Madigan et al., 2003).

OTU3 and OTU4 are more closely related to previously identified uncultured clones and likely have a similar function associated with low sulfate and oxic-anoxic environments. Cluster II only contains one isolate from 4-5cm and its closest relation is from an oxic, low sulfate, freshwater wetland in Australia (Rees et al., 2010).

Cluster III contains the first branch of Gram-positive Fimicutes, *Desulfotomaculum spp.*, associated with the 14-17 cm zone. The BLAST clones are from high sulfate environments, suggesting that either SRB or SB are likely present (Zhou et al., 2011).

Cluster IV groups with BLAST isolates from high sulfate, anoxic environments that are most closely related to Syntrophobacteraceae from δ-Proteobacteria. These bacteria are most notable for their ability to oxidize propionate and for syntrophic growth with acetogens when using acetate under low sulfate conditions (Loy et al., 2004; Stahl et al., 2007). All of the clones that form OTU7 are located between 8-9 cm, the proposed oxic/anoxic interface. These bacteria are likely taking advantage of the abundance of electron acceptors present and may be growing in syntrophy and using the byproducts from other species. They are also likely to be somewhat oxygen tolerant and may be the organisms responsible for the transfer of sulfur-compounds across the interface to continue the cross-boundary sulfur cycle.

OTU8 constitutes an unknown singleton, as it has no association with any of the other isolated clones or the sequences from the GenBank database.

Cluster V is the second branch of Firmicutes, *Desulfotomaculum*. The separation of Firmicutes branches is due to the lateral *Dsr* gene transfer described by Klein (2004). Four

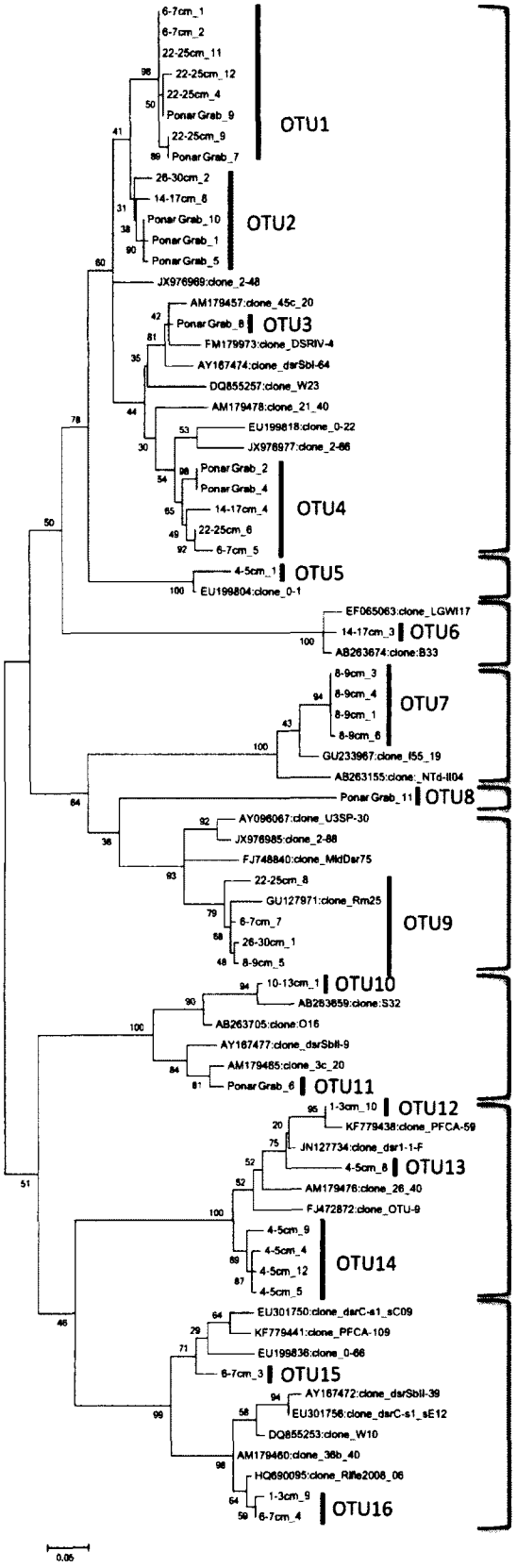

Figure 5.7: Maximum likelihood tree of truncated *dsrA* genes (177 amino acids) using the Whelan and Goldman model. Numbers correspond to 500 bootstrap replicates and percentage of replicate trees in which the associated taxa were clustered as shown. Clusters are based on 87% amino acid identity and associated Classes are divided by the dotted lines. Operational taxonomic units (OTU) are based on 97% amino acid identity and require at least two environmental clones

Unidentified and Uncultured SRB Clusters
Cluster I: oxic-anoxic, low-high SO4-

Cluster II: oxic, low SO4-

***Firmicutes**, Desulfotomaculum* (Gram Positive)
Cluster III: unknown oxygen, high SO4-

***Deltaproteobacteria**, Syntrophobacteraceae*
Cluster IV: anoxic, high SO4-

Unknown singleton

***Firmicutes**, Desulfotomaculum*, (Gram Positive)

Cluster V: oxic-anoxic, low-high SO4-

Deltaproteobacteria

Sytrophaceae
Cluster VI: oxic-anoxic, low SO4-

Unknown Family
Cluster VII: oxic, low SO4-

Sytrophaceae
Cluster VIII: oxic-anoxic, low SO4-

clones located between 6-25 cm are grouped into OTU9 and are most closely related to a clone from an acidic fen. The other environmental clones in the cluster are from both oxic/anoxic and low/high sulfate conditions.

The final three clusters are all found in the δ-Proteobacteria with the associated environmental clones from low sulfate zones and mostly oxic with a few growing in anoxic conditions. All of the isolates are from above 7 cm except one clone from 10-13 cm.

Both Clusters VI and VIII are associated with environmental clones related to the *Syntrophacae* family, which is from the same order Syntrophobacteraeles as *Syntrophobacteraceae*. These bacteria are known to operate in syntrophy with other bacteria. Between the two clusters there are four OTUs that are all associated with bacteria from a low sulfate and a mix of oxic and anoxic environments.

These two Clusters are separated by Cluster VII, which is not identified to any family. It is possible that these are also *Syntrophacae*, however they may be another bacterium and separated due to lateral gene transfers or some other mechanism (Klein et al., 2001). This is the only cluster that is associated with strictly oxic bacteria along with low sulfate.

5.3.4 Outcomes of Phylogeny

An interesting outcome of the phylogeny is the dominant presence of syntrophic bacteria. This suggests that under oligotrophic, presumably low sulfur conditions, SMB are dependent on other organisms to provide substrates and electron donors other than their

preferred sulfur-compounds to enable growth. Another observation is the absence of δ-Proteobacteria species that are typically associated with high sulfate anoxic environments such as orders Desulfobacterales, Desulfovibrionales, and Desulfurellales. It is possible they may be present in the deeper sediments or they were not successfully amplified, however it does signify that they are likely not abundant in the Subarctic, low sulfate and low to high oxygen environment of Kusawa Lake.

Chapter 6 Mercury in Kusawa Lake

6.1 Introduction

6.1.1 Origins of Mercury in the Yukon

Mercury (Hg) is a ubiquitous heavy metal that has been widely studied for its toxicity, industrial applications and its volatile biogeochemical cycle around the globe. Mercury is most recognized as a silver liquid in thermometers and has many other liquid, solid or gas forms (Table 6.1). Through these states, Hg is capable of transport within geological, atmospheric, aquatic and biological systems (Fitzgerald & Lamborg, 2005).

Table 6.1: Speciation and the common measurements of Hg in environmental samples. Adapted from (Chételat et al., 2012).

Species	Atmosphere	Aquatic	Organic/Tissue
Hg(II)	Gas and Particle-Associated	Inorganic reactive particulate and dissolved in water column and sediments	Inorganic

As a solid, Hg is commonly found mineralized with sulfur to form cinnabar, HgS, which is found throughout the Yukon, especially in conjunction with antimony deposits (Panteleyev, 2005). Solid Hg is naturally released to the environment by rock weathering or

discharge of stores from the cryosphere, driven by permafrost and glacial melt (Poissant et al., 2008). Cinnabar has been mined for over 3000 years, starting in the Peruvian Andes (Cooke et al., 2009) and has been used in many industrial products and applications throughout history such as thermostats, batteries, fluorescent lights, dentistry, chemical catalysis and pharmaceuticals (Fitzgerald & Lamborg, 2005).

Mercury is anthropogenically emitted to the atmosphere through industrial combustion processes such as coal and fossil fuel burning, waste incineration, cement

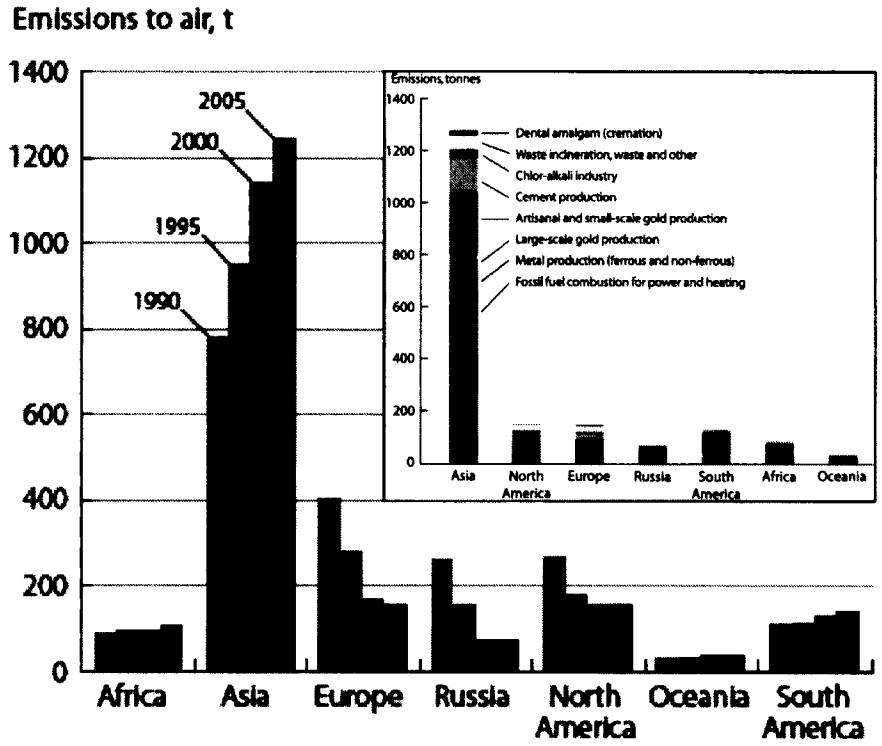

Figure 6.1: Global anthropogenic emissions of mercury to air by continent from 1990, 1995, 2000 and 2005 that depicts a decrease in developed countries and increase in developing countries, particularly Asia. The inset shows a breakdown of the industrial activity associated with Hg emissions by each continent, where again Asia is the primary producer. Both figures from United Nations Environmental Programme (2013).

production and smelting (Fitzgerald & Lamborg, 2005). This has led to a global increase in Hg emissions that parallels increasing CO_2 emissions beginning at the onset of the industrial revolution (Lamborg et al., 2002). Global Hg emissions produced by the developed world peaked and began to decrease in the 1990s, however, developing countries, particularly those in Asia, have rapidly increased Hg emissions from an array of industrial activities (Fig 6.1).

Traditionally, the primary source of anthropogenic Hg was from coal burning, more recently this has been greatly augmented by artisanal and small scale gold mining. The inset of Figure 6.1 outlines the industrial-associated global anthropogenic Hg contributions by continent in 2005. Pacyna et al. (2010) predicts that by 2020 Hg emissions should decrease in all continents with the exception of Asia, where the most conservative model estimates Asian emissions at 450 tonnes/year and the most pessimistic predicts almost no change from 2005 (Pacyna et al., 2010).

Mercury is also naturally emitted to the atmosphere by volcanic eruptions, wildfire and photo- or biological reduction of Hg(II) in water and soils. This natural release is compounded by additions from human activity to the point where anthropogenic contributions have raised the Hg level several-fold above the pre-industrial conditions (United Nations Environment Programme, 2013).

6.1.2 Long-Range Atmospheric Transport

Once emitted to the atmosphere, Hg is converted to Gaseous Elemental Mercury (GEM) or Hg(0), which has a very long residence time from 6 months to 2 years in the troposphere (Lamborg et al., 2002). Regional and seasonal-associated shifts in the atmospheric redox potential results in the oxidation of GEM and production of reactive gaseous Hg and particle-associated Hg, both of which have an atmospheric residency of just days. These are deposited to the Earth's surface through precipitation scavenging (i.e. with snow and rain) (Chételat et al., 2012). In the high Arctic, atmospheric Hg-scavenging is most notable in the spring through a phenomenon called Atmospheric Mercury Depletion Events (ADME) where a substantial amount of atmospheric Hg is suddenly deposited with snowfall due to seasonal changes in ocean chemistry (Schroeder et al., 1998; Steffen et al., 2007; United Nations Environment Programme, 2013). Dunford et al. (2010) catalogued the origin of GEM in Arctic, Subarctic and mid-latitude regions, including the Little Fox Lake Air Quality Monitoring Station, located ~125 km northeast of Kusawa Lake. At Little Fox Lake and another Subarctic station, ADMEs were not observed, instead, atmospheric GEM concentrations were somewhat constant throughout the year with the maximum occurring in early summer and minimum from late summer into autumn. Inputs from Asian countries were more prominent in regions closer to the Pacific at both the Subarctic and mid-latitude stations and inputs from Russia and North America were also detected at Little Fox Lake but at substantially lower levels than the contributions from Asia (Durnford et al., 2010).

6.1.3 Terrestrial and Aquatic Transport and Fates

Local anthropogenic, natural and atmospherically deposited Hg can be cycled between terrestrial, freshwater, atmospheric and if in proximity, marine environments. Some Hg transportation mechanisms include rapid reduction and evasion to the atmosphere, transportation in fluvial systems and deposition throughout watersheds including the ocean and bioaccumulation through the food web (Fig 6.2) (Schroeder et al., 2005; Chételat et al., 2012). Mercury enters aquatic fluvial systems via precipitation, runoff, erosion and release from the cryosphere. It is capable of flux back to the atmosphere, depending on Hg concentration, aquatic pH, wind and available substrates such as

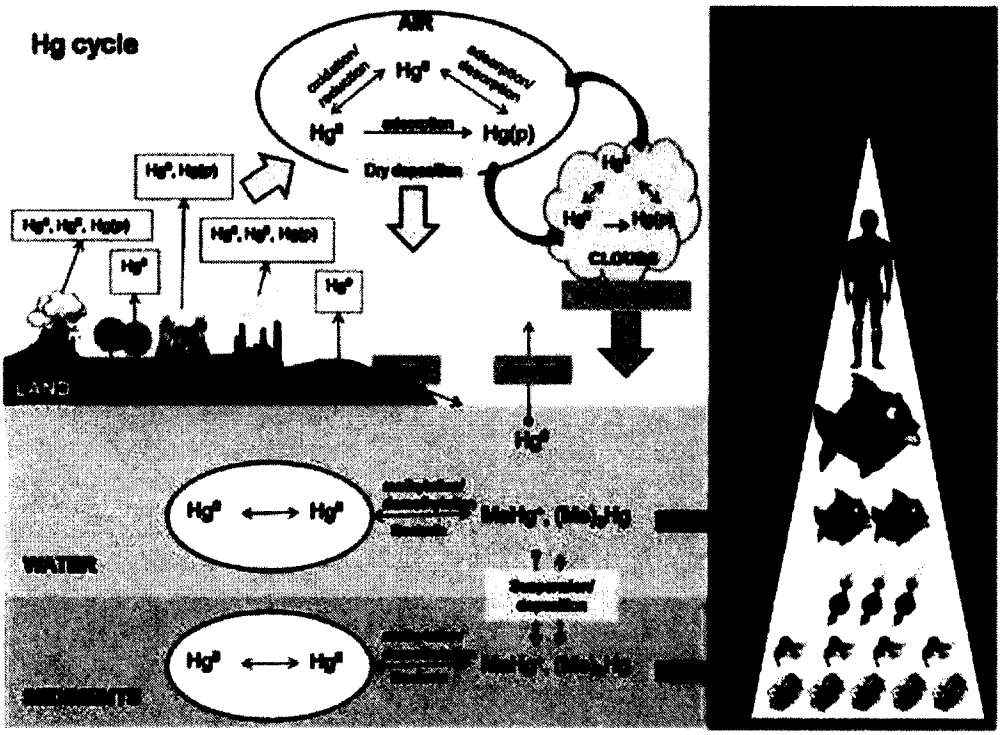

Figure 6.2: General overview of the global Hg cycle from the atmosphere to terrestrial and aquatic systems and the transfer to and bioaccumulation through the food web as methylmercury. From GMOS (2012)

dissolved organic carbon and particulate matter (Schroeder et al., 2005). In Subarctic systems, there are many long-term stores of Hg in soils, sediments and the cryosphere (AMAP, 2011). In lakes, a major storage site is the bottom sediment, where Hg has been sequestered and deposited from the water column to the lower sediments where it remains (Evans et al., 2005).

6.1.3.1 Algal-Derived Organic Matter Hg Scavenging

There is a well-recognized interaction between Hg and OM in both terrestrial and aquatic systems (Fitzgerald & Lamborg, 2003). This is due to the thermodynamically favourable bond between Hg (II) ions and the thio (-SH) group of various organic compounds (Hesterberg et al., 2001). One well-studied affiliation is the ability of labile algal-derived OM to scavenge Hg from the water column and transfer it to the bottom sediments during settling of suspended particulate-associated OM. This is measured by assessing the correlation between the $S2_{400}$ fraction detected by Rock Eval Pyrolysis and Total Hg (THg) content of lake sediment records (Stern et al., 2009; Sanei et al., 2014). The efficiency of this interaction is based on the concentration balance between Hg and labile OM. For example, if Hg is in excess of available OM it will remain in the water column and be flushed from the aquatic system or taken up by the food web, or if there is an abundance of OM then available Hg can be readily transported to the sediments (Sanei et al. 2014). Kusawa has been identified as a high Hg-binding capacity lake, meaning that although the concentrations of both OM and THg are exceeding low, the sediment OM is saturated with

Hg. This also means that any small increase in THg input may quickly overwhelm the OM scavenging capacity and lead to increasing amounts of Hg available to enter and bioccumulate through the food chain (Sanei et al., 2014).

Understanding algal-Hg scavenging is important in northern systems to ensure an accurate estimate of the contribution to historic and recent atmospheric inputs. Several studies have attributed the rising concentration of Hg in lake sediment records to industry-related anthropogenic inputs, however this does not account for climate change related inputs such as erosion from bedrock and release from the cryosphere. It also does not consider the increasing rates of lake primary productivity that corresponds to increased rates of algal-derived OM Hg scavenging. As a result, current estimates of sinks in the global Hg budget may be erroneous regarding the level of atmospheric Hg deposition and fates in northern ecosystems (Outridge et al., 2007; Stern et al., 2009; Sanei et al., 2014).

6.1.4 Mercury Methylation and Sulfate-Reducing Bacteria

One of the main reasons for the extensive study of Hg is its ability to bioaccumulate through the food chain as toxic organic methylmercury (MeHg). Microbial-mediated methylation of Hg(II) takes place at oxic/anoxic interfaces found within the environment, such as within the water column of eutrophic systems or within soils and lake sediments (Fig 6.3). The most widely recognized and studied species of Hg-methylating bacteria are SRB, Iron(III)-Reducing Bacteria and methanogens. Mercury methylation is an anaerobic process

that is inherently linked to both the sulfur and iron cycles and most readily occurs at the zones of sulfate and ferric iron reduction (Benoit et al., 1999; Mason & Lawrence, 1999; Hammerschmidt et al., 2006).

The ability of SRB to methylate Hg is dependent on community composition, as only certain strains are confirmed Hg-methylators, all of which are found under Deltaproteobacteria (Gilmour et al., 2011). The most common strain used to study SRB Hg-methylation is *Desulfovibrio desulfricans,* from the order *Desulfovibrionales*, which are obligate anaerobic SRB. *D. desulfuricans* both produces and degrades MeHg, where in most cases the rate of demethylation exceeds that of methylation. Therefore, as observed in many environments, only a small percentage of THg is present as MeHg (Hollweg et al., 2009; Gilmour et al., 2011).

The exact mechanism of SRB Hg-methylation is still poorly understood. It has been proposed that dissolved $HgS_{(aq)}$ readily diffuses across SRB cell membranes, is methylated and MeHg is then excreted. Some SRB may employ the acetyl-CoA pathway, which is used to completely oxidize carbon to CO_2, while incomplete oxidizers that are capable of growth outside the acetyl-CoA pathway may methylate mercury through some other process (Ekstrom et al., 2003). Further study of *D. desulfuricans* has identified two proteins, punative corrinoid protein (HgcA) and a 2[4Fe-4S] ferredoxin protein (HcgB) that can carry a methyl group from the reductive acetyl-CoA pathway and transfer it to Hg to produce MeHg (Gilmour et al., 2011).

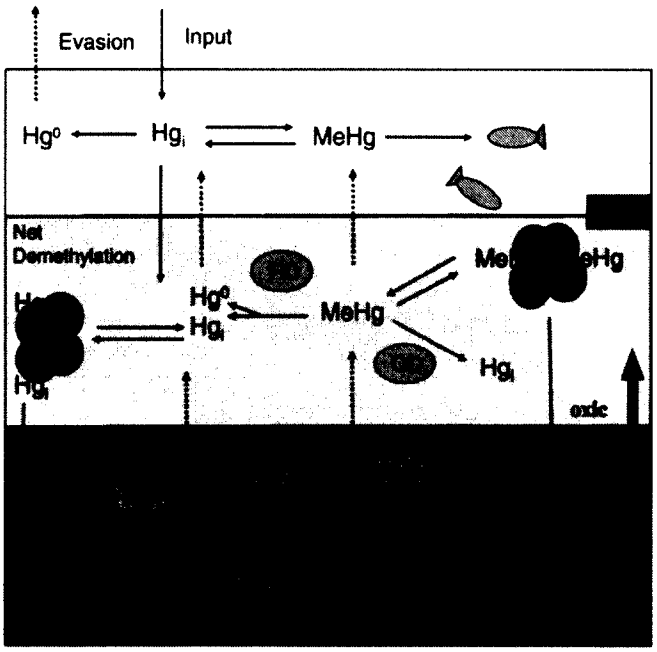

Figure 6.3: Overview of Hg cycling in the sediments of estuarine and coastal environments as described by Merritt et al. (2008). Where Hg enters oxic soils from the water column and is transported to anoxic sediments by diffusion via sediment association where it is methylated by SRB. MeHg is then re-transported to the sediment water interface (SWI) where it may enter the food chain or be converted to another species. Circles depict sediment particles, Hgi=inorganic divalent Hg or Hg(II), RD=reduction, OD=oxidation, MiR =bacterially independent reduction. (Merritt & Amirbahman, 2009)

6.1.5 Biochemical Controls of Mercury Methylation

Methylmercury production is dependent on several factors. First, is the concentration of THg where in many studies MeHg is positively correlated to THg (Hammerschmidt et al., 2006; Goulet et al., 2007; Hollweg et al., 2009; Jiang et al., 2011). However, in systems with very low microbial activity a threshold can be reached and a log relation between increasing THg and stable or decreasing levels of MeHg is observed that is likely related to saturation of methylating enzymes (Gilmour et al., 2011).

Organic matter also influences the bioavailability of Hg, where $S2_{400}$ has a strong correlation with THg in Subarctic and Arctic lake sediment records and as discussed can scavenge Hg from the water column and transport it to the bottom sediments (Stern et al., 2009; Sanei et al., 2014). .

Sulfate (SO_4^{2-}) also strongly regulates the rate of methylation, where increasing levels of SO_4^{2-} correspond to an increase in MeHg productivity in low sulfate environments, such as Kusawa Lake. Under high sulfate conditions, such as marine systems, SRB enzymes can be saturated with preferred electron acceptors, thereby inhibiting Hg-methylation (Gilmour et al., 1992; Fitzgerald & Lamborg, 2003; Norici et al., 2005; Sievert et al., 2007; Ouddane et al., 2008). Sulfide (H_2S) also controls the rate of methylation as it promotes the formation of dissolved $HgS_{(aq)}$ to enable diffusion across cell walls. However, under high sulfide conditions other sulfur-Hg species are formed, such as $Hg(SH)_2$, HgS_2 and polysulfides that cannot be methylated and consequently inhibit methylation. Sulfur-oxidizing bacteria also play a role in this balance by continuously oxidizing H_2S to sulfate to regulate H_2S or SO_4^{2-} inhibited methylation. This is a reason why methylation typically occurs around the oxic/anoxic zone as neither sulfate or sulfides are in excess (Gilmour et al., 1992; Benoit et al., 1999; Ouddane et al., 2008).

In sediments, MeHg is produced almost completely within the pore water, where diffused $HgS_{(aq)}$ is transported across cell walls, methylated by bacteria, excreted and finally diffused to the water column. Studies where MeHg was not diffused found it was promptly demethylated in the presence of Fe-oxides within the suboxic zone. Once MeHg is in the

water column it can be readily taken up by the food chain or may be lost by photo-demethylation and photo-reduction and emitted to the atmosphere. (Hammerschmidt et al., 2006; Goulet et al., 2007).

6.1.6 Bioaccumulation, Biomagnification and Toxicity

Bioaccumulation is defined as the ability of a toxic substance to reside within an organism for longer than it takes to degrade. Biomagnification in when the concentration of the toxic substance is compounded as it moves up the food chain. For example, the MeHg concentrations of fish continuously increase as it ingests MeHg contaminated invertebrates (United Nations Environment Programme, 2013).

Mercury is designated as a global threat to human and environmental health because of the varying degrees of toxicity experienced by those exposed to high concentrations (United Nations Environment Programme, 2013). In elemental form, Hg can cause respiratory tract failure when inhaled as a highly concentrated vapour, inorganic Hg(II) can lead to kidney failure and gastrointestinal damage and finally MeHg, the most toxic species, can be absorbed through the gastrointestinal tract and distributed throughout the body. These risks are of particular concern to pregnant and breastfeeding women (Health Canada, 2009). Mercury is also known to reside for long periods in the brain and historically the psychological symptoms associated with extreme mercury poisoning from felt hat manufacturing coined the term 'Mad as a Hatter'.

The World Health Organization guidelines set the tolerable daily intake of Hg in adults to 0.71 μg/kg body weight. Health Canada has also set the commercial standard that fish and seafood Hg levels must be below 0.50 μg/g of tissue (Health Canada, 2009). In the north, exposure to mercury is of large concern due to the sustained practice of harvesting food such as plants and berries, small and large game and fish. The Inuit Health Survey found that Inuit who regularly consume country foods have a higher blood mercury concentration than other Canadians though they were generally below the Health Canada blood toxicity thresholds, with a few exceptions. The report also emphasized that the nutrients and wellbeing obtained by consuming country foods outweighs the contaminant risks (Chan, 2011).

In the Yukon, Hg concentrations in fish are at very low levels and therefore there is no limit to the amount of fish that may be consumed. However, pregnant and nursing women are advised to limit their intake, especially of predatory fish such as trout, burbot and northern pike (Environment Yukon, 2010). The annual Hg concentrations of trout in Kusawa Lake are shown in Figure 6.4 where the average level over a 17-year period was 0.38 μg/g. The record trout Hg level was 0.54 μg/g in 1993 and the average level that year was 0.45 μg/g. This high decreased to 0.23 μg/g in 2009, with the most recent measurement in 2010 at 0.31 μg/g. These levels are nearing the Health Canada standard limit of 0.50 μg/g, indicating that Hg is present, bioaccumulating and biomagnifying in the Subarctic environment (Stern et al., 2011). The decrease in average trout Hg levels from

1993 is presumably associated with the decrease in atmospherically generated Hg from developed countries (i.e. North America and Europe), however the drop between 1999-2001 and 2007-2008 corresponds to the second and third highest recorded discharge years in 2000 and 2007, respectively for the Takhini river (Water Survey of Canada, 2012), indicating that the drop in trout Hg concentrations may be attributed to flushing of the drainage basin, photo-reduction and dilution of bioavailable Hg in the watershed.

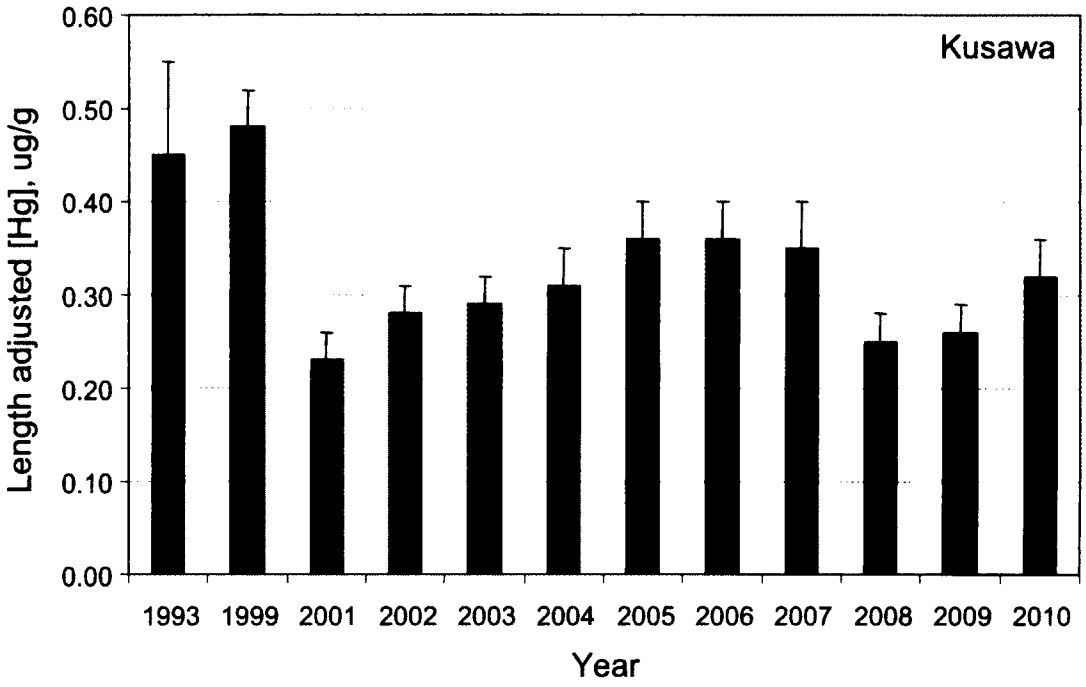

Figure 6.4: Level of Hg detected in trout tissue from Kusawa Lake from 1993-2010. From Stern et al. (2011).

6.2 Methods

6.2.1 Total Mercury and Methylmercury Quantification

Core A subsamples were used to quantify Total mercury and methylmercury at the University of Manitoba by Cold Vapour Atomic Absorption Spectrometry under the QA/QC set by the Northern Contaminants Program (Stern et al., 2009). The normalized downcore Hg measurements (1/Hg) were correlated with other variables including particle size, Rock Eval Pyrolysis, Tbac and SMB.

6.3 Results and Discussion

6.3.1 Total Mercury

The downcore profile of THg is depicted in Figure 6.5. The maximum THg sediment concentration of 0.034 μgg^{-1} occurs at 4 cm, the minimum, 0.016 μgg^{-1} at 19 cm and 22 cm and the overall average was 0.022 ± 0.0009 μgg^{-1} (±SE). The THg concentrations below 15 cm remain somewhat constant and fluctuate between 0.016 μgg^{-1} to 0.021 μgg^{-1}, while the top 5 cm has the highest concentration that continuously decreases down the core. A 1.5-fold increase in the THg concentration is observed from 1915-2010 that corresponds with increasing global temperature and industrial activity.

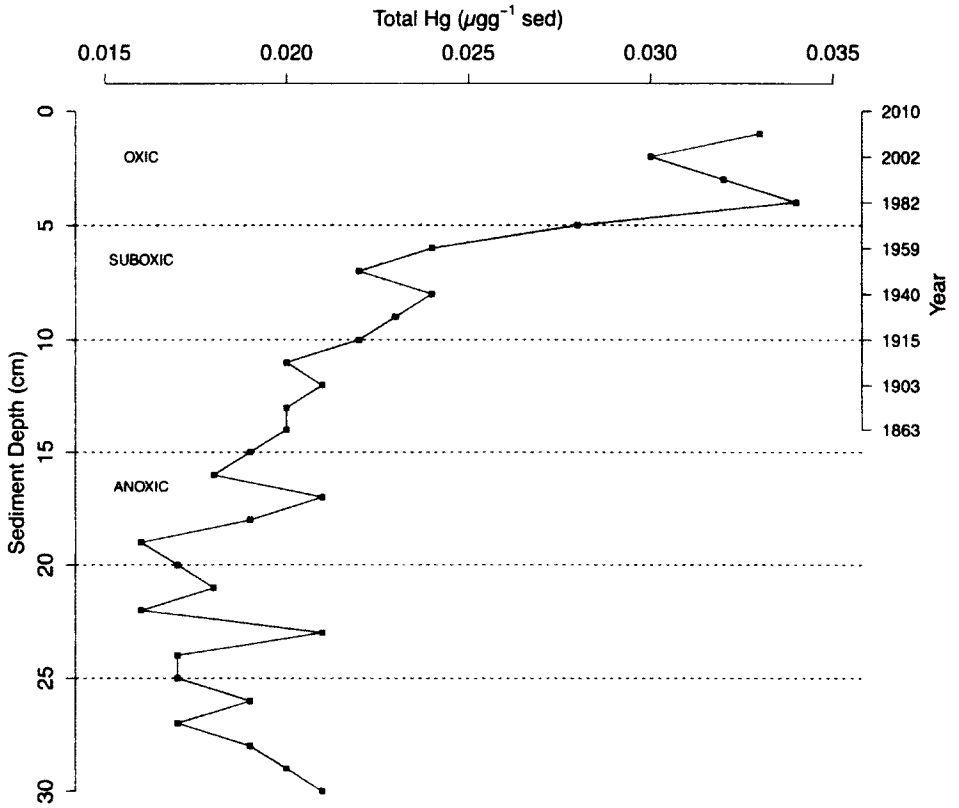

Figure 6.5: Downcore profile of Hg concentration in Kusawa Lake sediments. There is a 1.5-fold increase in THg concentration from 1915-2010 over the top 10 cm.

6.3.2 Methylmercury

The level of methylmercury (MeHg) throughout the core was below the limit of detection. This is not surprising considering the low THg concentration, low levels of OM, SRB and presumably sulfate concentrations. As well, the majority of MeHg is likely dissolved and associated with the pore water instead of the sediments. The inability to detect MeHg does not indicate that MeHg production is not occurring, only that the level is so low that it cannot be detected by the method used.

6.3.3 Total Mercury and Particle Size

The strongest association of Hg with the various particles size measurements was with fine silt (8-16 μm) that makes up 41-49% of the sediment. The other size measurements resulted in correlations that had slopes close to zero. Other studies have shown that Hg does not strongly associate with clay or very small particles. Jiang et al., (2011) proposed that aluminosilicates and other clay associated metals such as tin and potassium could be diluting the Hg concentrations in the sediments, rather than directly binding Hg. A biplot relation of % fine silt with the 1/Hg profile is depicted in Figure 6.6

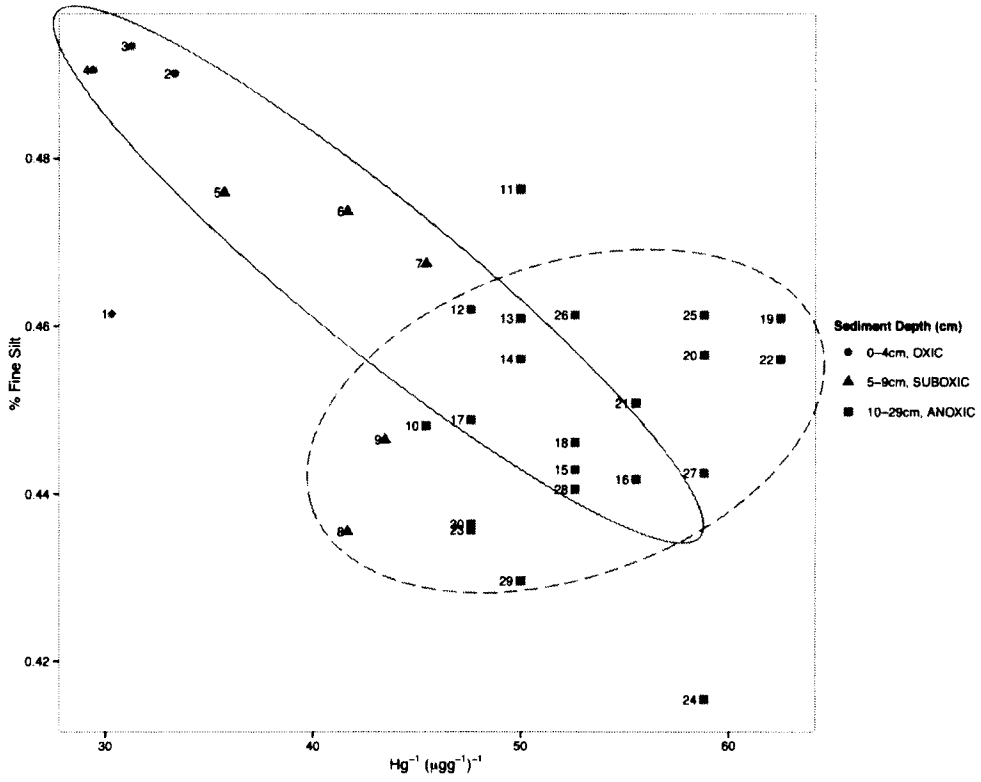

Figure 6.6: Downcore profile of 1/Hg association with % Fine Silt. There are two associations of sediments associated with the top 7cm, 12-18cm and 28cm (solid line oval) and the lower sediments (dotted line oval). Outliers are 1 cm, 11 cm and 24 cm.

where two notable trends are observed. The first is grouped by the solid line oval where a negative relation includes sediment from 2-7 cm, 12-18 cm and 28 cm indicating increasing THg concentrations with increasing amounts of fine sediment. The second association is shown by the dotted line oval that contains sediments from 8-11 cm and <19 cm. There is also a major overlap between the two ovals that encloses samples from 12-18 cm and 28 cm. The outliers from these two groupings includes the surface at 1 cm, influenced by reactions at the sediment-water interface, 11 cm, associated with the 1911 sedimentation event and 24 cm, which cannot be accounted for with the available data. As others have indicated that clay minerals do not directly bind Hg, the process that may be reflected in the pattern seen here could be OM-mediated aggregation of fine inorganic sediment.

6.3.4 Total Mercury and Organic Matter

The association between organic matter and Hg is well studied. There is a strong regression (r^2=0.51, p<0.001) between the normalized reciprocals of THg and the Hydrogen Index (HI) (mg HC g^{-1} TOC^{-1}), where HI is a measure of S2/TOC determined by Rock Eval Pyrolysis (Fig 4.1l). Hg is known to have a strong association with the labile HI_{400} fraction and a weak relation with HI_b (Sanei et al., 2014). In this study, sediment from the surface to 8 cm and 14 cm were all detected below 400°C, making the remainder a part of HI_b (Fig 4.2).

A full profile biplot of the reciprocal of both HI and Hg (Fig 6.7) shows a clear separation of the HI_{400} and HI_b fractions. The affinity of Hg with the more labile HI_{400}

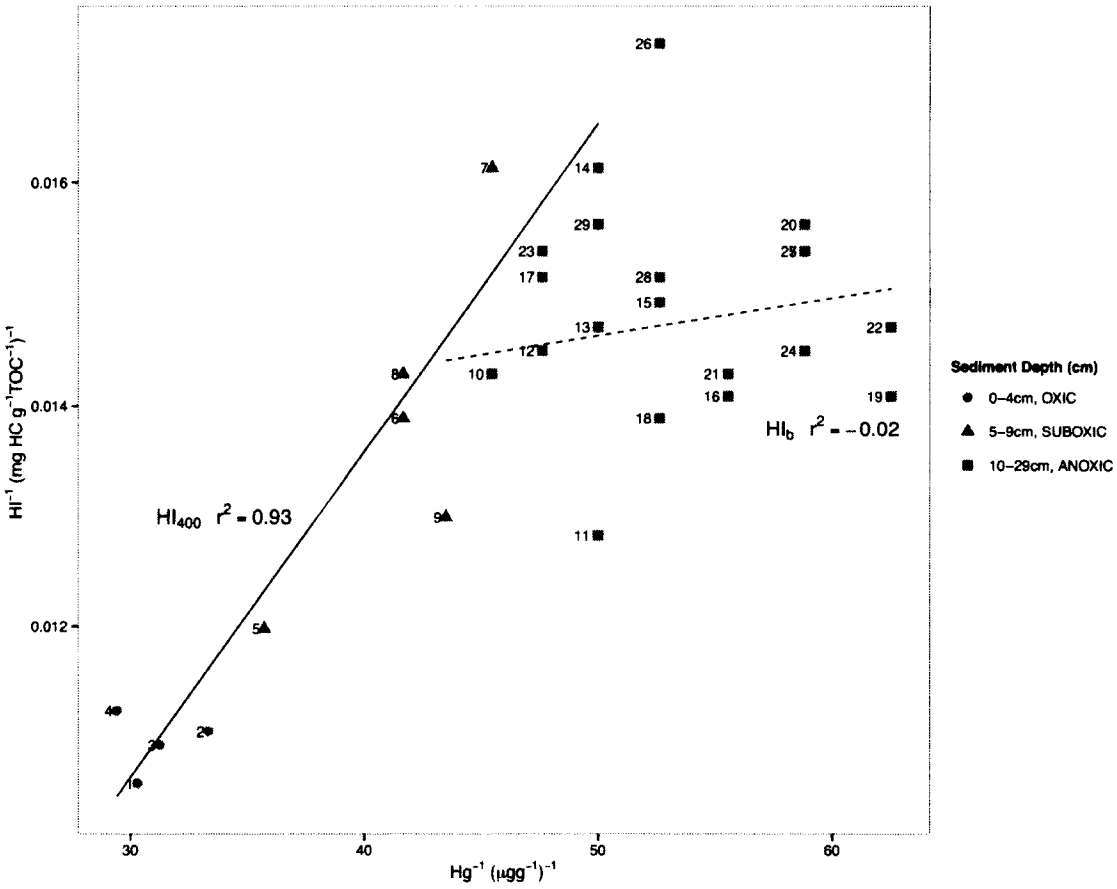

Figure 6.7: Biplot of Hg^{-1} and HI^{-1} with the regressions denoted for the strong relation between Hg and the HI_{400} (solid line) labile OM measurements and the degraded HI_b fractions (dotted line).

fraction is evident with its strong regression (r^2=0.93, p<0.0001, slope=2.9x10^{-4}), denoted by the solid line. The relation with the remaining sediments below 9 cm and excluding 14 cm are shown by the dotted line where no significant relation was found (r^2= -0.02, p>0.4).

These findings are expected and in line with Sanei et al.'s (2014) study that classifies Kusawa as a high-capacity binding lake due to its constantly strong correlation between HI_{400} and THg. Lakes with Hg-HI slopes >1 are considered low Hg binding capacity lakes where the input of Hg exceeds the available binding capacity of labile OM. This indicates

that although there are very low levels of OM and Hg at Kusawa, there is still sufficient OM available to scavenge the low Hg influxes from the water column and deliver it to the bottom sediments. This finding also suggests that any small increase in Hg may rapidly overwhelm the system resulting in increased amounts of available Hg in the water column (Sanei et al., 2014).

6.3.5 Total Mercury and Total Bacteria

To investigate patterns which could provide further insight to the various redox-driven reactions occurring down the core, Figure 6.8 is presented to depict the interaction between 1/Hg and Log(Tbac), where a three possible associations are observed. First, the surface sediments to 5 cm have a weak and steep positive trend. The second interaction, depicted by the solid line oval includes sediments associated with suboxic and anoxic zones from 6-15 cm, 26 cm and 28-29 cm. Here the concentration of bacteria decreases, as does the concentration of Hg. It is assumed that the decreases are related to downcore microbial redox interactions and loss of MeHg to the pore water although this was not directly measured. The third interaction occurs in the sediments below 11 cm and excluding 20-22 cm where a tight association between increasing Tbac and decreasing Hg is observed by the dotted line oval.

One interesting observation is that the relation between Hg and Tbac depicts a similar pattern observed in Figure 6.6, the biplot between Hg and % fine silt. It is proposed

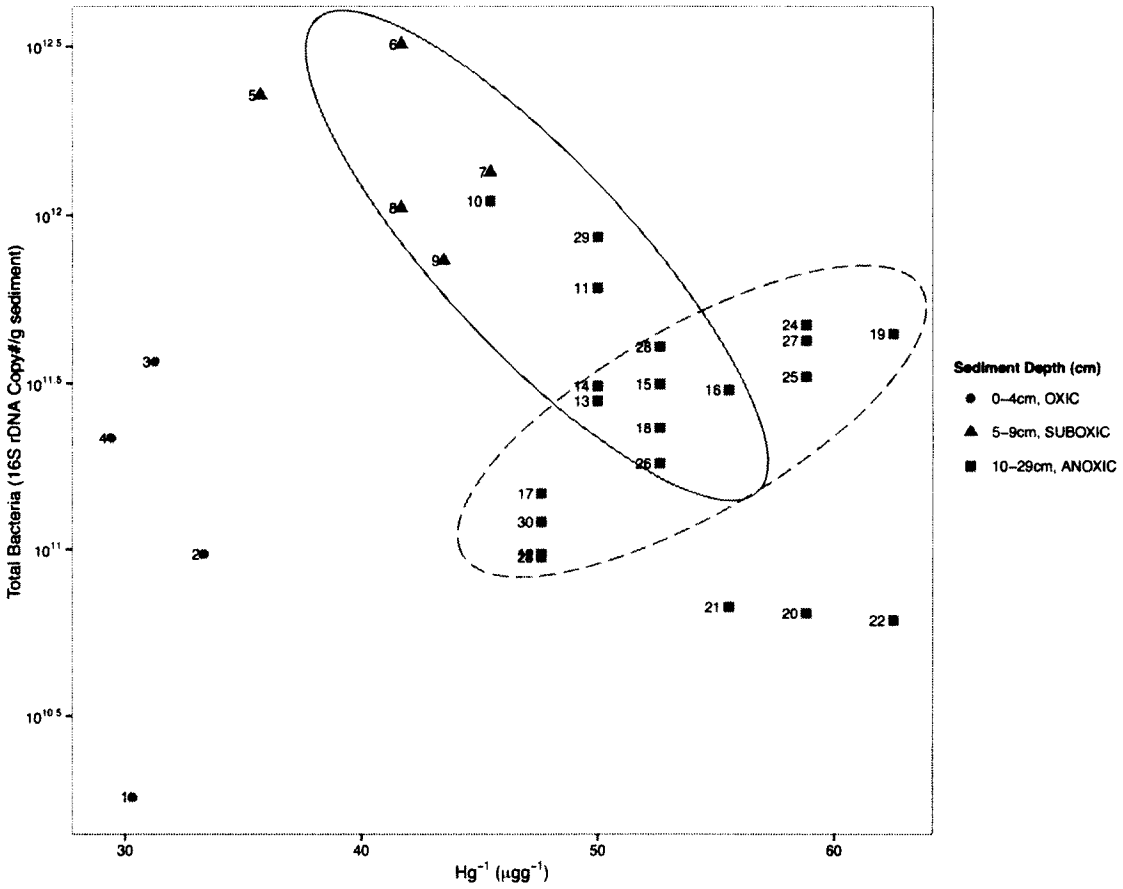

Figure 6.8: Biplot of 1/Hg association with Log(Total bacteria). The sediments from 1-5 cm show a steep positive relation at the left of the graph. The solid line oval includes sediments where a negative relation between Hg and Tbac for samples from 6-18 cm and 26-29 cm. The dotted oval contains samples from below 12 cm. Samples from 20-22 cm are considered outliers from these trends.

that these interactions are influenced by three different redox reaction regimes: (1) the steep positive relation in the near surface oxic sediments corresponds to recently deposited sediment-OM-bacterial-Hg aggregates formed in the water column, (2) a downcore dependent negative trend through the suboxic zone and oxic/anoxic transition boundary associated with microbial redox reactions and (3) the lower anoxic sediments where Hg has a weak relation with both bacteria and sediment that is independent of core depth. The

samples from 20-22 cm do not fit into any of these redox regimes and cannot be accounted for with the available data. These trends are suggestions based on correlation and cannot be verified with the available data.

6.3.6 Total Mercury and Sulfur-Metabolizing Bacteria

The final explanatory variable to describe the presence and cycling of Hg in the bottom sediment of Kusawa Lake is its interaction with SMB. The log(Ratio) was compared to 1/Hg in two separate biplots in Figure 6.9. The top panel (Fig 6.9a) includes sediments from the oxic (denoted by the solid oval) and suboxic (denoted by the dotted oval) zones. The lower sediments observed in Figure 6.9b are scattered and exhibit no evident relation. There is a distinct redox-dependent separation of the top 10 cm that complements earlier suggestions that the near surface sediments consist of recently deposited sediment-OM-Hg-bacterial aggregates followed by redox driven associations through the suboxic zone. Again though, these inferences are based on visual pattern and correlation and further study is required to verify these proposed trends. Recall from Figure 5.7 that sediments from 8-9 cm house *Syntrophobacteraceae* sp. that require high sulfate, anoxic conditions, which in turn are favourable for Hg-methylation. Therefore, the most probable depth for SRB-mediated Hg-methylation and demethylation is at the oxic/anoxic boundary from 8-9 cm. Though, no species from known SRB Hg-methylating orders were detected. Overall, the results suggest that conditions are not favourable for Hg-methylation by SRB as there are no obvious Hg-SMB interactions and no known Hg-methylators were detected.

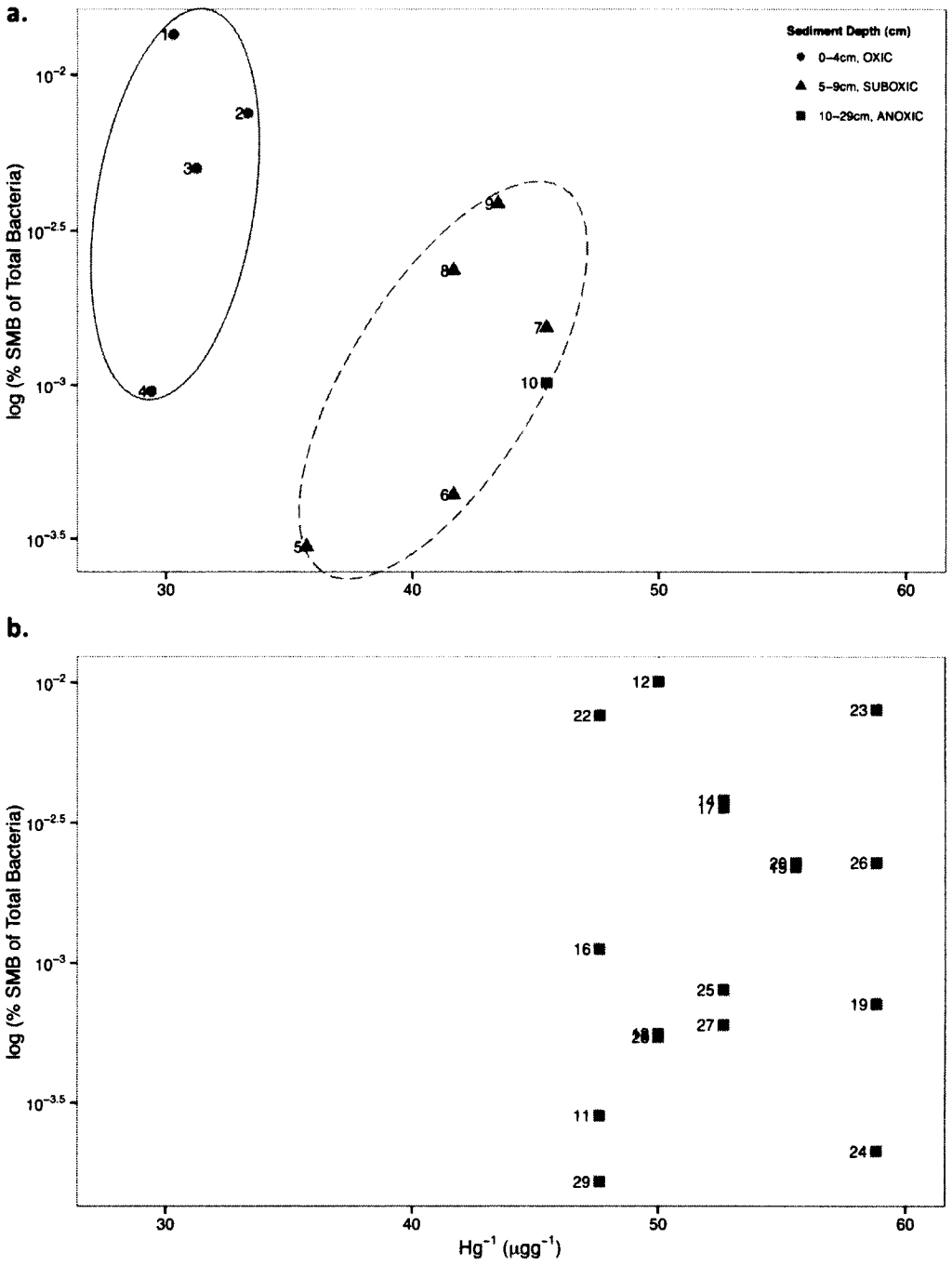

Figure 6.9: Biplot of log(%SMB) vs. 1/Hg where, a: depicts the separation of the oxic and anoxic zones in the top 10 cm, and b: shows the lack of structure within the anoxic sediments from below 11 cm.

6.3.7 Summary of Sediment, Organic Matter and Bacterial Interactions with Mercury

There are several factors that appear to control mercury in Kusawa Lake sediments:

- The concentration of THg is very low in the sediment record.
- THg is strongly correlated with $S2_{400}$ characterizing Kusawa as a high-capacity binding lake,
    - therefore, any increase in THg, without a concomitant increase in algal OM could overwhelm the OM-binding capacity and lead to increased Hg availability in the water column for bioaccumulation.
- Both Tbac and fine silt have a similar redox driven correlation to THg where three proposed trends are noted:
    1. a positive association with recently deposited near surface sediments, suggesting that sediment-bacteria-Hg interactions are established in the water column, presumably as floc formations;
    2. a negative trend through the suboxic zone where it is proposed that bacteria-mediated breakdown of sediment-OM flocs result in the release of Hg;
    3. a weak relation in sediments below 12 cm, indicating loss of interaction due to breakdown of sediment-OM flocs.
- There is a very low %SMB of total bacteria and no known Hg-methylating SRB were detected indicating that Hg-methylation by SRB in the sediments is likely minimal.
    - Subarctic, oligotrophic and orthograde lake conditions are unfavourable for SMB and SRB-mediated Hg-methylation.

6.4 Mercury in Kusawa Lake and the Implications of Climate Change

There are several measurable changes and potential risks associated with climate change in the Subarctic. In regards to Kusawa Lake, the major impacts will be as a result of annual warmer temperatures and varying levels of snow and rainfall (Environment Yukon, 2014).

6.4.1 Increased Allochthonous Sediment and Organic Matter

Increases in temperature and precipitation will inherently cause an increase in sediment transport from a range of origins. Glacial melt is expected to increase and release large concentrations of fine sediment as well as anthropogenic contaminants such as Hg, nutrients and other heavy metals. Similarly, the increased rates of permafrost melt will also release stored heavy metals and greenhouse gases such as methane and carbon dioxide. Furthermore, the loss of permafrost will cause land instability leading to erosion, land and mudslides and increased instability of torrent systems (Walsh, 2005; AMAP, 2011). All of this along with the expected higher rates of discharge and water levels will result in the increased distribution and diversity of both aquatic and terrestrial OM throughout Kusawa Lake.

6.4.2 Increased Primary Productivity

Longer ice-free seasons and warmer winter and summer temperatures will enable higher rates of aquatic primary productivity. Since algal scavenging of Hg to the lake sediments has been demonstrated as the principle control of Hg delivery (Sanei et al., 2014), warmer temperatures will likely result in an increase in stored Hg and in MeHg available for bioaccumulation in the water column. If more OM were available in the lake system it would decrease the control OM has on Hg by becoming a low Hg-binding capacity binding lake (Sanei et al., 2014). Another outcome is that increased primary productivity could promote environments more closely related to meso-eutrophic systems where the sediments may be fully anoxic with an oxygen clinograde (oxygen depleted in the lower water column), allowing Hg to be methylated within the water column and the sediments.

6.4.3 SRB Community Composition

A study by Robador et al. (2009) assessed the *in situ* adaptation of psychrophilic SRB from the Arctic Ocean and mesophilic temperate SRB to long-term temperature changes. The result was that the Arctic SRB communities incubated for one year at 20°C maintained the capacity to reduce sulfate at 0°C and also gained sulfate reduction ability at warmer temperatures. Concurrently, temperate SRB were subject to the same conditions and never acquired the ability to efficiently reduce sulfate at 0°C. These findings indicate that psychrophilic bacteria are more readily adaptable to changing climates than temperate

bacteria. This is likely due to the extreme shifts in seasonal temperatures in cooler compared to more temperate climates. Robador et al. (2009) also found that there was more diversity in the community composition of Arctic SRB compared to temperate and during incubation certain populations from the Arctic samples declined while others increased, however no populations were completely lost. They concluded that Arctic SRB select for organisms that are more readily adapted to the current temperature.

From this study, it can be assumed that in Kusawa Lake SRB communities are adapted to both winter and summer temperatures and in the event of ongoing warming the most efficient species of SRB will be selected for. If the lake becomes more eutrophic the level of available sulfate increases it could promote population increases of Hg-methylating SRB and as a result, MeHg production will increase.

Chapter 7 Conclusion

This thesis has provided background and insight into the biogeochemical sediment process of Hg cycling by SMB in Subarctic oligotrophic Kusawa Lake, Yukon. It also contributes to the limited literature regarding SMB at Subarctic latitudes and establishes a baseline for use in future studies. Each chapter of this work expands on the previous to develop a sediment-based concept of OM and SMB-mediated Hg-cycling from its delivery to the bottom sediments to either its storage as inorganic Hg or release to the water column as bioaccumulating MeHg.

Chapter 2 introduced Kusawa Lake, its history, climate and hydrology. Chapter 3 provided an overview of the lake's limnology and sedimentology of the core sites to elucidate the historic and contemporary sediment processes. One major sedimentation event was observed at 11 cm sediment depth, which was dated to 1911. As well, estimates of the redox zones were established using trace metal profiles, which provided guidance for interpretation of OM and bacterial processes. Chapter 4 presented OM composition and source as determined from Rock Eval Pyrolysis. $S2_{400}$ OM consisting of recently deposited algal cell wall material was detected from the surface to 8 cm and 14 cm depth. All remaining samples grouped as $S2_b$ and consisted of more refractory compounds. All of the samples were from autochthonous sources with the exception of 7 cm (unknown) and 26 cm, the proposed White River Ash layer. One major OM accumulation event was detected from 14-15 cm and lack of direct evidence restricted identification of its source.

Chapter 5 introduced the downcore distribution of Tbac and SMB along with the SMB diversity. There was an extremely low ratio of SMB to Tbac likely associated with oligotrophic Subarctic lake conditions. Four distinct layers of SMB were identified: (i) 1 – 5 cm: SOB (*Deltaproteobacteria,* unknown; (ii) 1 – 7 cm: SOB and SRB (*Deltaproteobacteria, Syntrophaceae*); (ii) 8 – 9 cm: SRB (*Deltaproteobacteria, Syntrophobacteraceae*) and; (iii) below 7 cm: SRB (uncultured clones and *Firmicutes, Desulfotomaculum*). No known Hg-methylators were detected, however, species that operate in syntrophy were identified. This suggests that because the SMB are metabolizing under low sulfate conditions, syntrophic species are selected for to enable ongoing cycling of SO_4^{2-} and H_2S across the oxic/anoxic boundary.

These lines of evidence were used to draw conclusions about Hg transport and fate in the lake sediments, which are summarized in Figure 7.1. Overall, Kusawa Lake is oligotrophic, has a low rate of primary productivity and OM, which strongly influences the controls of Hg-methylation. The cycle of Hg in Kusawa Lake begins in the water column, where it binds with labile OM associated with fine sediment and bacterial aggregates. This is a strongly influential control as Kusawa is considered a high Hg-binding capacity lake, due to the low levels of both Hg and OM. These aggregates or flocs settle to the lake bottom sediments. There is a very low percent of SRB present and no known Hg-methylating SRB were detected, therefore, opportunities for SRB Hg-methylation are assumed to be minimal. Methylation is occurring at some location within the lake ecosystem as elevated levels were

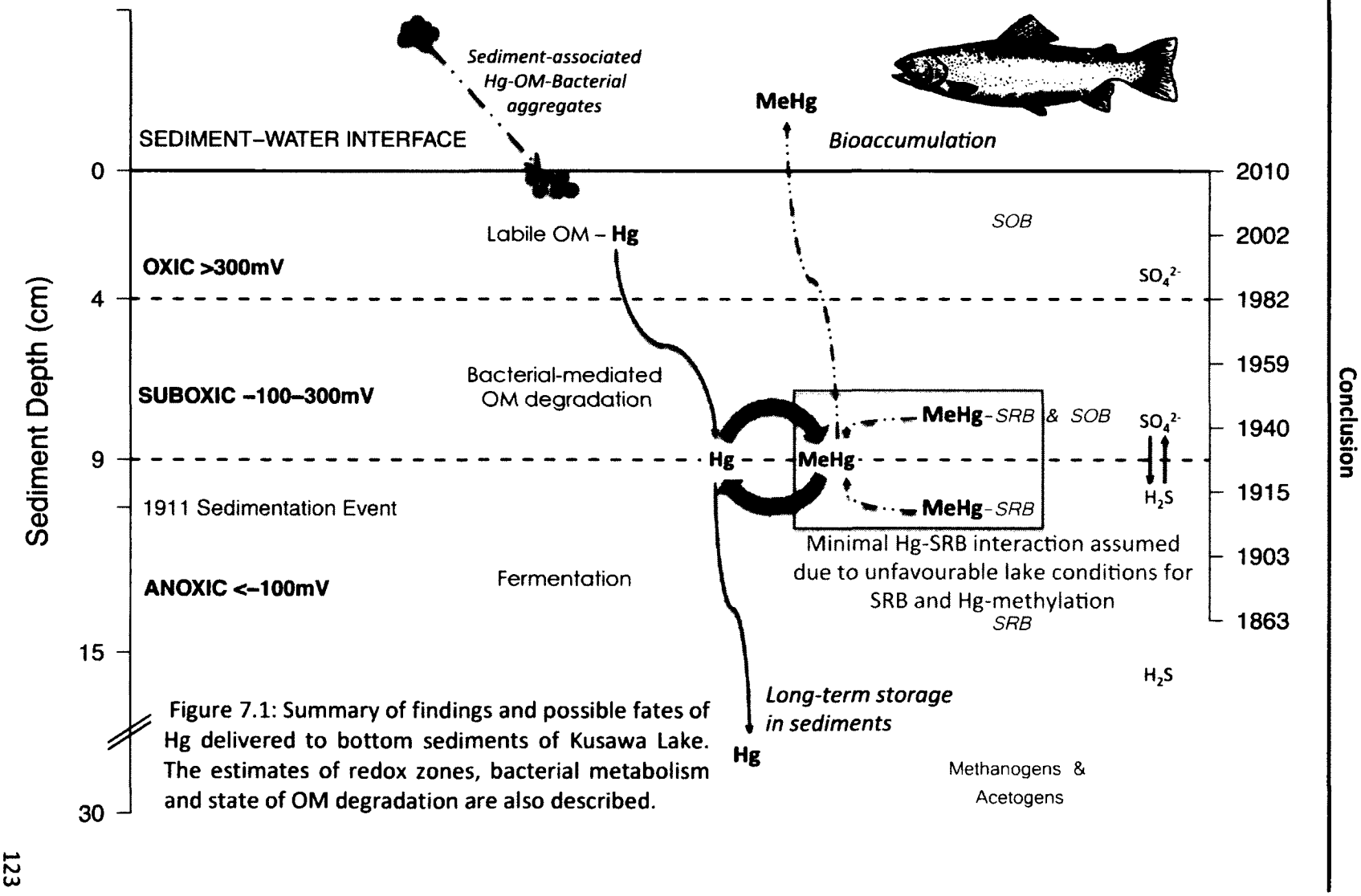

Figure 7.1: Summary of findings and possible fates of Hg delivered to bottom sediments of Kusawa Lake. The estimates of redox zones, bacterial metabolism and state of OM degradation are also described.

detected in the trout. The most likely location for methylation in the bottom sediments would be at the oxic/anoxic transition boundary, located at 8-9 cm depth. There, particulate Hg can be dissolved in association with sulfide and cross SRB (or some other methylating bacteria) cell walls, be methylated, excreted and diffuse through the pore water to the water column where it readily enters the food chain.

Overall, the major factors regulating the potential for Hg-methylation by SRB in Subarctic Kusawa Lake are:

1. the rate of primary productivity and water column concentration of sediment-associated algal-derived OM that can scavenge Hg and transport it to the sediments,
2. the concentration of mercury in the water column for scavenging by algal-derived OM and in the sediments for availability to SRB at the oxic/anoxic boundary and,
3. the diversity and concentration of SRB, where more eutrophic lake conditions are likely needed to promote SMB populations and select for SRB Hg-methylators.

7.1 Limitations and Future Work

As this study was completed in conjunction with a larger Hg research project at Kusawa, many of the limitations are related to the core sampling procedures that could have been modified to allow for analysis of additional variables and sampling sites.

The following is a list of limitations to this study and suggestions for future work:

- The sample site location appears to have been influenced by less regular sediment delivery than initially assumed, therefore future cores should be taken closer to the Stern et al. (2009) 2005 core,
- Only a single core was collected for the bacterial component of the study, another core from higher in the basin within a more eutrophic ecosystem, such as a wetland, could provide better detail regarding the mechanism of Hg-methylation,
- No sulfate reduction rates or sulfate or sulfide measurement were taken, which would have helped provide further insight to SMB metabolism,
- Sediment-associated methymercury levels were below the limit of detection and no pore water measurements were taken, which would have provide a better understanding of sediment-pore water exchanges, and
- Only SMB distribution and diversity was assessed. Detection of other known Hg-methlyating microbes such as iron-reducing bacteria would have been beneficial.

One suggestion for a future study would be to collect a core from a more eutrophic system in the upper reaches of the Takhini River basin and another core from the current sample site for comparison. Along with some of the measurements used in this study, *in situ* comparisons of sulfate reduction rates, mercury methylation rates, Hg-OM binding and interactions of stored inorganic Hg would help contribute to the understanding of the fate of Hg in Subarctic ecosystems.

Overall, this work contributes to the understanding of the controls of Hg transport and potential for SRB-mediated methylation in the sediments. More specifically it elucidates the microbial distribution and diversity that play a role in Hg processing, which are factors that have not been adequately studied at Subarctic latitudes. As well, identifying factors presumed to control Hg processes in Kusawa Lake will help infer and identify climate change implications and aid in assessing the impacts of Hg inputs from distant industrial sources, particularly Asia. Finally, this work will contribute to ensuring the environmental safety for Yukon people and future Yukon generations.

References

AMAP. (2011) *Snow, Water, Ice and Permafrost in the Arctic (AWIPA): Climate Change and the Cryosphere*. Arctic Monitoring and Assessment Programme. ISBN-978-82-7971-071-4. Oslo, Norway.

Applied Biosystems (2006) *SYBR® Green PCR Master Mix and RT-PCR reagents*. Applied Biosystems, Carlsbad, CA.

Applied Biosystems. (2010) TaqMan ® and SYBR ® Green Chemistries [online]. Available from http://www.appliedbiosystems.com/absite/us/en/home/applications-technologies/real-time-pcr/taqman-and-sybr-green-chemistries.html [cited June 10, 2014]. Applied Biosystems by Life Technologies.

Barton LL & Hamilton WA (2007) *Sulfate-Reducing Bacteria: Environmental and Engineering Systems*. Cambridge University Press, New York, U.S.A.

Benoit JM, Gilmour CC, Mason RP & Heyes A (1999) Sulfide controls on mercury speciation and bioavailability to methylating bacteria in sediment pore waters. *Environ Sci Technol.* **33:** 951-957.

Bio-Rad (2014) Mini-Opticon Real-Time PCR System | Life Science Education | Bio-Rad [online]. Available from http://www.bio-rad.com/en-ca/product/miniopticon-real-time-pcr-system. [cited May 28, 2014]. Bio-Rad Laboratories, Inc.

Brankatschk R, Bodenhausen N, Zeyer J & Bürgmann H (2012) Efficiency of real-time qPCR depends on the template: a simple absolute quantification method correcting of qPCR efficiency variations in microbial community samples. *App Environ Microb.* **78**: 4481-4489.

Brune DC (1995) Sulfur compounds as photosynthetic electron donors. *Anoxygenic Photosynthetic Bacteria.* (Blankenship RE, Madigan MT & Bauer CE, eds). Kluwer Academic Publishers, Dordrecht, Netherlands.

Bruschi M, Barton LL, Goulhen F, Plunkett RM (2007) Enzymatic and genomic studies on the reduction of mercury and selected metallic oxyanions by sulphate-reducing bacteria. *Sulfate-Reducing Bacteria: Environmental and Engineering Systems* (Barton LL & Hamilton WA, eds). Cambridge University Press, New York, NY.

Cao H, Wang Y, Lee OO, Zeng X, Shao Z, Qian P-Y (2014) Microbial sulfur cycle in two hydrothermal chimneys on the Southwest Indian Ridge. *mBio.* **5**(1): 1-11.

Carrie J, Sanei H & Stern G (2012) Standardization of Rock-Eval Pyrolysis for the analysis of recent sediments and soils. *Org Geochem.* **46:** 38-53.

Castro H, Reddy KR & Ogram A (2002) Composition and function of sulfate-reducing prokaryotes in eutrophic and pristine areas of the Florida Everglades. *App Environ Microb.* **68**(12): 6129-6137.

Catalan J, Pla-Rabés S, Wolfe AP, Smol JP, Rühland KM, Anderson NJ, Kopácek J, Stuchlík E, Schmidt R, Koinig KA, Camarero L, Flower RJ, Heiri O, Kamenik C, Korhola A, Leavitt PR, Psenner R, Renberg I (2013) Global change revealed by paleolimnological records from remote lakes: a review. *J of Paleolimnol.* **49**(3): 513-535.

Chakraborty K, Finkelstein SA, Desloges JR & Chow NA (2010) Holocene paleoenvironmental changes inferred from diatom assemblages in sediments of Kusawa Lake, Yukon Territory, Canada. *Quaternary Res.* **74:** 15-22.

Champagne and Aishihik First Nation (CAFN) (2010) *Dän Kéyi Kwändür: Stories From Our Country.* Haines Junction, Yukon. **ISBN 0-9731315-1-9.**

Chan L (2011) *Inuit Health Survey 2007-2008: Contaminant Assessment in Nunavut*. Nunavut Steering Committee of the International Polar Year, Inuit Health Survey. Iqaluit, NU.

Chételat J, MacDonald R, Munthe J, Pacyna J, Sundseth K, Wang J & Wilson S (2012) Chapter 2: Sources, Processes and Pathways. *Canadian Arctic Contaminants Assessment Report III 2012* (Chételat J & Braune B, eds). Northern Contaminants Program, Ottawa, ON.

Chok NA (2010) *Pearson's versus Spearman's and Kendall's Correlation Coefficients for Continuous Data.* MSc Thesis. University of Pittsburg, Pittsburg, PA.

Chow NA (2009) *Late glacial and Holocene environmental change inferred from sedimentary archives of Kusawa Lake, boundary range mountains, Yukon Territory, Canada.* MSc. Thesis. University of Toronto, Toronto, ON.

Church M & Gilbert R (1975) Pro-glacial fluvial and lacustrine environments. *Glaciofluvial and Glaciolacustrine Sedimentation* (Jopling AV, McDonald BC, eds). Society of Economic Paleontologists and Mineralogists Special Publication. **23:** 22-100.

CodonCode Corporation. Sequence Assembly and Alignment with CodonCode Aligner [online]. Available from http://www.codoncode.com/aligner/. [cited May 28, 2014]. CodonCode Corporation.

Coleman ML, Hedrick DB, Lovely DR, White DC, Pye K (1993) Reduction of Fe(III) in sediments by sulphate-reducing bacteria. *Nature*. **361**: 436-438.

Cooke CA, Balcom PH, Biester H & Wolfe AP (2009) Over three millennia of mercury pollution in the Peruvian Andes. *PNAS*. **106**(22): 8830-8834.

Cypionka H (2000) Oxygen respiration by *Desulfovibrio* species. *Annu Rev Microbiol.* **54**: 827-848.

Dahl C, Engels S, Pott-Sperling AS, Schulte A, Sander J, Lübbe Y, Deuster O & Brune DC (2005) Novel genes of the *dsr* gene cluster and evidence for close interaction of Dsr proteins during sulfur oxidation in the phototrophic sulfur bacterium *Allochromatium vinosum. J Bacteriol.* **187**(4): 1392-1404.

Dhillon A, Teske A, Dillon J, Stahl DA & Sogin ML (2003) Molecular characterization of sulfate-reducing bacteria in the Guaymas Basin. *App Environ Microb.* **69**(5): 2765-2772.

Dickson C (2008) Regionally relevant health risk assessments for mercury levels in fish. *Yukon Synopsis of Research Conducted Under the 2007-2008 Northern Contaminants Program.* **ISBN 978-0-662-06025=3:** pp. 20-25.

Dodson SI (2005) *Introduction to Limnology.* Kemp, M.J., McGraw-Hill Companies Inc, New York, NY.

Dolla A, Fournier M & Dermoun Z (2006) Oxygen defense in sulfate-reducing bacteria. *J Biotechnol.* **126**: 87-100.

Donohue I, Molinos JG (2009) Impacts of increased sediment loads on the ecology of lakes. *Biol Rev.* **84**: 517-531.

Durnford D, Dastoor A, Figueras-Nieto D & Ryjkov A (2010) Long range transport of mercury to the Arctic and across Canada. *Atmos Chem Phys.* **10:** 6063-6086.

Eisbacher GH & Clague JJ (1984) *Destructive mass movements in high mountains: hazards and management.* Geological Survey of Canada. Paper 84-16: pp 230.

Ekstrom EB, Morel FMM & Benoit JM (2003) Mercury methlayion independent of the actyle-coenzyme A pathway in sulfate-reducing bacteria. *App Environ Microb.* **69:** 5414-5422.

Elsen S, Efthymiou G, Peteinatos P, Diallinas F, Kyritsis P & Moulis J (2010) A bacteria-specific 2[4Fe-4S] ferredoxin is essential in *Pseudomonas aeruginosa. BMC Microbiol.* **10:** 271.

Environment Canada (2014a) Canadian Climate Normals 1981-2010 Station Data – Whitehorse [online]. http://climate.weather.gc.ca/ climate_normals /results_1981 *2010-*e.html?stnID=1617&lang=e&dCode =0&StationName=WHITEHORSE &SearchType=Co [cited Apr 15, 2014].

Environment Canada (2014b) Historical Hydrometric Data – WaterOffice – Environment Canada [online]. http://wateroffice.ec.gc.ca/mainmenu/historical_data_index_e.html [cited Apr 20, 2014].

Environment Yukon (2007, 2008 and 2010) Yukon Snow Survey Bulletin & Water Supply Forecast: May 1 - 2007, 2008 and 2010. Whitehorse, Yukon. **ISSN 1705-883X**

Environment Yukon (2010) *Yukon Freshwater Fishes*. Government of Yukon. **ISBN 978-1-55362-461-5.** Whitehorse, Yukon.

Environment Yukon (2011) *Yukon Water: An Assessment of Climate Change Vulnerabilities.* Government of Yukon. **ISBN: 978-1-55362-516-2**. Whitehorse, Yukon.

Environment Yukon (2014) *Yukon State of the Environment: A Report on Environmental Indicators – 2014*. Government of Yukon. Whitehorse, Yukon.

Evans MS, Muir D, Lockhart WL, Stern G, Ryan M & Roach P (2005) Persistent organic pollutants and metals in the freshwater biota of the Canadian Subarctic and Arctic: an overview. *Sci Total Environ.* **351-352**: 94-147.

Favorgen Biotech (2009*) FavorPrep Genomic DNA Clean-up Kit Manual*. Favorgen Biotech, Ping-Tung, Taiwan.

Fitzgerald WF & Lamborg CH (2005) Geochemistry of Mercury in the Environment. *Treatise on Geochemistry* (Sherwood Lollar B, Holland HD & Turekian KK, eds). Elsevier.

Freidrich CG, Rother D, Bardischewsky F, Quentmeier A & Fischer J (2001) Oxidation of reduced inorganic sulfur compounds by bacteria: emergence of a common mechanism? *App Environ Microb.* **67**(7): 2873-2882.

Frostegard AS (1999) Quantification of bias related to the extraction of DNA directly from soils. *App Environ Microb.* **65**: 5409-5420.

Gilbert R & Desloges JR (2005) The record of glacial Lake Champagne in Kusawa Lake, southwestern Yukon Territory. *Can J Earth Sci.* **42:** 2127-2140.

Gilmour CC, Elias DA, Kucken AM, Brown SD, Palumbo AV, Schadt CW & Wall JD (2011) Sulfate-reducing bacterium *Desulfovibrio desulfricans* ND132 as a model for understanding bacterial mercury methylation. *App Environ Microb.* **77**(12): 3938-3951.

Gilmour CC, Henry EA & Mitchell R (1992) Sulfate stimulation of mercury methylation in freshwater sediments. *Environ Sci Technol.* **26**(11): 2281-2287.

Giovannoni SJ & Stingl U (2005) Molecular diversity and ecology of microbial plankton *Nature.* **437**: 343-348.

Global Mercury Observation System (GMOS) (2012) GEOSS Science and Technology Porfolio [online]. Available from http://www.geo-tasks.org/geoss_portfolio/health_gmos.php [cited June 10, 2014]. Group on Earth Observations. Geneva, Switzerland.

Goulet RR, Holmes J, Page B, Poissant L, Siciliano SD, Lean DRS, Wang F, Amyot M & Tessier A (2007) Mercury transformations and fluxes in sediments of a riverine wetland. *Geochim Cosmochim Ac.* **71:** 3393-3406.

Gregersen LH, Bryant DA, Frigarrds N-U (2011) Mechanism and evolution of oxidative sulfur metabolism in green sulfur bacteria. *Front Microbiol.* **2**(116): 1-14.

Gudasz C, Bastviken D, Premke K, Steger K & Tranvik LJ (2012) Constrained microbial processing of allochthonous organic carbon in boreal lake sediments. *Liminol Oceanogr.* **57**(1): 163-175.

Hammerschmidt CR, Fitzgerald WF, Lamborg CH, Balcom PH & Tseng CM (2006) Biogeochemical cycling of methylmercury in lakes and tundra watersheds of arctic Alaska. *Environ Sci Technol.* **40:** 1204-1211.

Hare AA, Kuzyk ZZA, Macdonald RW, Sanei H, Barber D, Stern GA & Wang F (2014) Characterization of sedimentary organic matter in recent marine sediments from Hudson Bay, Canada by Rock-Eval pyrolysis. *Org Geochem.* **68**: 52-60.

Hare PG, Greer S, Gotthardt R, Farnell R, Bowyer V, Schweger C & Strand D (2004) Ethnographic and archaeological investigations of alpine ice patches in Southwest Yukon, Canada. *Arctic.* **57:** 260-272.

Health Canada. (2009) It's your health - Mercury and human health [online]. Available from http://www.hc-sc.gc.ca/hl-vs/iyh-vsv/environ/merc-eng.php. [cited June 10, 2014]. Government of Canada. Ottawa, ON.

Hesterburg D, Chou JW, Hutchinson KJ, Sayers DE (2001) Bonding of Hg(II) to reduced organic sulfur in humic acid as affected by S/Hg ratio. *Environ Sci Technol.* **35**: 2741-2745.

Hines ME, Faganeli J, Adatto I & Horvat M (2006) Microbial mercury transformations in marine, estuarine and freshwater sediment downstream of the Idrija Mercury Mine, Slovenia. *App Geochem.* **21**:1924-1939.

Hockin SL & Gadd GM (2007) Bioremediation of metals and metalloids by precipitation and cellular binding. *Sulfate-Reducing Bacteria: Environmental and Engineering Systems* (Barton LL & Hamilton WA, eds). Cambridge University Press, New York, NY.

Hogg EHT & Wein RW (2005) Impacts of drought on forest growth and regeneration following fire in southwestern Yukon, Canada. *Can J Forest Res.* **35:** 2141-2150.

Hokenbrink C, Ocón S, Mellerup A, Otakit H & Frigaard N (2011) Sulfur globule oxidation in green sulfur bacteria is depending on the dissimilatory sulfite reductase system. *Microbiology.* **157**: 1229-1239.

Hollweg TA, Gilmour CC & Mason RP (2009) Methylmercury production in sediments of Chesapeake Bay and the mid-Atlantic continental margin. *Mar Chem.* **114**: 86-110.

Holmer M & Storkholm P (2001) Sulphate reduction and sulphur cycling in lake sediments: a review. *Freshwater Biol.* **46**: 431-451.

Hughes OL, Campbell RB, Muller JE & Wheeler JO (1969) *Glacial limits and flow patterns, Yukon Territory, south of 65 degrees North Latitude.* Geological Survey of Canada. Paper 68-34.

Invitrogen (2010a) *TOPO ® XL PCR Cloning Kit Manual.* Life Technologies, Carlsbad, CA.

Invitrogen (2010b) *Qubit™ dsDNA HS Assay Kit Manual.* Life Technologies, Carlsbad, CA.

Invitrogen (2010c) *Platinum ® Taq DNA Polymerase Manual.* Life Technologies, Carlsbad, CA.

Jackson LE, Ward B, Duk-Rodkin A & Hughes OL (1991) The last Cordilleran ice sheet in southern Yukon Territory. *Geogr phys quatern.* **45:** 341-354.

Janowicz JR (2010) Observed trends in the river ice regimes of northwest Canada. *Hydrol Res.* **41:** 462-470.

Janssens, M (2014) personal communication. Whitehorse, Yukon.

Jiang S, Liu X & Chen Q (2011) Distriubution of total mercury and methylmercury in lake sediments in Arctic Ny-Ålesund. *Chemosphere.* **83**: 1108-1116.

Joe-Strack J (2012) *Respect, Resilience and Prosperity: Recommendations for a Yukon Water Strategy.* Walter and Duncan Gordon Foundation. Toronto, ON.

Johnstone JF, Chaplin FS, Foote J, Kemmett S, Price K & Viereck L (2004) Decadal observations of tree regeneration following fire in boreal forests. *Can J Forest Res.* **34:** 267-273.

Jørgensen B (2000) Bacteria and marine biogeochemistry. *Marine Geochemistry* (Schultz HD & Zabel M, eds). Springer, Heidelberg, Germany.

Kaneko J, Hayashi T, Tanahashi M & Naganuma T (2007) Phylogenetic diversity and distribution of dissimilatory sulfite reductase genes from deep-sea sediment cores. *Mar Biotechnol.* **9**: 429-436.

Klein M, Friedrich M, Roger AJ, Hugenholtz P, Fishbain S, Abicht H, Blackall LL, Stahl DA & Wager M (2001) Multiple lateral transfers of Dissimilatory Sulfite Reductase genes between major lineages of Sulphate-reducing prokaryotes. *J of Bacteriol.* **183**:20 6028-6035.

Kondo R, Nedwell DB, Purdy KJ & de Queiroz Silva S (2004) Detection and enumeration of sulphate-reducing bacteria in estuarine sediments by competitive PCR. *Geomicrobiol J.* **21**: 145-157.

Krekeler D, Teske A & Cypionka H (1998) Strategies of sulphate-reducing bacteria to escape oxygen stress in a cyanobacterial mat. *FEMS Microbiol Ecol.* **25**: 89-96.

Kusawa Park (2014) Kusawa Park Steering Committee [online]. Available from www.kusawapark.ca [cited Feb 13, 2014].

Kuzyk G, Russell DE, Farnell RS, Gotthardt RM, Hare PG & Blake E (1999) In pursuit of prehistoric caribou on Thandlät, southern Yukon. *Arctic.* **52:** 214-219.

Laerd Statistics (2013) Spearmans' Rank-Order Correlation [online]. Available from https://statistics.laerd.com/statistical-guides/spearmans-rank-order-correlation-statistical-guide.php. [cited May 28, 2014]. Lund Research Ltd.

Lamborg CH, Engstrom DR, Fitzgerald WF & Balcom PH (2013) Apportioning global and non-global components of mercury deposition through ^{210}Pb indexing. *Sci Total Environ.* **448**: 132-140.

Lamborg CH, Fitzgerald WF, Damman AWH, Benoit JM, Balcom PH & Engstrom DR (2002) Modern and historic atmospheric mercury fluxes in both hemispheres: Global and regional mercury cycling implications. *Global Biogeochem Cy.* **16**(4): 1104.

Leloup J, Fossing H, Kohls K, Holmkvist L, Borowski C & Jørgensen B (2009) Sulfate-reducing bacteria in marine sediment (Aarhus Bay, Denmark): abundance and diversity related to geochemical zonation. *Env Microbio.* **11**(5): 1278-1291.

Leloup J, Loy A, Knab NJ, Borowski C, Wager M & Jorgensen BB (2007) Diversity and abundance of sulfate-reducing microorganisms in the sulfate and methane zones of a marine sediments, Black Sea. *Environ Microbiol.* **9**(1): 131-142.

Lopez-Gutierrez JC, Henry S, Hallet S, Martin-Laurent F, Cartroux G & Philippot L (2004) Quantification of a novel group of nitrate-reducing bacteria in the environment by real-time PCR. *J Microbiol Meth.* **57**: 399-407.

Lowey GW (2002) Sedimentary processes of the Kusawa Lake torrent system, Yukon, Canada, as revealed by the September 16, 1982 flood event. *Sediment Geol.* **151:** 293-312.

Loy A, Küsel K, Lehner A, Drake HL & Wagner M (2004) Microarray and functional gene analyses of sulfate-reducing prokaryotes in low-sulfate, acidic fens reveal co-occurrence of recognized genera and novel lineages. *App Environ Microbiol.* **70**(12): 6998-7009.

Madigan MT, Martinko JM & Parker J (2003*) Brock Biology of Microorganisms*. Prentice Hall, Pearson Education Canada Ltd., Toronto, ON.

Manske A, Glaeser J, Kuymers MMM and Overmann J. (2005). Physiology and phylogeny of Green Sulfur Bacteria forming a monospecific phototrophic assemblage at a depth of 100 meters in the Black Sea. *App Environ Microbiol.* **71**(12): 8049-8060.

Mason RP & Lawrence AL (1999) Concentration, distribution and bioavailability of mercury and methylmercury in sediments of Baltimore harbour and Chesapeake Bay, Maryland, USA. *Environ Toxicol.* **18**(11): 2438-2447.

Merritt KA & Amirbahman A (2009) Mercury methylation dynamics in estuarine and coastal marine environments - A critical review. *Earth-Sci Rev.* **96**: 54-66.

MO BIO Laboratories Inc. (2009*) Power Soil ® DNA Isolation Kit Manual.* Carlsbad, CA, U.S.A.

MO BIO Laboratories Inc. (2010*) UltraClean® Microbial DNA Isolation Kit Manual.* MO BIO Laboratories Inc., Carlsbad, CA, USA.

Mussmann M, Ishii K, Rabus R & Amann R (2005) Diversity and vertical distribution of cultured and uncultured *Deltaproteobacteria* in an intertidal mud flat of the Wadden Sea. *Environ Microbiol.* **7**: 405-18.

Muyzer G & Stams AJ (2008) The ecology and biotechnology of sulfate-reducing bacteria. *Nat Rev Microbiol.* **6**: 441-454.

Ng C, DeMaere MZ, Williams TJ, Lauro FM, Raftery M, Gibson J.A.E, Andrews-Pfannkoch C, Lewis M, Hoffman JM, Thomas T, Caviccioli, R. (2010). Metaproteogenomic analysis of a dominant green sulfur bacterium from Ace Lake, Antarctica. *ISME J.* **4**: 1002-1019.

Norici A, Hell R & Giordano M (2005) Sulfur and primary productivity in aquatic environments: an ecological review. *Photosyn Res* **86:** 409-417.

Omelchenko MV, Makarova KS, Wolf YI, Rogozin IB & Koonin EV (2003) Evolution of mosaic operons by horizontal gene transfer and gene displacement in situ. *Genome Biol.* **4**: R55.

Ouddane B, Mikac N, Cundy AB, Quillet L & Fischer JC (2008) A comparative study of mercury distribution and methylation in mudflats from two macrotidal estuaries: The Seine (France) and the Medway (United Kingdom). *Appl Geochem.* **23**: 618-631.

Outridge PM, Sanei H, Stern GA, Hamilton PB & Goodarzi F (2007) Evidence for control of mercury accumulation rates in Canadian high arctic lake sediments by variations in aquatic primary productivity. *Environ Sci Technol.* **41:** 5259-5265.

Pacyna EG, Pacyna JM, Sundseth K, Munthe J, Kindbom K & Wilson S (2010) Global emission of mercury to the atmosphere from anthropogenic sources in 2005 and projections to 2020. *Atmos Environ.* **44**(20): 2487-2499.

Panteleyev, A. (2005) *Stinite veins and disseminations I09.* Yukon Geological Survey, Mineral Deposit B.C. Profiles and British Columbia Geological Survey. Whitehorse, Yukon.

Pester M, Knorr K, Friedrich MW, Wager M & Loy A (2012) Sulfate-reducing microorganisms in wetlands - fameless actors in carbon cycling and climate change. *Front Microbiol.* **3**(72): 1-19.

Pickhardy PC, Folt CL, Chen CY, Klaue B & Blum JD (2002) Algal blooms reduce uptake of toxic mercury in freshwater food webs. *PNAS.* **99:** 4419-4423.

Poissant L, Zhang HH, Canario J & Constant P (2008) Critical review of mercury fates and contamination in the arctic tundra ecosystem. *Sci Total Environ.* **400**: 173-200.

Promega (2011) *Technical Manual: Assembly of Restriction Enzyme Digestions Part# TM367.* Promega Corporation. Madison, WI.

Qiagen ® (2006*) QIAprep ® Miniprep Handbook: Plasmid.* Qiagen.

Qiagen ® (2008*) QIAquick ® Spin Handbook: QIAquick Gel Extraction Kit.* Qiagen.

Ravichandran M (2004) Interactions between mercury and dissolved organic matter - a review. *Chemosphere* **55:** 319-331.

Rees GN, Baldin DS, Watson GO & Hall KC (2010) Sulfide formation in freshwater sediments, by sulfate-reducing microorganisms with diverse tolerance to salt. *Sci Total Environ.* **409**: 134-139.

Robador A, Brüchery V & Jørgensen B (2009) The impact of temperature change on the activity and community composition of sulfate-reducing bacteria in arctic versus temperature marine sediments. *Environ Microbiol.* **11**(7): 1692-1703.

Ruby EG, Wirsen CO, Fannasch HW. (1981) Chemolithotrophic sulfur-oxidizing bacteria from the Galapagos Rift hydrothermal vents. *App Environ Microbiol.* **42**(2): 317-324.

Sanei H, Outridge PM, Stern GA & Macdonald RW (2014) Classification of mercury-labile organic matter relationships in lake sediments. *Chem Geol.* **373**: 87-92.

Sass H & Cypionka H (2007) Response of sulphate-reducing bacteria to oxygen. *Sulphate-Reducing Bacteria: Environmental and Engineered Systems* (Barton LL & Hamilton WA, eds). Cambridge University Press, New York, NY.

Sass H, Berchtold M, Branke J, König H, Cypionka H & Babnzien H (1998) Psychrotolerant sulfate-reducing bacteria from an oxic freshwater sediment, description of *Desulfovibrio cuneatus* sp. nov. and *Desulfovibrio litoralis* sp. nov. *Syst Appl Microbiol.* **21**: 212-219.

Schmalenberger A, Drake HL & Küsel K (2007) High unique diversity of sulfate-reducing prokaryotes characterized in a depth gradient in an acidic fen. *Environ Microbiol.* **9**(5): 1317-1328.

Schroeder WH, Anlauf KG, Barrie LA, Lu JY & Steffen A (1998) Arctic springtime depletion of mercury. *Nature.* **394**: 331-332.

Schroeder WH, Beauchamp S, Edwards G, Poissant L, Rasmussen P, Tordon R, Dias G, Kemp J, Van Heyst B & Banic CM (2005) Gaseous mercury emissions from natural sources in Canadian landscapes. *J Geophys Res.* **110**: 1-13.

Sievert SM, Kiene RP & Schulz-Vogt HN (2007) The sulfur cycle. *Oceanography.* **20**(2) 117-123.

Smith CAS, Meikle JC & Roots CF. (2004) *Ecoregions of the Yukon Territory: Biophysical properties of Yukon landscapes.* Agriculture and Agri-Food Canada, PARC Technical Bulletin No. 04-01, Summerland, BC.

Stahl DA, Loy A & Wagner M (2007) Molecular strategies for studies of natural populations of sulphate-reducing microorganisms. *Sulphate-Reducing Bacteria: Environmental and Engineering Systems* (Barton LL & Hamilton WA, eds). Cambridge University Press, New York, NY.

Steffen A, Douglas T, Amyot M, Ariya P, Aspmo K & Mergm T (2007) A synthesis of atmospheric mercury depletion event chemistry linking atmosphere, snow and water. *Atmos Chem Phys Discuss.* **7**: 10837-10931.

Stern GA, Sanei H, Roach P, Delaronde J & Outridge PM (2009) Historical interrelated variations of mercury and aquatic organic matter in lake sediment cores from a subarctic lake in Yukon, Canada: Further evidence toward the algal-mercury scavenging hypothesis. *Environ Sci Technol.* **43:** 7684-7690.

Stern, GA, Roach P, Dickson C, Fuchs C, DeLaronde J, Friesen S, Pleskach K and Tomy G. (2011) Trace Metals and Organohalogen Contaminants in fish from selected Yukon lakes: a temporal and spatial study. *Synopsis of Research, Northern Contaminants Programme.* Aboriginal Affairs and Northern Development Canada. Ottawa, ON.

Stewart FJ, Dmytrenko O, DeLong EF & Cavenaugh CM (2011) Metatranscriptomic analysis of sulfur oxidation genes in the endosymbiont of *Solemya velum. Front Microbiol.* **2**(134): 1-10.

Tamura K, Stecher G, Peterson D, Filipski A & Kumar S (2011) MEGA6: Molecular Evolutionary Genetic Analysis using Maximum Likelihood, Evolutionary Distance and Maximum Parsimony Methods. *Mol Biol and Evol.* **28**: 2731-2739.

Thamdrup B, Fossing H & Jørgensen B (1994) Manganese, iron and sulfur cycling in a coastal marine sediment, Aarhus Bay, Denmark. *Geochim Cosmochim Ac.* **58**: 5115-5129.

Thauer RK, Stackenbrandt E & Hamilton WA (2007) Energy metabolism and phylogenetic diversity of sulphate-reducing bacteria. *Sulphate-Reducing Bacteria: Environmental and Engineered Systems* (Barton LL & Hamilton WA, eds). Cambridge University Press, New York, NY.

UBC Okanagan (2012) DNA Services, DNA Sequencing, Fragment Analysis | FADSS at UBC's Okanagan Campus [online]. Available from http://www.ubc.ca/okanagan/ikbarberschool/research/analytical/fadss/dnasequencing.htm. UBC Okanagan.

United Nations Environment Programme (2013) *Global Mercury Assessment 2013: Sources, Emissions, Releases and Environmental Transport.* UNEP Chemicals Branch. Geneva, Switzerland.

von Wachenfeldt E, Tranvik LJ (2008) Sedimentation in boreal lakes – the role of flocculation of allochthonous dissolved organic matter in the water column. *Ecosystems.* **11**: 803-814.

Wagner M, Roger AJ, Flax JL, Brusseau GA, Stahl DA. (1998). Phylogeny of dissimilatory sulfate reductases supports an early origin of sulfate respiration. *J Bacteriol.* **180**: 2975-2982.

Walsh JE (2005) Cryosphere and hydrology. *Arctic Climate Impact Assessment* (Symon C, Arris L & Heal B, eds). Cambridge University Press, New York, U.S.A.

Water Survey of Canada. (2012). Water Survey of Canada: Takhini River Near Whitehorse (09AC001) [online]. Available from http://www.wsc.ec.gc.ca/applications/H2O/

grapheng.cfm? station=09AC001&report=daily&year=2012. [cited March 3, 2015]. Environment Canada.

Wrona FJ, Prowse TD & Reist JD (2005) Freshwater Ecosystems and Fisheries. *Arctic Climate Impact Assessment* (Symon C, Arris L & Heal B, eds). Cambridge University Press, New York, NY.

Wu X-J, Pan J-L, Liu X-L, Tan J, Li D-T, Yang H. (2009) Sulfate-reducing bacteria in leachate-polluted aquifers along the shore of the East China Sea. *Can J Microbiol.* **55**: 818-828.

Yukon Permafrost Network (2011) Yukon Permafrost Network [online]. Available from www.permafrost.gov.yk.ca. [cited April 15, 2014]. Government of Yukon, Whitehorse, YT.

Zhou J, He Q, Hemme CL, Mukhopadhyay A, Hillesland K, Zhou A, Van Nostrand JD, Hazen TC, Stahl DA, Wall JD, Arkin AP. (2011) How sulphate-reducing microorganisms cope with stress: lessons from systems biology. *Nat Rev Microbiol.* **9**: 452-46.

Appendix: Trace Metal Profiles

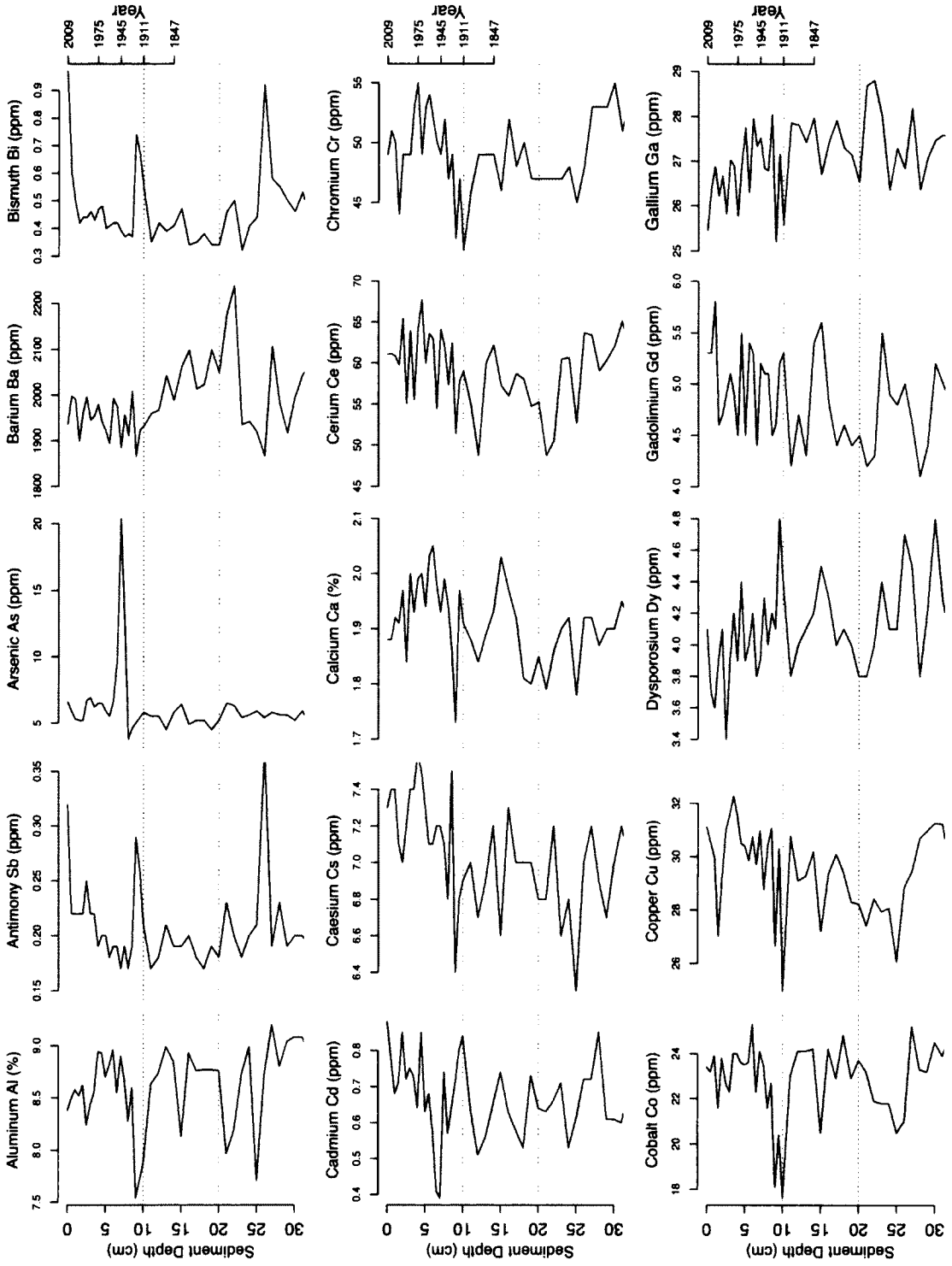

Appendix: Trace Metal Profiles

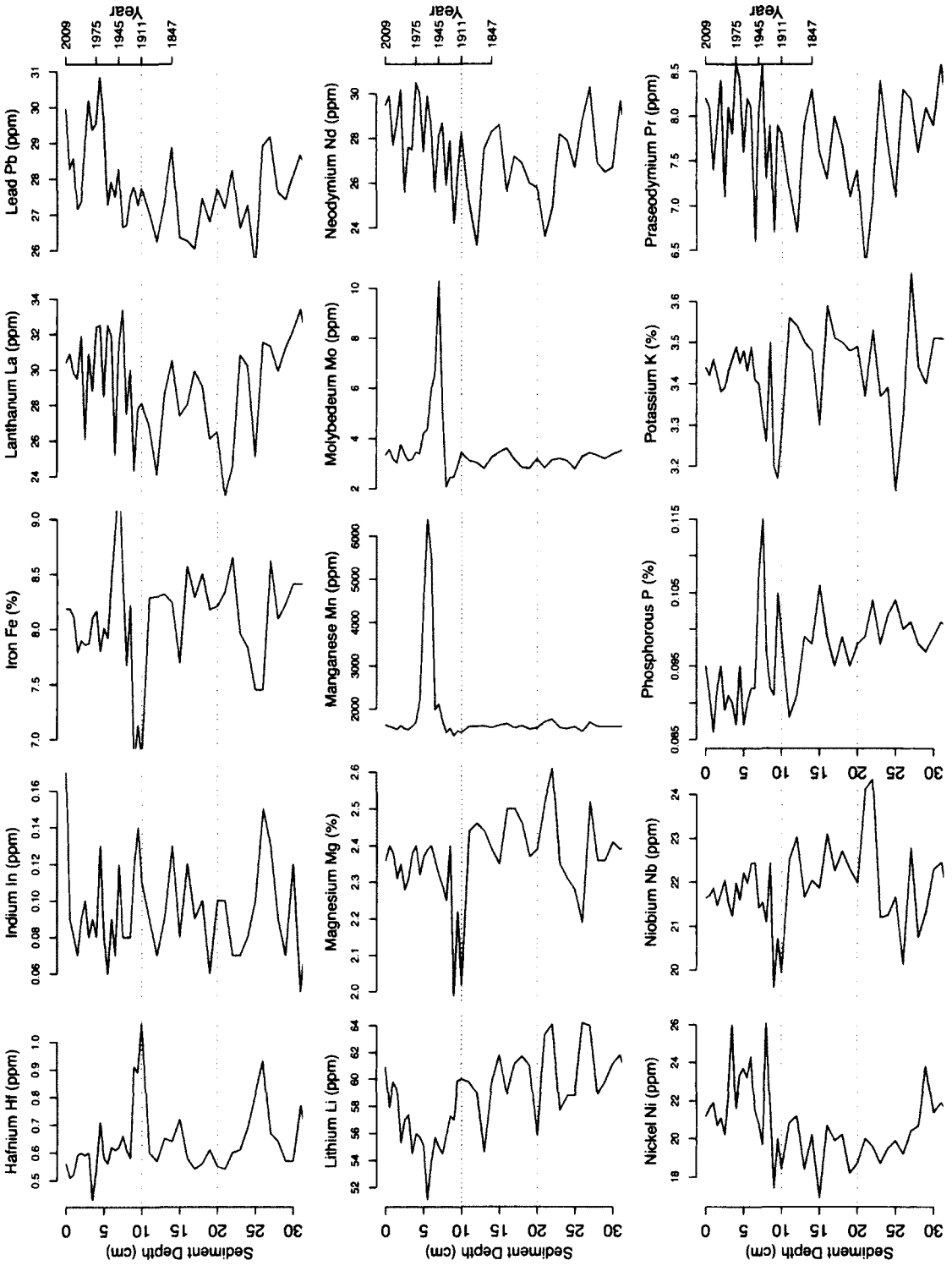

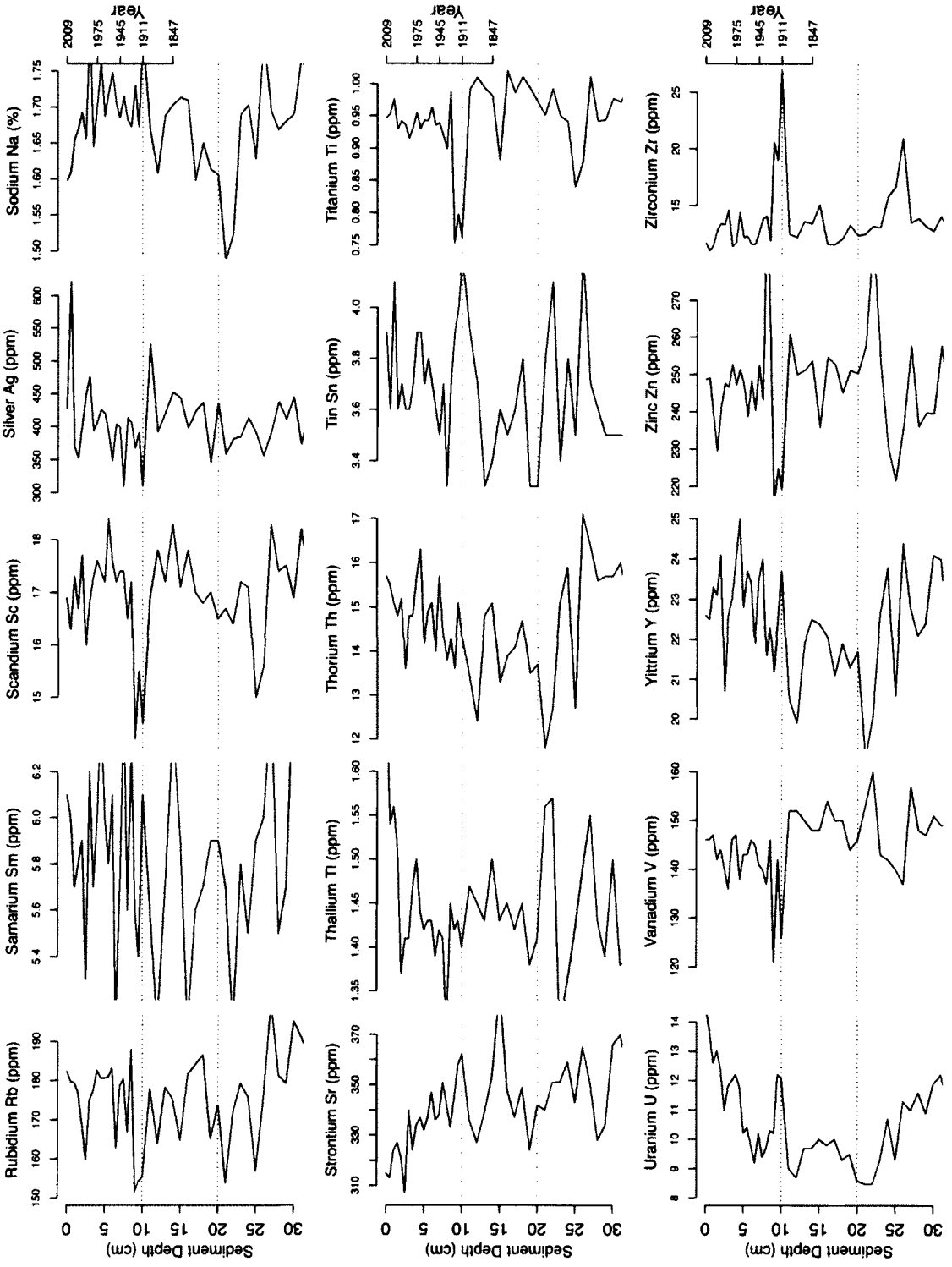
Year
2009
1975
1945
1911
1847
Sodium Na (%)
Titanium Ti (ppm)
Zirconium Zr (ppm)
Silver Ag (ppm)
Tin Sn (ppm)
Zinc Zn (ppm)
Scandium Sc (ppm)
Thorium Th (ppm)
Yttrium Y (ppm)
Samarium Sm (ppm)
Thallium Tl (ppm)
Vanadium V (ppm)
Rubidium Rb (ppm)
Strontium Sr (ppm)
Uranium U (ppm)
Sediment Depth (cm)